Membrane-Disrupting Activity of Antimicrobial Peptides and the Electrostatic Bending of Membranes

by

Sattar Taheri-Araghi

A thesis
presented to the University of Waterloo
in fulfilment of the
thesis requirement for the degree of
Doctor of Philosophy
in
Physics

Waterloo, Ontario, Canada, 2010

AUTHOR'S DECLARATION

I hereby declare that I am the sole author of this thesis. This is a true copy of the thesis, including any required final revisions, as accepted by my examiners.

I understand that my thesis may be made electronically available to the public.

Abstract

Antimicrobial peptides (AMPs) are not only fast microbe-killing molecules deployed in the host defense of living organisms but also offer valuable lessons for developing new therapeutic agents. While the mode of action of AMPs is not clearly understood yet, membrane perturbation has been recognized as a crucial step in the microbial killing mechanism of many AMPs.

In this thesis, we first present a physical basis for the selective membrane-disrupting activity of cationic AMPs. To this end, we present a coarse-grained physical model that approximately captures essential molecular details such as peptide amphiphilicity and lipid composition (e.g., anionic lipids). In particular, we calculate the surface coverage of peptides embedded in the lipid headgroup-tail interface and the resulting membrane-area change, in terms of peptide and membrane parameters for varying salt concentrations. We show that the threshold peptide coverage on the membrane surface required for disruption can easily be reached for microbes, but not for the host cell – large peptide charge ($\gtrsim 4$) is shown to be the key ingredient for the optimal activity-selectivity of AMPs (in an ambient-salt dependent way). Intriguingly, we find that in a higher-salt environment, larger charge is required for optimal activity.

Inspired by membrane softening by AMPs, we also study electrostatic modification of lipid headgroups and its effects on membrane curvature. Despite its relevance, a full theoretical description of membrane electrostatics is still lacking – in the past, membrane bending has often been considered under a few assumptions about how bending modifies lipid arrangements and surface charges. Here, we present a *unified* theoretical approach to spontaneous membrane curvature, C_0, in which lipid properties (e.g., packing shape) and electrostatic effects are self-consistently integrated. Our results show that C_0 is sensitive to the way lipid rearrangements and divalent counterions are modeled. Interestingly, it can change its sign in the presence of divalent counterions, thus stabilizing reverse hexagonal (H_{II}) phases.

Acknowledgements

I would like to take this opportunity to acknowledge those who have helped me complete this thesis. First and foremost, I would like to express my gratitude to my supervisor, Professor Bae-Yeun Ha – his encouragement, support, and thoughtful advice have been immensely valuable, both in personal and professional terms. Besides, I am indebted to other members of my defense and advisory committee. I am grateful to Professor Cècile Fradin who kindly accepted to be the external examiner of my thesis. I enjoyed her deep and thoughtful questions during my defense. Professors Michael Palmer, Russell Thompson and Zoya Leonenko have been on my advisory committee for a few year and I have always found their comments and suggestions constructive in improving my work. I am also thankful to other members of our research group, Yang Li, Roham Farzami, and Zheng Ma, whose cooperation helped me a lot.

I would like to say a special thank to my wife, Farinaz, to whom I would like to dedicate this thesis. Her love and companionship has been so heartwarming during my *not-so-easy* PhD years. Without her this thesis would not be possible. My gratitude goes to my parents who wisely provided me with extraordinary environment and education during my childhood. Their efforts has had a key role in the formation of my todays thinking style. I would also like to thank my elder brother, Sina, who first showed me the interesting world of physics in my youth. His support has been so heartwarming through the years. I owe to him all the confidence I got to stay in physics as my professional career.

I have been always blessed to be surrounded by wonderful friends. They have made my life joyful and shaped my personality. We have shared happy and sad moments of our lives. I am not able to thank each of them here, but, name a few who played a role in my education: Mojtaba Ghadimi, Khosrow Allaf-Akbari, Hamid Molavian, Ali Tabei, Samad Bazargan, Azad Qazi-Zade, Alireza Shayesteh, and Majid Safari.

Finally, I would like to thank Natural Sciences and Engineering Research Council (NSERC) of Canada and Ontario Ministry of Education for their financial support.

This thesis is dedicated to my love, Farinaz,

and my parents for their constant support.

Contents

Author's Declaration ii

Abstract iii

Acknowledgments iv

Dedication vi

Table of Contents vii

List of Figures xi

1 Introduction 1

1.1 Motivation and Goals 1

1.2 Antimicrobial Peptides 3

1.2.1 Discovery 3

1.2.2 Biological and physiochemical properties 4

1.2.3 Mechanism of action 5

1.3 Biological Cells 14

1.3.1 Structure of the cell 14
1.3.2 Bacteria 14
1.3.3 Bacterial cell membranes 16
1.4 Organization of The Thesis 18

2 Electrostatics in Biological Environments 20
2.1 Poisson-Boltzmann Theory 20
2.2 Debye-Hückel Theory 22

3 Cationic Antimicrobial Peptides: a Physical Basis for their Selective Membrane-Disrupting Activity 24
3.1 Introduction 24
3.2 Theoretical Methods 29
3.2.1 Molecular model 29
3.2.2 Free energy calculations 31
3.3 Results and Discussion 38
3.3.1 Wigner-Seitz cell free energy 38
3.3.2 Membrane binding 39
3.3.3 Variation of peptide charge 44
3.3.4 Effect of peptide hydrophobicity 46
3.3.5 Dependence on bulk peptide concentration 47
3.3.6 Membrane disruption 48
3.3.7 Spontaneous pore formation 50
3.4 Conclusions 53

3.5 COMSOL scripts 55
3.5.1 Wigner-seitz cell free energy 55
3.5.2 Minimization of free energy 58

4 Spontaneous Bending of Lipid Bilayers: How are Lipid and Electrostatic Properties Interrelated? 66

4.1 Introduction 66
4.2 Model 69
4.2.1 Single-lipid free energy 69
4.2.2 Electrostatic free energy of a lipid membrane 71
4.3 Membrane Free Energy 77
4.3.1 Monolayers 77
4.3.2 Bilayers 78
4.4 Results 80
4.4.1 Monolayers 80
4.4.2 Bilayers: spontaneous curvature of asymmetrically charged bilayers 86
4.5 Conclusions 89

5 Conclusions and Proposal for Future Considerations 92

5.1 Conclusions 92
5.2 Proposals for Future Works 94
5.2.1 An analytical approach for peptide-lipid bilayer binding . . . 94
5.2.2 Threshold of pore formation by antimicrobial peptides . . . 99

Bibliography **104**

List of Figures

1.1 Electrostatic interactions, the origin of the selectivity of AMPs . . . 7

1.2 Antimicrobial peptide SMAP29 attached to a cell membrane 8

1.3 Insertion of antimicrobial peptides and expansion of the overall area of a lipid bilayer 10

1.4 Schematic cross-sectional view of barrel-stave and toroidal pores . . 11

1.5 Disruption of the structure of a lipid bilayer by excessive coverage of peptides 12

1.6 The energy as a function of radius for a simple pore on the lipid bilayer 13

1.7 Schematic cross sectional view of a bacterium 15

1.8 Amphipathic lipids can self-assemble in a variety of structures . . . 16

1.9 Schematic view of Gram-positive and Gram-negative bacterial cell membranes 18

3.1 Insertion of antimicrobial peptides into lipid bilayer 26

3.2 The disk model for peptide 27

3.3 Wigner-Seitz cell arrangements of peptides 28

3.4 Side view of WS cell 34

3.5 Free energy of a Wigner-Seitz Cell per lipid molecule 39
3.6 Membrane free energy per lipid 40
3.7 Membrane free energy per lipid for various peptide charge 41
3.8 Parallel plates, release and trap of counterions 43
3.9 Molar ratio of membrane-puturbing peptides to lipids, P_I/L 45
3.10 P_I/L as a function of peptide charge 46
3.11 P_I/L as a function of bulk peptide concentration 48
3.12 Fractional area stretch, $\Delta A/A$, as a function of peptide charge . . . 49
3.13 Energy of a pore as a function of the radius 51
3.14 The activation free energy for lipid-pore formation 52

4.1 The packing shape of a lipid, characterized by geometrical parameters 70
4.2 Charge discreteness of anionic lipids on a spherically curved membrane 73
4.3 A Wigner-Seitz cell for the monovalent and divalent counterios . . . 75
4.4 Relaxed headgroup area of lipids as a function of monovalent salt concentration 80
4.5 Location of neutral surface, δ_N, and thickness, l_{hc}, of a lipid monolayer 82
4.6 Spontaneous curvature of a charged lipid monolayer as a function of monovalent salt 83
4.7 Spontaneous curvature of an asymmetrically charged lipid bilayer . 86
4.8 Spontaneous curvature of an asymmetrically charged lipid bilayer as a function of θ 88

5.1 Side view of a cylindrical Wigner-Seitz cell 97

5.2 Free energy of a cylindrical Wigner-Seitz cell as a function of the radius 98

5.3 Formation of a peptide-stabilized pore 100

5.4 Schematic view of peptide energies in a pore and on the surface . . 101

5.5 Unit cells defined with constant area and varying number of anionic lipids 102

Chapter 1

Introduction

1.1 Motivation and Goals

The discovery of penicillin by Alexander Fleming in 1928 was arguably one of the most significant achievements in medicine. This discovery transformed medicine and saved millions of lives in less than a century. It sounded like a miracle to cure a then-untreatable disease within a few days or possibly a few hours. However, the great service of antibiotics to public health has been accompanied by an ever growing side effect: the development of antibiotic-resistant bacteria [1]. Alexander Fleming was aware of this and had cautioned about the usage of antibiotics. In his Nobel Lecture in 1945, Fleming states that "it is not difficult to make microbes resistant to penicillin in the laboratory by exposing them to concentrations not sufficient to kill them, and the same thing has occasionally happened in the body." [2] He continues, "the time may come when penicillin can be bought by anyone in the shops. Then there is the danger that the ignorant man may easily underdose himself and by exposing his microbes to non-lethal quantities of the drug make them resistant." [2]

Given the widespread use of antibiotics over several decades, the emergence of antibiotic-resistant microbes has been inevitable, even though their development

and spread could be slowed down by the way antibiotics have been prescribed and used. Moreover, antibiotic-resistant bacteria could arise as a natural result of mutations and natural selection in the microbial populations of multicellular organisms [1]. For instance, consider a population of bacteria treated with antibiotics. The more resistant ones, who survive the antibiotic attack, multiply and constitute a higher portion of the population. They can spread around and the same process can repeat over and over again. The eventual result is that some treatable disease will again become untreatable. In a point of view, this is a bitter reality to see how an achievement in medicine brings about a more challenging trouble to the society.

Regardless of its cause and origin, scientific community are trying to find methods to respond to the growing threat of antibiotic-resistant microbes. One direction has been designing and developing novel antimicrobial compounds as an alternative or supplement to antibiotics. Among different candidates, antimicrobial peptides (AMPs) have gained a great deal of attention over the last couple of decades [3–6]. These "evolutionary ancient weapons" [4] have been protecting multicellular organisms (e.g., plants and animals) from microbial challenges through billions of years. Constant exposure of multicellular organisms to pathogenic microbes is, at the first stage, counteracted by their innate immunity in which AMPs are one of the main combatants. The long term service of AMPs backs the notion that microbes cannot easily develop resistance against them. This is a promising feature which could rectify the current threat of antibiotic resistance [3].

Extensive research on antimicrobial peptides, followed by some clinical trials, has not yet been successful in designing and synthesizing modified antimicrobial peptides to be used as therapeutic agents [3, 5]. One or two AMPs have received approval from Food and Drug Administration as anti-infective drugs [3, 5]. The failure of many attempts has been rooted in AMPs' weak antimicrobial activity or their high toxicity for the host cells [3]. During the experiments, the AMP was not strong enough to kill the invading pathogenic microbes. When it was, it was also

toxic toward host cells that should not have been harmed. These results have left the scientific community with a major question: How can AMPs be made more active (microbe-killing) and, at the same time, more selective (having the ability to discriminate host cells). The prospects for an answer in the genetical landscape are grim: the biological activity of peptides arises from their amino acid sequence. Peptides are made of typically 15-40 amino acid residues. There are 20 types of standard amino acids in nature. To get a sense of the variety of possible peptides, let's consider a 20-amino acid long peptide, permutation of amino acids results in $20^{20} = 10^{26}$ different peptides. How can the "best" peptides from such a big pool be found? What should be the criteria to determine the activity or selectivity of peptides based on their amino acid composition? These fundamental questions have not been adequately addressed so far.

In this thesis, we present a physical basis for membrane-perturbing activity of AMPs. To this end, we develop a coarse-grained model of a AMP-membrane system, which allows us to examine how peptide-membrane parameters control peptide activity and selectivity. The emerging physical picture is that peptide charge is a key ingredient for determining the optimal activity and selectivity of AMPs, such that the optimal charge depends on the ambient salt. Inspired by the experimental observations of AMP-induced membrane softening, we also examine how the charge properties of membranes influence their conformational properties.

1.2 Antimicrobial Peptides

1.2.1 Discovery

The earliest investigation of the antimicrobial activity of normal tissues and body fluids dates back to the last decades of the nineteenth century when antimicrobial substances were observed in blood, leucocytes and lymphatic tissues [6, 7]. At

the same time, the precise identity of these substances was, however, not clearly understood [7]. Later, in the first decades of the twentieth century, antimicrobial substances were classified based on the physiological properties of their targets, such as gram-staining properties by which bacteria were classified as Gram-negative or Gram-positive. (Table 1 in reference [7]). Based on the limited knowledge about the structure of the discovered antimicrobial agents, they were named "small basic proteins", "basic peptides", "basic linear peptides", etc. [7]. Few decades later, in the 1980s, antimicrobial peptides became the center of attention following a few discoveries in which AMPs were isolated from multicellular organisms: amphibian magainins from skin of the frog by Michael Zasloff [8], insect cecropins by Hans Boman [9], and mammalian defensins by Robert Lehrer [10]. These discoveries, along with the increasing resistance of bacteria to conventional antibiotics, have directed the research of novel therapeutic substances to antimicrobial peptides. So far, more than 890 different antimicrobial peptides have been identified and listed in databases (for an excellent collection you may visit http://www.bbcm.units.it/~tossi/amsdb.html). Among them, the 3D structures of more than 50 AMPs have been determined.

1.2.2 Biological and physiochemical properties

Antimicrobial peptides are ubiquitous in nature [4]. They are genetically encoded and form an essential component of the innate immunity in both plants and animals [11]. Three families of AMPs have been observed in humans: defensins, cathelicidins, and histatins [12–14]. The term "evolutionarily ancient weapons" [4] points out the long term contribution of AMPs to the innate immunity and their role in the evolution of multicellular organisms. Besides, the long term presence of AMPs in nature for over two billion years suggests the notion that microbes cannot easily develop resistance against them [3].

Generally speaking, peptides are short proteins. They are made of about 10-50 amino acid residues [15]. There are 20 different amino acids in nature with different physical and chemical properties. Table 1.1 (adopted from reference [16]) shows their chemical and physical properties. The properties of peptides and proteins are defined by the amino acid sequence in their structure [15]. Each protein has its own biological function owing to its unique amino acid sequence. Antimicrobial peptides are typically cationic: they contain several positively charged amino acid residues [4, 6]. As it turns out, this contributes to their selective activity, making them potent for negatively charged membranes such as microbial membranes [17, 18]. AMPs have amphipathic structure, that is, their amino acid sequence and their spatial structures are such that the hydrophilic residues and the hydrophobic residues are located on opposite sides of the molecule [4, 6]. This enables AMPs to interact with both water (polar) and the lipid part (non-polar) of the cell membranes. The cationic charge and the amphipathic structure are the two major factors granting AMPs their cell-membrane-disrupting ability [6]. Understanding the exact mechanisms by which AMPs disrupt lipid bilayers and cell membranes have been the subject of extensive research over the last couple of decades. In the next section we briefly present the discoveries and the advances in this particular area of research.

1.2.3 Mechanism of action

In the last couple of decades there has been extensive research on the mechanisms of activity of AMPs (a comprehensive review can be found in reference [4]). There has also been a great deal of interest in discovering the optimal parameters that enable AMPs to selectively attack microbes while leaving the host cell intact [19]. A few specific steps are involved in microbial killing. As discussed in reference [6] (with some modifications), the steps are: (*i*) cell discrimination; (*ii*) binding and

Table 1.1: Amino acids and their physical properties

Amino Acid	3-Letter name	Side chain polarity	Net charge
Alanine	Ala	nonpolar	0
Arginine	Arg	polar	+1
Asparagine	Asn	polar	0
Aspartic acid	Asp	polar	-1
Cysteine	Cys	nonpolar	0
Glutamic acid	Glu	polar	-1
Glutamine	Gln	polar	0
Glycine	Gly	nonpolar	0
Histidine	His	polar	0
Isoleucine	Ile	nonpolar	0
Leucine	Leu	nonpolar	0
Lysine	Lys	polar	+1
Methionine	Met	nonpolar	0
Phenylalanine	Phe	nonpolar	0
Proline	Pro	nonpolar	0
Serine	Ser	polar	0
Threonine	Thr	polar	0
Tryptophan	Trp	nonpolar	0
Tyrosine	Tyr	polar	0
Valine	Val	nonpolar	0

membrane association; (*iii*) membrane perturbation and rupture.

Cell discrimination

Antimicrobial peptides were shown to kill bacteria in 15-90 minutes [6]. One of the most important features of the action of AMPs is their ability to recognize the target cell in the crowd of host cells [4]. AMPs are known to utilize one of the structural differences between host cell and microbial cells to achieve this goal. The outer leaflet of the outer membrane of bacterial membranes is abundant in anionic lipids, while the host cell is overall neutral on its outer layer [4]. AMPs, typically, bear a few cationic amino acid residues in their structure and are mainly

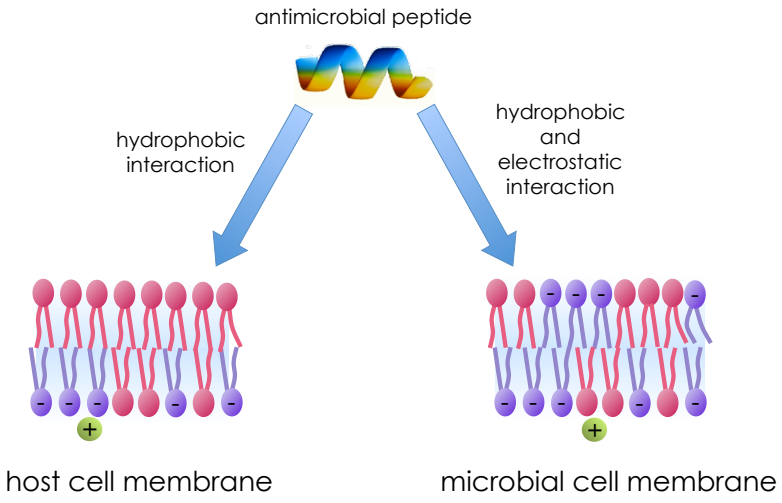

Figure 1.1: The attraction between antimicrobial peptide and microbial membrane is increased by electrostatic interaction.

cationic. Their interaction with microbial membranes is boosted by the coulomb interaction between the cationic residues and anionic lipids on the membrane [4,18]. This is the origin of peptide selectivity (Fig. 1.1). At first glance, one may conclude that the more highly charged peptides would be more potent against microbes. This view is, however, not consistent with the experimental observations [19]. As will be elaborated in this thesis, cell discrimination and association with cell membranes are the combined effect of several different interactions. Even though the electrostatic interaction plays a central role, it is influenced by other effects, such as hydrophobocity of peptides, and is complicated with "many-body Coulomb interactions" so that the AMP activity diminishes if the peptide charge exceeds an optimal value which is around +5 (electronic charges) [19, 20].

This picture of membrane discrimination is somehow complicated by the fact that the microbial membranes are much more than a pure lipid bilayer [15]. Gram-negative and Gram-positive bacteria have more complex structures, as will be discussed later in this chapter. Nevertheless, the outer membranes of Gram-negative

Figure 1.2: Antimicrobial peptide SMAP29 attached to the outer leaflet of the cell membrane. Reprinted by permission from Macmillan Publishers Ltd: Nature Reviews Microbiology (K. A. Brogden, **3**:238-250), copyright (2005).

organisms contain negatively charged *lipopolysaccharides* (LPS) [15]. Most likely, AMPs are first attracted to this cell envelope and subsequently interact with the lipid matrix of the cell membrane.

A fundamental method to identify the main target site of antimicrobial peptides is microscopy. Some AMPs, like *Magainin 2*, are observed to bind to the cell surface while some others, like *biotinylated buforin* II, enter the cytoplasm [21]. Fig. 1.2, adapted from reference [6], shows the membrane structure of bacteria which is damaged as treated by AMPs (SMAP29).

Binding and membrane association

Once an AMP is brought into close proximity to a lipid bilayer by the electrostatic interactions, it may interact more effectively with the cell membrane through its hydrophobic residues [4, 6, 18, 22]. Note that hydrophobic interactions, unlike electrostatic forces, are not long-ranged. In a series of studies by Huang *et al.* a clear picture of the activity of AMPs against model lipid bilayer has been pre-

sented [23–25]. In these studies, oriented circular dichroism (OCD) was used to find the orientation and the secondary structure of peptides bound to the lipid membranes. X-ray diffraction was used to measure the thickness of the membrane. These studies suggest that association of peptides with lipid bilayers reduces the thickness of the bilayer. Membrane thinning indicates that the peptides associated with the lipid bilayer tend to reside on the headgroup-tail interface, parallel to the membrane, stretching the bilayer. Because the volume of the hydrocarbon chain (the lipidic area of the membrane) remains constant, membrane thinning must be the direct consequence of its area stretch (Fig. 1.3). Experiments have clearly shown that there is a linear relationship between the molar ratio of peptide to lipids (P/L) and the thickness of the lipid if (P/L) is smaller than a certain value, $(P/L)^*$. Beyond $(P/L)^*$, the thickness remains constant, which is thought to indicate a somewhat different type of peptide-lipid interactions [23, 25]. These results have been remarkably important in clarifying the mechanism of action of AMPs.

The parallel association of peptides with lipid membranes is driven mainly by the amphipathicity of the AMPs: the spatial organization (secondary structure) of the AMPs is such that hydrophobic residues are separated from the hydrophilic ones [4, 6, 18, 26]. The hydrophobic residues stay in contact with lipid tails, while hydrophilic residues are in contact with the solution. In this arrangement, AMPs remain parallel to the surface and thus stretch the overall area of the membrane [23, 25, 26]. This is analogous to the situation where the the membrane is stretched by external pressure. In other words, peptide binding results in reduced membrane integrity. Once (P/L) exceeds the threshold, $(P/L)^*$, pores start to form in the membrane. In the next subsection, we discuss the details of pore formation.

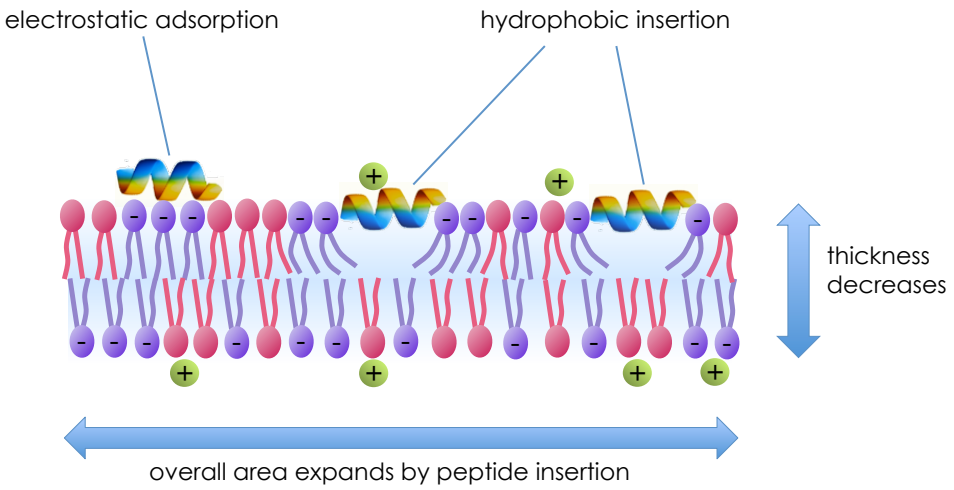

Figure 1.3: The expansion in the overall area of a lipid bilayer can be measured by thickness change. This picture is correct for $(P/L) < (P/L)^*$. Above $(P/L)^*$, the thickness remains constant - extra peptide take part in pore formation and not membrane thinning.

Membrane perturbation and rupture

Bilayer tension increases due to peptide crowding (high (P/L) value). As a result, the peptide and the membrane have to be rearranged to relieve the excess pressure. In general, the structure of the lipid bilayer is distorted in response to the tension. There are two major mechanisms by which the bilayer is distorted. As summarized in reference [6], in one mechanism pores are formed in the membrane, while in the other, the membrane is ruptured and micelles are developed (the *carpet-model*). Both of these mechanisms lead to the membrane's collapse and the cell's death. In some cases, however, membrane collapse lags the loss of viability of the cell [6]. Two types of AMP-mediated pores are observed in lipid bilayers: *barrel-stave* pores and *toroidal* pores (Fig. 1.4) [26, 27]. The type of the pore that forms on the lipid bilayer depends on the structure of AMP rather than on the lipid's composition [6]. In what follows, we discuss the different pores and the *carpet-model* that supports

the micellization of the lipid bilayer (Fig. 1.5).

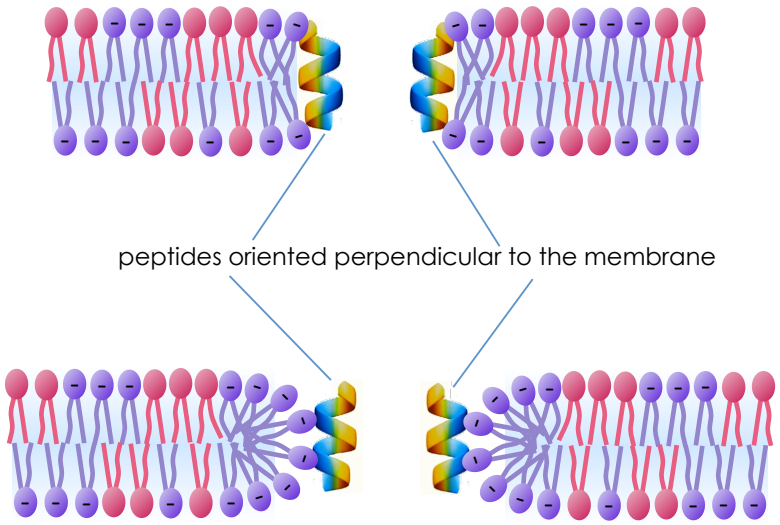

Figure 1.4: Schematic cross-sectional view of pores induced by α-helical peptides. (a) In *barrel-stave* pores, the hydrophobic side of the peptide faces hydrocarbon tails of lipids and the hydrophilic side faces water. (b) In *toroidal* model, lipid head groups form a curved edge separating lipid tails from water. The pore is stabilized by 4-7 peptides aligned perpendicular to the membrane around the pore.

One way to assess the pore formation and membrane permeabilization is to monitor the voltage across a lipid membrane [6]. AMPs such as Cecropins and their synthetic peptide analogs were found to form large voltage-dependent ion channels on lipid membranes. Comparison of different AMPs also sheds light on some structural requirements for pore formation [28].

The *barrel-stave* pore is a unique type of pore formed by the peptide alamethicin [6, 26]. In this model, the pore is stabilized by arrangement of α-helical peptides around the pore where the peptides are aligned perpendicular to the surface of the membrane [26]. The edge of the pore is covered by peptides, such that their hydrophobic side faces the lipid area of the membrane and their hydrophilic side is in contact with water. In other words, peptides bridge between the lipid

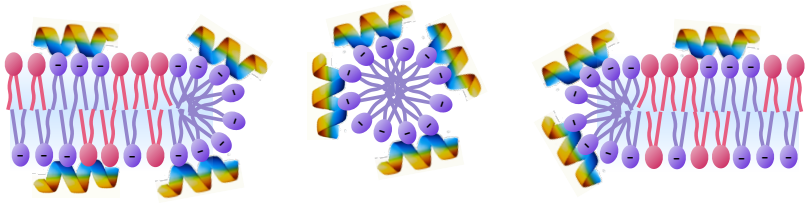

Figure 1.5: Excessive coverage of a lipid bilayer by peptides disrupts their structure by creation of micelles.

area of the membrane and water to reduces the unfavorable hydrophobic energy. The number of peptides in the barrel-stave pore ranges from 3 to 11, and the inner radius of the pore falls within the range $\approx 1.8 - 4.0$nm depending on the lipid bilayers composition [29, 30].

The *toroidal* pore is different from the barrel-stave pores in the arrangement of lipids on the edge of the pore [27]. Here, lipid part is separated from water by the polar headgroups of the phospholipids, just like that in the lipid bilayer. At the edge of the pore, each layer bends continuously The pore is stabilized by vertical alignment of the peptides around the pore [31]. Unlike in the *barrel-stave* pore, the charged (polar) side of the peptides in a *toroidal* pore faces the lipid bilayer and the headgroups of the lipids. Magainin is one of the antimicrobial peptides that form *toroidal* pores [26]. Toroidal pores are larger than barrel-stave pores in size and include 4-7 peptides per pore [26].

In the *carpet model*, there is no pore formed in the membrane. Instead, the extensive coverage of the membrane by peptides destroys the lipid bilayers by breaking apart its structure in a detergent-like manner [22,32]. At some point, peptides make the lipid molecules form micelles and disrupt the integrity of lipid bilayer [22, 32].

The general mechanism of pore formation by AMPs can be explained through the energetics of a spontaneous pore in a pure bilayer [25]. If a membrane is subjected to some external tension, the bilayer expands in order to sustain the

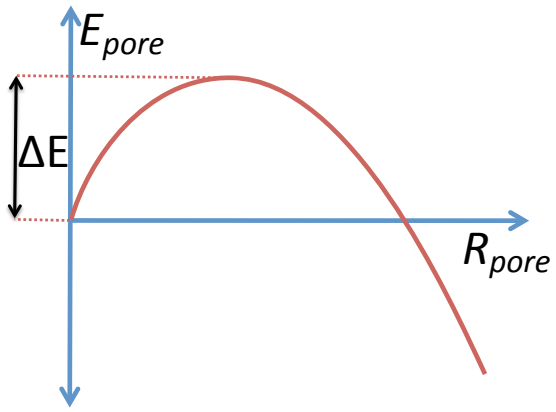

Figure 1.6: The energy of a simple pore , E_{pore}, on the lipid bilayer as a function of the radius of the pore , R_{pore}. The energy barrier to the growth of the pore, ΔE, is determined by surface tension of the bilayer and the line tension on the edge of the pore. See text for the equation governing the energy, Eq. 1.1.

tension. Once the tension is large enough, pores start forming in the bilayer. The initiation of a single pore is not straightforward to analyze. However, once a pore is opened, its fate is determined by the competition between the line tension on its edge and the tension of the membrane [33, 34]. Quantitatively, the energy of a pore of radius R_{pore} can be expressed as

$$E_{\text{pore}} = 2\pi R_{\text{pore}}\lambda - \pi R_{\text{pore}}^2\gamma \tag{1.1}$$

where λ is the line tension and γ the surface tension. The first term accounts for the energy cost associated with the pore edge that resists pore expansion. The second term reflects the energy gain through the surface tension. Based on this picture, pores are unstable: there is an energy barrier beyond which a pore expands indefinitely and below which it closes. This energy barrier is shown by ΔE in Fig. 1.6. In the case of peptide-induced pores, the spontaneous pores formed this way will be then stabilized by peptides as explained above. In the third chapter we will elaborate on pore formation, treating it as a barrier crossing process.

1.3 Biological Cells

1.3.1 Structure of the cell

Cells are often referred to as the "building blocks of life" [15]. They are probably the smallest entities that exhibit the basic life activities such as division and passing on genetic information [15]. The number of cells in human body is "literally astronomical" [35] , greater than the number of stars in the Milky Way. Their variety is, however, limited to around 200 types [35], each exhibiting a specific physical structure. Some, like nerve cells, are long with branched structure, some like red blood cells are remarkably flexible. The basic structure of all cells is, however, similar in the sense that all of them have a cell membrane that encapsulates the cytoplasm and the cell compartments [35]. The structure of the cell membrane and the cell compartments vary from species to species. In a microscopic view, cells can be divided into two categories: *eukaryotic* and *prokaryotic* [15]. In eukaryotes, their DNA is packed inside a space called the nucleus, a membrane bound organelle. DNA in prokaryotes is not encapsulated in a specific compartment. Eukaryotic cells also possess other membrane-bounded compartments, or organelles, such as mitochondria and the Golgi apparatus. Cells in plant, animal, and fungi are eukaryotes. Bacteria are prokaryotes. Next, we discuss the structure of bacteria in more detail.

1.3.2 Bacteria

Unlike the simple view held by many, not all bacteria induce disease. A healthy adult has about 10^{12} bacteria on the skin and about 10^{14} in the intestines. Some bacteria are parasitic, while the majority of them live freely in soil and water. [36]. Bacteria vary widely in shape [37]; some are rounded or spherical cells, called *cocci*, while others are elongated or rod-shaped, called *bacilli* [37]. There are also spiral

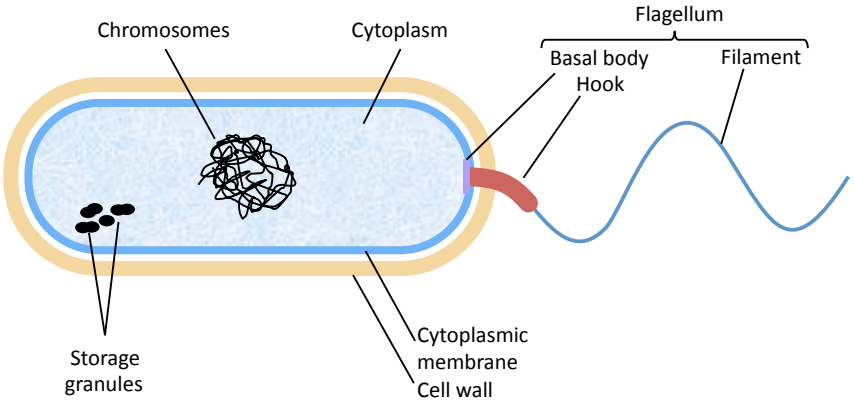

Figure 1.7: Schematic cross sectional view of a bacterium. In bacteria, chromosomes are not encapsulated in nucleus. Not all details shown here are present in every bacterium. Modified by permission from *Bacteria in Biology, Biotechnology and Medicine* by P. Singleton, 4th edition, John Wiley and Sons. 1997.

bacteria called *spirilla* when they are rigid or *spirochaetes* when they are flexible [37].

Bacteria usually measure in the micrometer (μm) range: from 0.2μm for cells of *Chlamydia* to 250μm from some of the cells of *Spirochaeta* [37]. In most species, however, the maximum dimensions are within $1 - 10\mu$m [37].

Besides the physical shape, bacteria also differ in terms of both chemical composition and fine structure [37]. Fig. 1.7 depicts a 'general' schematic view of a bacteria. Note that not all bacteria have the features shown in this figure. Even though bacteria are sometime regarded as simple cells, owing to their lack of organelles (such as a nucleus and Golgi apparatus), they employ several very sophisticated mechanisms at the molecular level [37]. One example is a structural element called flagellum (plural: flagella) found in many species. Flagella are surface appendages that help a bacterium swim or attach to a desired surface.

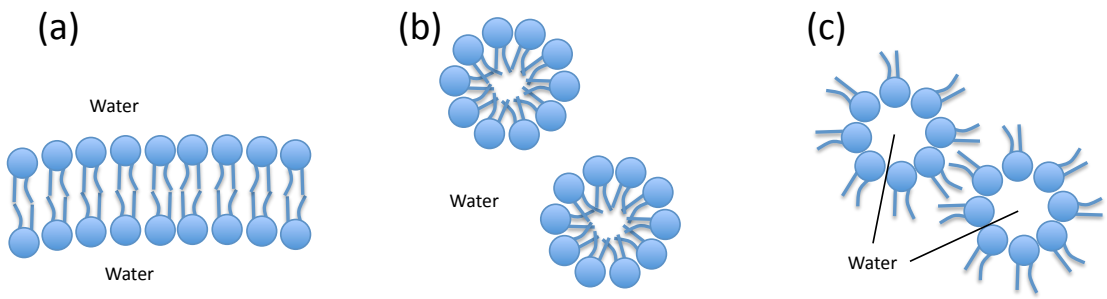

Figure 1.8: Amphipathic lipids can self-assemble in a variety of structures.

1.3.3 Bacterial cell membranes

A key structural element of all cell membranes is the lipid bilayer. Lipids account for 50% of the mass of cell membranes [15]. The constituent lipid molecules are amphipathic, that is, they have a polar (hydrophilic) head group and non-polar (hydrophobic) tails. In water, they can self-assemble into structures such that the polar head groups separate the non-polar tails from water. Depending on the concentration, size, and shape of the lipid molecules, the preferred structure can be a micelle, an inverted micelle or a lipid bilayer as depicted in Fig. 1.8 [35]. The thickness of a lipid bilayer is within the range of 4 - 5nm. One of the most abundant types of lipids in cell membranes, which also occurs in all bacteria, is the phospholipid. The schematic view of phospholipid molecules is shown in Fig. 1.8. Phospholipids have fatty acid tails whose length and saturation affect the flexibility of the lipid bilayer.

Lipid bilayers have unique elastic properties. In the first order approximation, they can be considered as elastic sheets [35]. In a more microscopic view, however, this model fails. One major issue is that, unlike an elastic sheet, a lipid bilayer has no shear resistance. That is why they are often referred to as "fluid membranes", referring to the lateral diffusion and flip-flop of lipid molecules (the rarely occurring

relocation from the inner layer to the outer layer or vice-versa). The *fluidity* of a lipid bilayer depends on its composition and temperature. At a freezing point, phospholipid molecules can undergo a phase transition and transform into rigid crystalline (gel) structures [15]. The composition of lipid bilayers can also strongly affect their rigidity. Presence of 20% cholesterol can double up the stiffness of a lipid bilayer [35].

In cell membranes, other molecules such as membrane proteins are anchored to the lipid bilayer in different ways [15]. Some proteins span across the membrane and are called *transmembrane proteins*, while others are attached to the surface through covalent bond or by hydrophobic regions of the protein [15]. The number of proteins is much smaller than that of lipids in a cell membrane. However, they account for almost half of the mass of the membranes on average [15]. Proteins are also responsible for significant membrane functions. It is the proteins that give membranes of different cells their characteristic functional properties [15].

The bacterial cell surface appears to be more complicated than that of eukaryotes. While lipid bilayers form the main part of the membrane (or a cytoplasmic membrane), a stiff envelope, the *cell wall*, protects the whole cell from mechanical damage and regulates the transport of ions and molecules. The cell wall structure varies in different species. There are two major types of cell walls: *Gram-negative* and *Gram-positive*. The cell wall structure can be determined by monitoring the bacterium's response to certain dyes. The methodology, *Gram stain*, was discovered by Danish scientist Christian Gram in the 1880s [37]. Figure 1.9, adapted from reference [15], shows a schematic view of the cell wall structure of Gram-positive and Gram-negative bacteria.

Gram-positive bacteria have a *peptidoglycan layer* that encapsulates the lipid bilayer (inner layer) of the membrane. Gram-negative bacteria have two membranes separated by a *periplasmic space*. The inner membrane is a phospholipid bilayer.

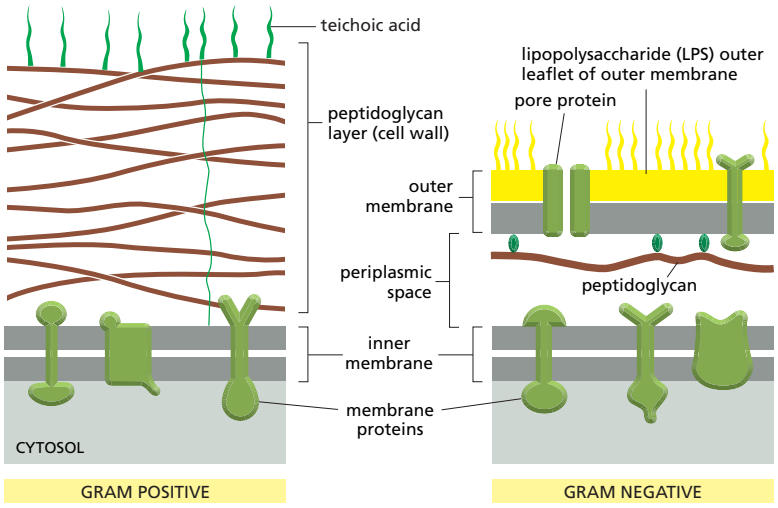

Figure 1.9: Bacterial membranes, categorized as Gram-positive or Gram-negative, have seemingly different structures. In both cases, the inner membrane is a phospholipid bilayer. ©2008 From Molecular Biology of the Cell 5E by Alberte et al. Reproduced by permission of Gerland Science/Taylor and Francis LLC.

The outer membrane has an outer leaflet made of *lipopolysaccharide* (LPS) and an inner leaflet made of phospholipids.

1.4 Organization of The Thesis

The first chapter of this thesis is an introduction detailing the motivation and the goals of this work. The Introduction chapter includes a brief overview on Antimicrobial Peptides (AMPs), their mechanism of action, as well as of biological cells and cell membranes.

In the second chapter, we present the basis of electrostatic interactions in electrolytes and derive the Poisson-Boltzmann equation.

The third chapter is devoted to the physical modeling of AMPs and lipid bilayers. Using a coarse-grained model for AMPs and lipid bilayers, we present a

physical basis for the membrane-disruptive activity of AMPs. We find that the activity of AMPs is maximized at a certain peptide charge (Q$\sim$ 5). We also show that in a high salt environment larger peptide charge is required for optimal activity.

In the forth chapter, we present a unified approach to the spontaneous bending of lipid bilayers consisting of neutral and anionic lipids immersed in a salty solution. We show that the spontaneous curvature of a membrane, C_0, can easily be influenced by electrostatic interactions in an ambient salt-dependent way. Interestingly, its sign can be inverted by the presence of a small concentration of divalent cations.

In the last chapter, we present conclusions and propose two potential projects for future considerations. First we propose a semi-analytical approach to membrane-AMP association. Next, we outline the steps required for studying AMP-stabilized pores.

Chapter 2

Electrostatics in Biological Environments

2.1 Poisson-Boltzmann Theory

The electrostatic interactions often play an important role in biological systems. Examples include packing of DNA molecules in the presence of divalent cations [38], curvature deformation of lipid bilayers in response to surrounding ions [79], and selective-activity of antimicrobial peptides (AMPs), the main focus of this thesis. In this chapter, we present a brief introduction to the fundamental theory of electrostatic interactions in electrolytes, as it is mostly the case in biological environments. To do so, we derive the Poisson-Boltzmann (PB) mean-field theory and its linearized version, known as Debye-Hückel (DH) theory.

To begin with, consider a charged molecule in an electrolyte that interacts with the surrounding ions in the solution. Oppositely charged ions, *counterions*, are attracted and *co-ions* are repelled from the charged molecule. This redistribution of counterions is a result of competition between energy and entropy. Energetically,

counterions tend to completely neutralize the molecule. This process, however, is opposed by entropy: ions prefer to move freely in the solution, maximizing the entropy. As the result of this competition, the density of counterions would be high near the charged molecule and decreases at larger distances. In the context of equilibrium statistical mechanics, the PB equation determines the density profile of counterions and co-ions around a charged object in an electrolyte. The PB equation can be derived by combining the Boltzmann distribution with the Poisson equation, which relates the charge distribution to the electrostatic potential. According to the Boltzmann weight, the probability of finding an ion of the ith kind at position $\mathbf{r}$ is exponentially related to the energy of that ion in position $\mathbf{r}$. In the following, we consider only electrostatic interaction. The energy of ion i is given by $Z_i e\psi(\mathbf{r})$, where Z_i is the valence of the ion which includes the sign of the ion, $-e$ the electronic charge, and $\phi(\mathbf{r})$ is the electrostatic potential at $\mathbf{r}$. The density of the ions at $\mathbf{r}$ is related to the probability of finding them at $\mathbf{r}$. Thus, we can write

$$n_i(\mathbf{r}) \propto \exp\left(\frac{-Z_i e\phi(\mathbf{r})}{k_B T}\right). \tag{2.1}$$

where $n_i(\mathbf{r})$ is the density of the ions of the ith kind and $k_B T$ is the thermal energy. On the other hand, in electrostatics, the Poisson equation relates the charge density to the divergence of the electric field as

$$\nabla.\left[\epsilon_0\epsilon(\mathbf{r})\nabla\phi(\mathbf{r})\right] = -4\pi\rho(\mathbf{r}) = -4\pi e\sum_i Z_i n_i(\mathbf{r}), \tag{2.2}$$

where ϵ_0 and $\epsilon(\mathbf{r})$ are, respectively, the electric permittivity of vacuum and the dielectric constant at $\mathbf{r}$, $\rho(\mathbf{r})$ the total charge density at $\mathbf{r}$, and $\sum_i$ is a sum over all existing ions in the solution. Combination of Eqs. 2.1 and 2.2 yields the well-known

Poisson-Boltzmann (PB) equation:

$$\nabla.\left[\epsilon_0\epsilon(\mathbf{r})\nabla\phi(\mathbf{r})\right] = -4\pi e\sum_i Z_i n_i^0 \exp\left(\frac{-Z_i e\phi(\mathbf{r})}{k_B T}\right). \tag{2.3}$$

In this equation, n_i^0 denotes the number density of the ions of the ith kind at infinity (assuming $\lim_{\mathbf{r}\to\infty}\phi(\mathbf{r}) = \mathbf{0}$).

For electrolytes containing only (1:1) salt (e.g., NaCl) Eq. 2.3 can be further simplified. By noting $Z_i = +1$ or -1, and $n_{+1}^0 = n_{-1}^0 = n_0$, for a (1:1) electrolyte with constant electric permittivity, we can rewrite Eq. 2.3 as

$$\nabla^2\Psi(\mathbf{r}) = \frac{-8\pi n_0 e^2}{\epsilon_0\epsilon k_B T}\left[\frac{\exp\left[-\Psi(\mathbf{r})\right] - \exp\left[\Psi(\mathbf{r})\right]}{2}\right] = \kappa^2\sinh\left[\Psi(\mathbf{r})\right], \tag{2.4}$$

where $\Psi(\mathbf{r}) = e\phi(\mathbf{r})/k_B T$ is the *reduced* electrostatic potential and κ^{-1} is the Debye screening length defined by $\kappa^2 = 8\pi n_0 e^2/\epsilon_0\epsilon k_B T$.

2.2 Debye-Hückel Theory

Now we consider the case where particles in the solution are not highly charged, the electric potential is low ($\Psi(\mathbf{r}) \ll 1$). In this case, the PB equation can be expanded to first order of $\Psi(\mathbf{r})$, yielding a linear differential equation for the potential known as the Debye-Hückel (DH) equation. The DH equation for (1:1) electrolyte reads:

$$\nabla^2\Psi(\mathbf{r}) = \kappa^2\Psi(\mathbf{r}). \tag{2.5}$$

The DH potential at distance r from a small spherical charge, q, is given as

$$\phi(r) = \frac{1}{\epsilon_0\epsilon}\frac{q\exp(-\kappa r)}{r}. \tag{2.6}$$

The electric potential decays exponentially (as compared to the long-ranged Coulomb potential) due to the screening effect of the salt ions. The screening length, κ^{-1}, ranges from 10 Å for 100mM NaCl to 1 μm for a pure water with H^+ and OH^- ions.

Note that PB and DH theories rely on the following important assumptions: (*i*) the solvent is considered as a continuum medium, (*ii*) dipole interactions are ignored, (*iii*) effects of finite ion sizes are ignored. It is also worthwhile to note that PB and DH ignore the local fluctuations of the charge densities and are thus called mean-field approaches. These density fluctuations can become important in some specific circumstances as will be discussed in chapter 4 in detail.

Later, we introduce a modified PB approach, which enables us to incorporate finite ion sizes and charge correlations.

Chapter 3

Cationic Antimicrobial Peptides: a Physical Basis for their Selective Membrane-Disrupting Activity

3.1 Introduction[1]

Living organisms can flourish, even in the face of constant challenges of invading microbes such as viruses, fungi, and bacteria. A crucial step in their host defense is to deploy antimicrobial peptides (AMPs), i.e., fast-acting microbicidal molecules with distinct "microbe-greedy" structure [4, 6, 40]. How they *selectively* kill microbes is not clearly understood yet, but their membrane association has long been recognized as an essential step in the microbial killing mechanism [18, 22, 23, 25, 41–43]. Indeed, many cationic peptides (e.g., magainin 2) kill microbes in a "collective" or concentration-dependent manner by their pore-forming activities on the microbial membrane (see Refs. [4, 6] for a comparative view on barrel-stave, carpet, or

[1] A brief version of this chapter including some figures is publihsed as an article in the journal Soft Matter, **6**, 1933- 1940, 2010.

toroidal-pore mechanisms and Refs. [44, 45] for recent reviews on cationic AMPs). Some peptides such as pyrrhocoricin target intracellular components [46]. Nevertheless, these membrane-targeting peptides are of particular interest, since they do not easily induce microbial resistance, which would require the 'costly' work of redesigning lipid membranes [4,18]. Furthermore, they act via a non-specific mechanism, thus killing a wide range of microbial pathogens [4, 6, 18, 40]. What makes AMPs so potent against microbes, without posing a significant threat to their host? Cationic peptides exploit the 'compositional' difference between microbial and host cell membranes [4,6,18,22,40]: the abundance of anionic lipids in the outer layers of the former [see Fig. 3.1]. In contrast, anionic lipids in the host cell membrane mostly face the cytoplasm. Accordingly, peptide *cationic* charge enables the peptides to recognize microbial membranes as their primary target. Indeed, this 'membrane discrimination' is a crucial requirement of cationic AMPs [4, 6, 18, 22, 40, 47].

Understanding the microbial killing mechanism is not only of fundamental interest in biology but also of therapeutic value. The emergence of antibiotic-resistant strains has spurred great effort in searching for new anti-infective agents [3, 44, 45]. Along this line, Nature's chosen antibiotics, i.e., AMPs, especially membrane-active ones, offer promising design principles for developing peptide antibiotics [3, 4, 6, 44, 45]. Even though peptide antibiotics have, so far, demonstrated potency only as topical agents [3, 44, 45], their exceptional quality (fast-killing and broad spectrum) has motivated a great interest in maximizing their potential as anti-infective drugs. While there is extensive experimental evidence of its significance [4,6,18,22,40], a quantitative picture of the physical mechanism that underlies membrane discrimination and disruption is elusive. Our theoretical understanding of how peptide parameters may be optimized for enhanced selectivity, for instance, has remained far behind the experimental advances, despite its potential therapeutic benefit for cost-effective peptide-sequence designs.

The work in this chapter is devoted to developing a unified theoretical ap-

proach to the selective membrane-disrupting activity of cationic AMPs [48] – one which allows us to predict the parameters required for optimal peptide activity under various physiological conditions. The objective is two-fold: we first present a quantitative basis of membrane discrimination, often postulated in the literature [4,6,18,22,40,47]; we then map out a physical picture of membrane disruption by peptide binding, as illustrated in Fig. 3.1. Here, we do not attempt to resolve discrepancies between various models of microbial killing (e.g., different pores and targets) but concentrate on finding general principles that may apply to a broad range of 'amphiphilic' AMPs [18, 22, 23, 25, 41] (see Fig. 3.1). In particular, we calculate the surface coverage of peptides embedded at the lipid headgroup-tail interface and the resulting fractional membrane-area change, $\Delta A/A$, for a wide range of peptide and membrane parameters, where A is the membrane area. Note that $\Delta A/A$ is often described as a good measure of surface activity of AMPs [23,25,42]. Nevertheless its relation with peptide and membrane parameters has yet to be established theoretically.

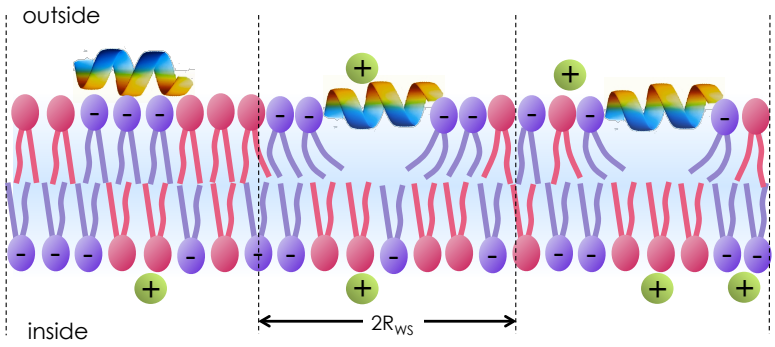

Figure 3.1: Asymmetric incorporation of AMPs into the outer layer of a microbial (cytoplasmic) lipid bilayer membrane. AMPs initially interact with the outer layer through their electrostatic attraction with anionic lipids (see the peptide on the left). Peptides inserted at the headgroup-tail interface (the two in the middle and on the right) stretch and disrupt the membrane. Notice the difference in the orientation of the peptide on the left from two others.

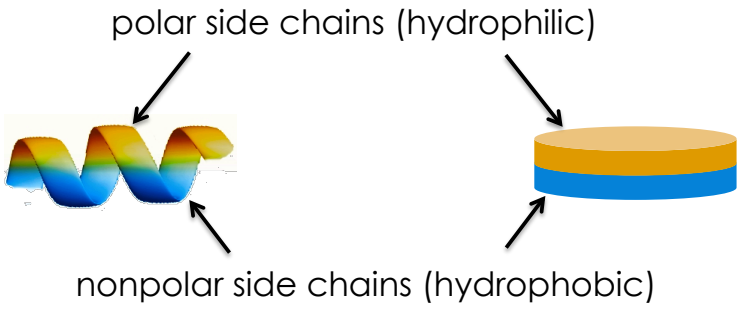

Figure 3.2: A peptide is modeled as a disk. Physical properties of the disk are chosen such that it reflects those of a peptide. One half of the disk (tangerine) has the same charge as the net charge of the peptide and the area of the disk matches the cross sectional area of the peptide.

Our results show that the membrane-perturbing activity of AMPs against microbes is optimized at a certain value of peptide charge ($Q \approx 5$) – larger for a higher salt concentration – such that the viability of the host cell membrane is well preserved, a limit on how one can optimize peptide sequences. We believe this to be the chief attribute of cationic AMPs. This view is consistent with experiments [19, 49] but has been only partially explored theoretically [20]. Importantly, our prediction of reduced optimal activity by ambient salt explains the observation that peptide activity is compromised in a high-salt environment which can result in lethal bacterial colonization [50]. One example is the airway of cystic fibrosis patients that has abnormally high NaCl [50]. Finally, our results imply that cholesterol in the host cell can significantly enhance the selectivity by reducing hemolytic activity, consistent with known results [4, 18].

It is worth noticing that membrane disruption requires concentration 'thresholds' (i.e., minimum peptide concentrations at which peptides are effective against a particular strain of bacteria) [18,22,23,25,41,47]: (i) the minimum inhibitory (bulk) concentration, denoted as 'MIC,' and (ii) the threshold coverage on the membrane surface. The latter is not too far from full membrane coverage, even though the

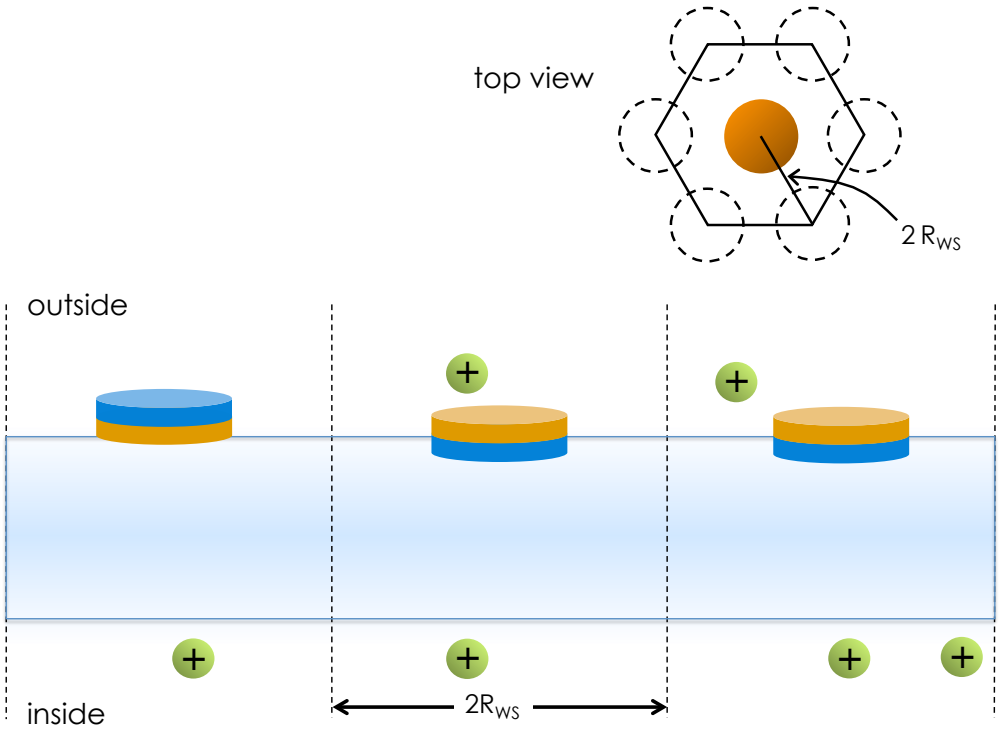

Figure 3.3: The Wigner-Seitz cell (WSC) arrangement of disks. Disks are either adsorbed on the surface (left) or inserted in the headgroup-tail interface (the two on the right). Disks make an hexagonal lattice as illustrated in the top view.

MIC is typically in the low micromolar range [47], contrary to our intuition. Our binding-affinity calculations suggest that for large peptide charge threshold membrane coverage can be reached easily for microbial membranes, but not for the host cell membrane. This is responsible for membrane discrimination.

In the literature, two different experimental approaches have been adopted to study the activity of AMPs: (i) a brute-force approach to cellular damage using biological cells and peptides (see Refs. [4, 6, 19] and references therein) and (ii) a biophysical approach based on the interaction of synthesized peptides with a model membrane, under controlled conditions [19,49]. Our approach is similar, in spirit, to the latter. Recent experiments [19,49] indeed suggest that some peptide parameters

(e.g., peptide charge and hydrophobicity) can be tuned almost independently.

In the next section, we present our model and free-energy analysis of membrane discrimination and disruption, followed by conclusions.

3.2 Theoretical Methods

3.2.1 Molecular model

First, we introduce a simplified model that we believe captures the most important aspects of our peptide-membrane system. One example is the amphiphilic (microbe-greedy) design, i.e., the clustering of polar and hydrophobic groups into distinct structural domains; this enables AMPs to interact simultaneously with lipid heads and tails (see Fig. 3.1), an important structural requirement for membrane disruption [51]. In our approach, the peptide is represented by a circular disk of finite thickness; its amphiphilic design is mimicked by partitioning the disk into two circular halves of the same thickness, represented in two different colors in Fig. 3.2. The polar part (orange) is characterized by its cationic charge, denoted as Q, and dielectric constant of $\epsilon_P = 40$. For simplicity, the peptide charge is assumed to be uniformly distributed over the polar part. Accordingly, our model does not take into account charge discreteness. As a result, neutral polar residues will not contribute to Q. For moderately large or large Q, we believe that the impact of this simplification will be minor. (With a similar spirit, we also ignore charge discreteness of membrane charges, as detailed below.) On the other hand, the hydrophobic part (blue) has a relatively low dielectric constant of $\epsilon_H = 4$ and a high affinity for lipid tails. The high affinity is incorporated in our model though the energy term accounting for bound peptides. One bound AMP, if inserted, releases the energy ϵ_I to the system due to favorable contact between hydrophobic side of the peptide and lipid area of the membrane.

The lipid bilayer, immersed in a salty solution, is considered as a "soft interface." It consists of a mixture of zwitterionic (dipolar) and anionic (e.g., PG) lipids, in the plane of the surface; the mobile charges interact not only with each other but also with the ambient salt ions and AMPs. The charge density of the membrane at position $\mathbf{r}_\perp$ is determined by the fraction of charged lipids, $\alpha(\mathbf{r}_\perp)$, and the headgroup area of lipids in the outer layer, a^{out}, as $-e\alpha(\mathbf{r}_\perp)/a^{out}$, where $-e$ is the electronic charge. While each lipid tends to occupy its preferred area, it can be compressed or swollen by thermal fluctuations and external perturbations, dominantly by peptide binding and electrostatic interactions on the outer layer. Lipids respond to the binding of a charged cationic peptide in two different ways: demixing and compressing. The former refers to the mobility of lipids and the latter refers to their headgroup area flexibility. In absence of peptides, neutral and charged lipids are ideally mixed. That is, the local fraction of charged lipids is constant, $\alpha(\mathbf{r}_\perp) = \bar{\alpha}$. The electric field due to peptide gathers anionic lipids in the vicinity of the peptide. Moreover, flexibility of the headgroups allow lipids to shrink to lower the free energy. In the case of insertion, lipid headgroups compress further to let peptides accommodate among the headgroups. In our model a^{out} refers to the average headgroup area in the outer layer.

Our primary concern is finding the density of peptides in the membrane-perturbing mode (denoted as mode 'I'), i.e., those partially-inserted at the lipid headgroup-tail interface with polar side chains in contact with water and hydrophobic side chains facing the membrane. We also need to consider those "bound" electrically on the membrane surface (mode 'S') illustrated in Fig. 3.3 as they influence the energetics (through mutual repulsion) and thus the density of those in 'I' mode. Peptides in both binding modes "compete" to attract anionic lipids to their vicinities, and we will treat them on equal footing. Because of this competition and peptide-induced membrane stretch, we will determine *simultaneously* peptide binding and lipid rearrangements, since these two feats can depend on one another. Perhaps, this is

the most serious technical challenge, which turns out to be crucial to deal with, but has been only partially accomplished in Ref. [20] as detailed later.

3.2.2 Free energy calculations

Wigner-Seitz Cell

Because of the aforementioned competition in attracting anionic lipids and considering that the lipid membrane is not an *un*limited supply of anionic lipids, and also because of the repulsion between bound peptides (those within the distances shorter than Debye screening length), bound peptides reside at equidistant spots with highest packing fraction. Following Refs. [20, 52], we capture this feature by considering bound peptides as forming a hexagonal lattice on their binding surface, assumed to lie in the x-y plane [54] [Fig. 3.3 and 3.4]. In fact, there is much evidence that AMPs embedded in the headgroup region are dispersed [23], especially when the tails are in the biologically active fluid phase.

On average, each peptide on the lattice experiences a radially-symmetric distribution of other peptides; it thus defines one circular Wigner-Seitz cell (WSC) of radius $R_{\rm WS}$. This model is expected to work fine in two limiting cases: *i*) when the density of bound peptides is high enough so that their lipid-mediated mutual repulsion plays an important role; *ii*) when the density of bound peptides is low enough so that the peptide arrangement on the surface is not a key factor.

The total free energy of one WSC, Fig. 3.4 , excluding the elastic energy cost for insertion, in our approach includes various contributions:

$$
\begin{aligned}
\mathcal{F} &= \frac{\epsilon_0}{2}\int \epsilon_r(\mathbf{r})\left[\nabla\Phi(\mathbf{r})\right]^2 d\mathbf{r} \\
&\quad + k_B T \int \left[n_+ \ln\frac{n_+}{n_0} + n_- \ln\frac{n_-}{n_0} - (n_+ + n_- - 2n_0)\right] d\mathbf{r} \\
&\quad + \frac{k_B T}{a^{out}} \int \left[\alpha \ln\frac{\alpha}{\overline{\alpha}} + (1-\alpha)\ln\frac{1-\alpha}{1-\overline{\alpha}}\right] d\mathbf{r}_\perp \\
&\quad + \frac{\lambda}{a^{out}} \int (\alpha - \overline{\alpha}) d\mathbf{r}_\perp + \varepsilon_I \delta_{Ii}. \qquad (3.1)
\end{aligned}
$$

The meaning of various symbols is as follows: ϵ_0 is the permittivity of free space, $\epsilon(\mathbf{r})$ the dielectric constant at $\mathbf{r}$, Φ the electric potential, k_B the Boltzmann constant, T the temperature, $n_+ = n_+(\mathbf{r})$ [$n_- = n_-(\mathbf{r})$] the density of cationic (anionic) salt ions, n_0 the density of salt ions at $z = \pm\infty$ ($\Phi = 0$ at $z = \pm\infty$), a^{out} the headgroup area of lipids in the outer layer (an average over neutral and anionic lipids), $\alpha = \alpha(\mathbf{r}_\perp)$ the local fraction of charged lipids (with $\overline{\alpha}$ the average fraction), and $\mathbf{r}_\perp = (x, y, z = 0)$. The Lagrange multiplier λ is to ensure the conservation of lipid charges in each WSC [20, 52], and ε_I is the (hydrophobic) free energy gain for insertion (the delta function is to ensure that this term vanishes for electric adsorption, i.e., when $i = S$). Finally, the surface ($\mathbf{r}_\perp$) integrals run over the outer layer within each WSC, while the volume ($\mathbf{r}$) integrals over the entire volume of a WSC, extending to $z = \pm\infty$.

The first term in Eq. 3.1 accounts for the electrostatic energy of a WSC, including contributions from charges both on the surface and in bulk; the second term describes the entropy of salt ions, as influenced by the peptide and anionic lipids in the cell, and the third term takes into account the entropic penalty for the redistribution of charged lipids around a bound peptide (in the absence of peptides, the fraction of charged lipids tends to a constant $\alpha(\mathbf{r}_\perp) = \overline{\alpha}$).

The free energy functional in Eq. 3.1 is to be minimized with respect to a few

functions: $\alpha(\mathbf{r}_\perp)$, $\Phi(\mathbf{r})$, and $n_\pm(\mathbf{r})$. For instance, minimization of Eq. 3.1 with respect to $\Phi(\mathbf{r})$ and $n_\pm(\mathbf{r})$ leads to the well-known Poission-Boltzmann equation:

$$\nabla^2\Psi(\mathbf{r}) = \kappa^2 \sinh\Psi, \tag{3.2}$$

where $\Psi(\mathbf{r}) = e\Phi(\mathbf{r})/k_BT$ is the reduced electric potential and the inverse Debye length, κ, is defined by $\kappa^2 = 2n_0e^2/\epsilon_w\epsilon_0k_BT$, with ϵ_w the dielectric constant of water and ϵ_0 the permittivity of free space. Eq. 3.2 has to be solved together with appropriate boundary conditions (for similar issues, see Refs. [20,52]). On the other hand, minimization of the Eq. 3.1 with respect to $\alpha(\mathbf{r}_\perp)$ results in [20, 52]

$$\alpha(\mathbf{r}_\perp) = \frac{\exp\left[\Psi(\mathbf{r}_\perp) - \lambda\right]}{\dfrac{1-\overline{\alpha}}{\overline{\alpha}} + \exp\left[\Psi(\mathbf{r}_\perp) - \lambda\right]}. \tag{3.3}$$

All the parameters, $\alpha(\mathbf{r}_\perp)$, $\Psi(\mathbf{r})$, and λ, except $\bar{\alpha}$, are to be determined self-consistently and simultaneously.

For a given value of λ and a^{out}, Eq. 3.2 can be solved subject to boundary conditions. There are four types of boundary conditions:

- the normal component of the electric field should vanish on the boundaries perpendicular to the membrane. This condition is to ensure that mutual interactions between peptides are taken into account.

$$\left.\frac{\partial\Phi}{\partial r}\right|_{r=R_{\mathrm{WS}}} = 0 \tag{3.4}$$

  where $r = x^2 + y^2$, the distance form the center of the WS cell.

- the electric potential at infinity, $z = \pm\infty$, vanishes. This also implies that total charge density becomes zero $\lim_{z\to\pm\infty}[n_+(\mathbf{r}) + n_-(\mathbf{r})] = 0$

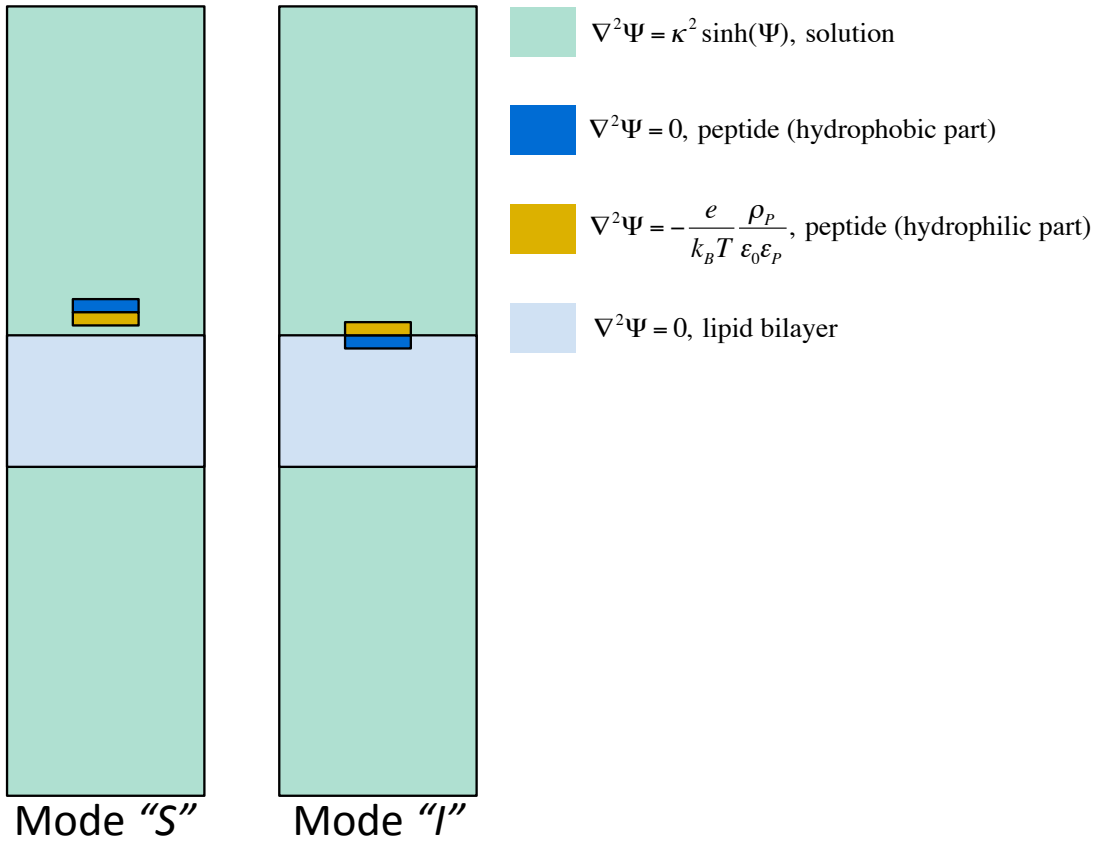

Figure 3.4: Side view of Wigner-Seitz cell containing one surface adsorbed peptide (mode S) and inserted peptide (mode I). Each cell has cylindrical symmetry. Different colors refer to different environments as specified. The electrostatic equation solved in each environment is shown beside the corresponding color. These equations are linked to each other through the boundary conditions. See text for the details of the boundary conditions.

- the electric field is discontinuous on the charged surface of the membrane. The discontinuity reflects the magnitude of the surface charge density:

$$\epsilon_w \epsilon_0 \frac{\partial \Phi}{\partial z}\bigg|_{0^+} - \epsilon_l \epsilon_0 \frac{\partial \Phi}{\partial z}\bigg|_{0^-} = -\frac{e\alpha(\mathbf{r}_\perp)}{a^{out}}. \tag{3.5}$$

- On other boundaries, where there is no net surface charge, the electric poten-

tial is continuous.

The resulting $\Phi(\mathbf{r})$, $\alpha(\mathbf{r}_\perp)$, and thus, the free energy are functions of λ and a^{out}. The Lagrange parameter λ is chosen iteratively based on the Secant method of root finding [53] such that the last second term in Eq. 3.1 vanishes. The procedure is repeated for a wide range of a^{out} to find the a^{out}-dependence of WS cell free energy. The WS cell free energy of Eq. 3.1 will be used to construct the free energy of the membrane and solvent system.

Free energy minimization

To find the equilibrium values of a^{out} and $R_{\rm WS}$ one has to calculate the total free energy of the system including the membrane, bound peptides, solvent, and free peptide (those in bulk). That free energy is based on Eq. 3.1 and comprises a few other important effects, including the entropy of mixing of bound peptides and the elastic energy of the membrane (thus free energy cost for insertion). In our approach, we include lateral deformations of the membrane, but not out-of-plane deformations (see below Eq. 3.6.) The elastic term is then uniquely determined by lipid headgroup areas a^{in} and a^{out}. Because of the bilayer coupling, a^{in} and a^{out} are not independent. This dependence comes from our assumption that for a flat membrane the deformation of the inner/outer layers are such that their total area always match. The total free energy per lipid molecule can be written as

$$\begin{aligned} F \;=\; & \frac{\theta\mathcal{F}_I + (1-\theta)\mathcal{F}_S}{\theta N_I + (1-\theta)N_S} + \left(\gamma a^{in} + \frac{k}{a^{in}}\right) + \left(\gamma a^{out} + \frac{k}{a^{out}}\right) \\ & + k_B T a^{in}\left[\sigma_I \ln\left(\frac{\sigma_I a_p}{c_p v_p}\right) + \sigma_S \ln\left(\frac{\sigma_S a_p}{c_p v_p}\right)\right. \\ & \left. + (\sigma_M - \sigma_I - \sigma_S)\ln\left(1 - \frac{\sigma_S + \sigma_I}{\sigma_M}\right) - (\sigma_M - \sigma_I - \sigma_S)\right]. \end{aligned} \tag{3.6}$$

The meaning of each symbol and term is as follows. The first term in Eq. 3.6 is the WS free energy per lipid molecule, which is averaged over two binding modes. In this term, θ is the fraction of peptides in the membrane-perturbing mode and N_I (N_S) is number of lipids within a WS cell with a peptide at its center in binding mode I (S). The second and third terms are, respectively, the elastic contribution of the inner and outer layer with γ the "unperturbed" interfacial tension (that in absence of electrostatic interactions) [35]; the parameter k is chosen such that the relaxed headgroup area of the lipids is 65 Å in absence of peptide binding. (Note that the area compression modulus of a bilayer is given by $K_A = 4\gamma$.) The last term accounts for the entropy of bound peptides; here σ_I (σ_S) is the planar density of bound peptides in binding mode I (S), a_p the area occupied by a bound peptide, c_p the density of peptides in bulk, v_p is the peptide volume, and σ_M is the total number of sites available to bound peptides per area, i.e., the maximum number of the disks per area on the surface required for full coverage.

In our approach, membrane elasticity influences peptide binding through the second and third terms on the right hand side of Eq. 3.6, which describe the energy cost for in-plane deformations of the membrane induced by peptide binding. In reality, membrane bending can also influence the energetics of peptide binding. However, this is a sub-dominant effect: Bending involves relative deformations of the inner and outer layers, which costs less energy than overall stretching or compression.

Note that not all the parameters $\theta, N_I, N_S, R_{\rm WS}, a^{in}, a^{out}$ are independent. For later convenience, we choose the following parameters as a complete set of independent parameters: $d = 2R_{\rm WS}$, a^{out}, and θ. Others are derivable from these. For instance, N_I (N_S) is considered as a function of d and a^{out}, i.e., $N_S = N_S(d, a^{out}) = \pi d^2/4a^{out}$ and $N_I = N_I(d, a^{out}) = (\pi d^2/4 - a_p)/a^{out}$. Similarly, $a^{in} = a^{in}(d, \theta, a^{out}) = a^{out} + \theta a_p/[\theta N_I + (1-\theta)N_S]$, $\sigma_I = \sigma_I(d, \theta) = 4\theta/\pi d^2$, $\sigma_S = \sigma_S(d, \theta) = 4(1-\theta)/\pi d^2$, and thus $\mathcal{F} = \mathcal{F}(d, a^{out})$. Minimization of the free energy per lipid F in Eq. 3.6

with respect to our preferred parameters, d, a^{out}, and θ, will determine their equilibrium values and thus the equilibrium values of σ_S and σ_I (with σ_I being the key parameter in our approach).

Initially, bound peptides will reside on the outer layer of their target membrane, as illustrated in Fig. 3.1. Some peptides, especially pore-forming peptides, can translocate into the inner layer, and their distribution will be eventually symmetrized between the inner and outer layers (see for example Ref. [17]). We mainly concentrate on analyzing the free energy F in Eq. 3.6 for the initial symmetrical binding. It should be noted that symmetrization is a kinetically-limited process coupled to pore formation [17]. Indeed, experiments with the pore-forming peptide magainin 2 interacting with lipid vesicles suggest how symmetrization and membrane permeabilization are interrelated (with the latter estimated by the efflux of encapsulated fluorescent dyes from the vesicles). Symmetrization lagged somewhat behind membrane permeabilization: in 10 min, about 30% of the total peptide molecules were shown to translocate into the inner leaflets of the vesicles, while about 80% of dyes were released from the vesicles [17]. Since our main focus here is on membrane perturbation prior to rupture (via pore formation, for instance), assymmetric binding merits our significant consideration. After detailing the asymmetrical binding, we comment on how peptide activity is influenced by symmetrization.

In the next section, we analyze our free energy and map out a physical picture of peptide binding.

3.3 Results and Discussion

3.3.1 Wigner-Seitz cell free energy

As the first step, we calculate the free energy of WS cell per lipid molecule inside the cell, F_{WS}/N_i ($i = S$ or I), depicted in Fig. 3.5 as a function of d. As shown in the figure, curves are calculated for the two binding modes, I (left), and, S (right). Different membranes are chosen: slightly charged membrane ($\bar{\alpha} = 0.05$ a typical value for host cell, top figures) and highly charged membranes ($\bar{\alpha} = 0.3$ for bacterial membrane, bottom figures). Recall $\bar{\alpha}$ is the average fraction of anionic lipids. We have chosen $a_p = 314\,\text{Å}^2$, $\epsilon_w = 80$, $\epsilon_l = 2$, $\epsilon_p = 4$, $\kappa^{-1} = 10\,\text{Å}$, $T = 300\,\text{K}$, and $a^{out} = 65\,\text{Å}^2$. Peptide charge, Q is increased from 1 to 10 to show the effect of peptide charge variation. The trend on membrane with $\bar{\alpha} = 0.05$ is not surprising. Free energy per lipid increases by decreasing d implying that smaller WS cell radius is not favorable. This depicts a "repulsion" between peptides while binding to the membrane is not strong. Note that this repulsion is not only from the electrostatic interactions between peptides but also from the entropic cost of the distribution of salt ions around peptides. Larger peptide charge results in stronger repulsion between peptides, and thus, the free energy increases more rapidly. On highly charged membranes with $\bar{\alpha} = 0.3$, the trend is, however, non monotonic. The F_{WS}/N_i has a minimum the location of which increases with respect to d by increasing Q. (For some curves the location is out of the plotted range). As a result, at a given d, variation of peptide charge can force the system to increase d (lower the density of bound peptides) or decrease d (increase the density of bound peptides). This can be found by following the slope of the curves in the Fig. 3.5. This observation seems contradictory to the intuitive expectation that the larger peptide charge would result in stronger binding to highly charged membranes, and thus, trigger more peptides bound to the surface. As will be discussed later in

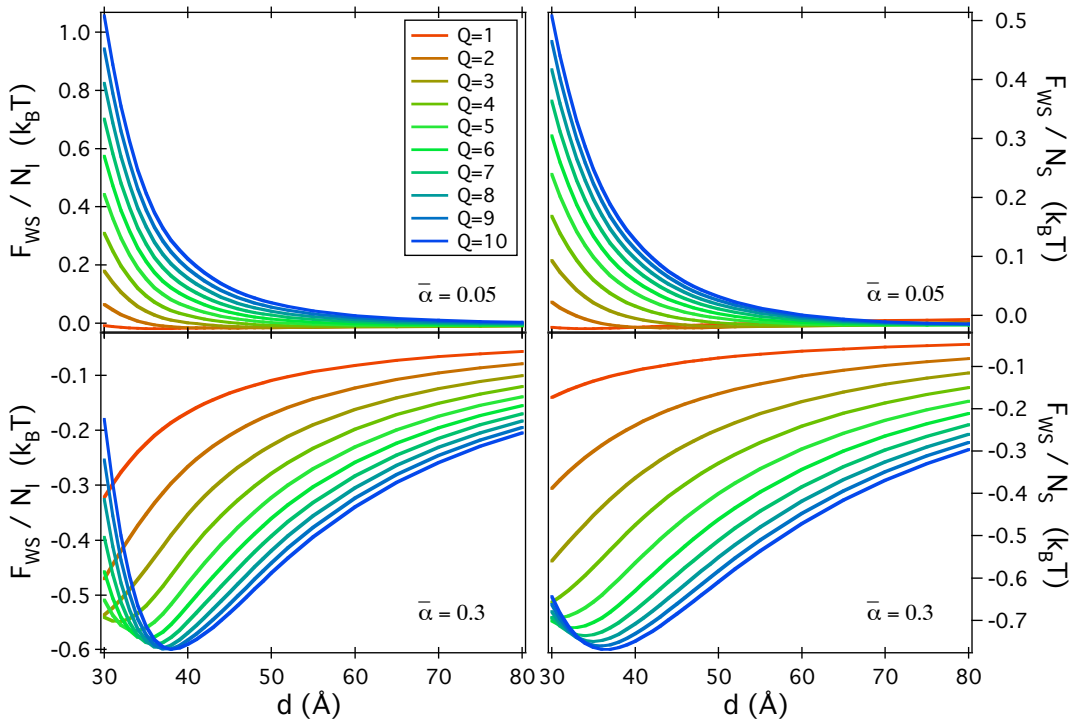

Figure 3.5: Free energy of a Wigner-Seitz Cell per lipid, F_{WS}/N_i ($i = S$ or I), for the two binding modes, I (left), and, S (right), for slightly charged membrane ($\bar{\alpha} = 0.05$, top figures) and highly charged membranes ($\bar{\alpha} = 0.3$, bottom figures). We have chosen $a_p = 314\,\text{Å}^2$, $a^{out} = 65\,\text{Å}^2$, $\epsilon_w = 80$, $\epsilon_l = 2$, $\epsilon_P = 40$, $\epsilon_H = 4$, $\kappa^{-1} = 10\,\text{Å}$, and $T = 300\,\text{K}$. Variation of peptide charge, Q, has non monotonic effect on F_{WS}/N_i depending on fraction of charged lipids, $\bar{\alpha}$ and R_{WS}.

this chapter, this phenomenon will explain an important feature of antimicrobial peptide activity, the optimal charge at which the activity is maximized.

3.3.2 Membrane binding

As an intermediate step, we minimize the free energy per lipid molecule F (Eq. 3.6) with respect to a^{out} for sizable ranges of d and θ (peptide-peptide distance and the fraction of surface-inserted peptides, respectively). Fig. 3.6 displays our result for F calculated at the equilibrium a^{out} for peptide charge $Q = 4$. We have chosen

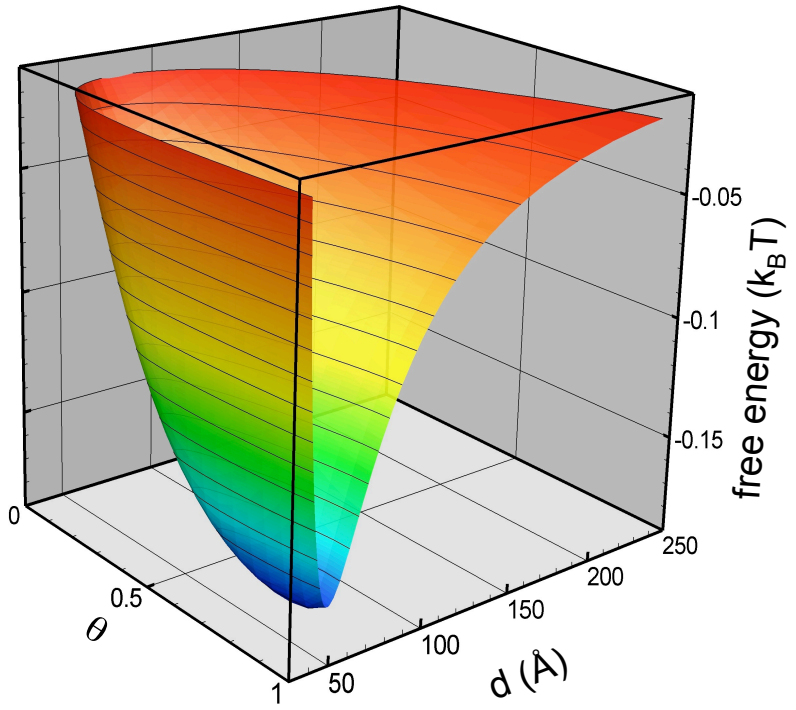

Figure 3.6: Free energy per lipid F (k_BT) as a function of peptide-peptide distance d and the fraction of peptides in the membrane-perturbing mode (mode I), θ, for $\bar{\alpha} = 0.3$ (typical for a bacterial membrane) and peptide charge $Q = 4$. The free energy changes non-monotonically and thus has a well defined minimum.

$\varepsilon_I = -12\,k_BT$ and $a_p = 314\,\text{Å}^2$, typical values for magainin 2 [55], as well as $\bar{\alpha} = 0.3$. Additionally, we have used $c_p = 10\,\mu\text{M}$, $\gamma = 0.14\,k_BT/\text{Å}^2 \approx 60\,\text{mJ/m}^2$ (or $K_A \approx 240\,\text{mJ/m}^2$ [56]), $\epsilon_w = 80$, $\epsilon_l = 2$, $\epsilon_p = 40$, $\epsilon_H = 4$, $\kappa^{-1} = 10\,\text{Å}$, and $T = 300\,\text{K}$. Finally, we allow a gap, chosen to be 3 Å, between the charged face of the peptide and the membrane surface for peptides in the state "S" (those adsorbed on the surface) as shown in Fig. 3.4. (Unless otherwise stated, we use these parameters throughout this chapter.)

As shown in the figure, the free energy changes non-monotonically with d and θ. As a result, there is a well-defined free energy minimum at a certain value of (d, θ) or (σ_S, σ_I). Obviously, the negativeness of the minimum indicates favorable

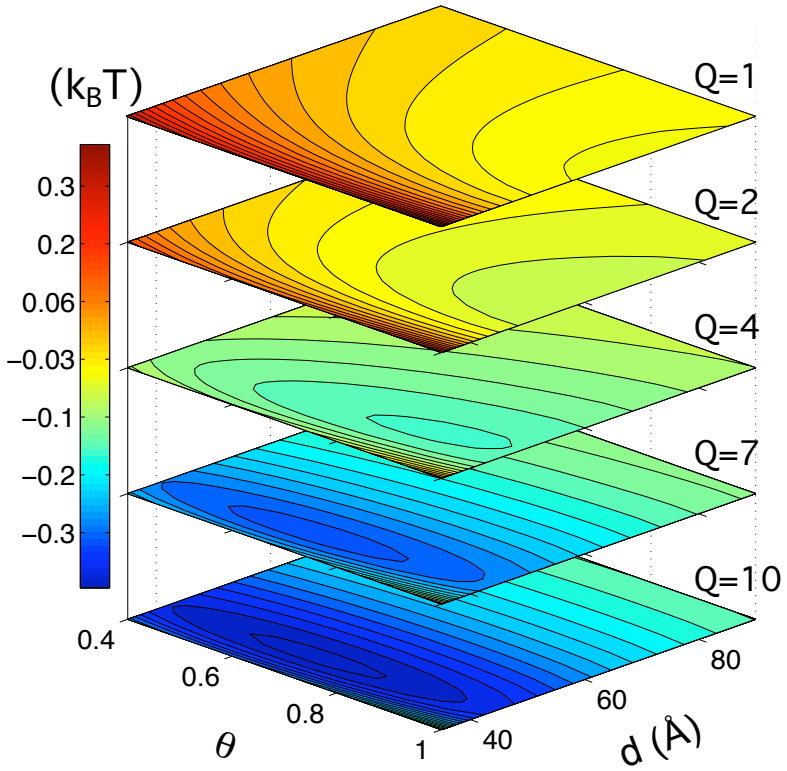

Figure 3.7: Contour-plot representation of F for various choices of peptide charge Q, showing how the location of the free energy minimum, $(d_{\min}, \theta_{\min})$, evolves as Q increases.

interactions of a peptide with an oppositely-charged membrane.

The non-monotonicity deserves some discussion. It can be understood in terms of the interplay between a few distinct effects, which we group into three subgroups:

(a) the entropic effect associated with lipid demixing, the confinement entropy of ions "trapped" around the membrane surface, the elastic energy cost for insertion, and the translational entropy of bound peptides,

(b) the hydrophobic attraction of an interfacially-inserted peptide as described by ε_I,

(c) the electrostatic interactions between a peptide and anionic lipids, (as influenced by surrounding salt ions, lipid demixing, and other bound peptides).

Those in (a) prefer large d – repulsive, while those in (b) favor small d – attractive. The competition between the two is partly responsible for the non-monotonicity. The electrostatic effect in (c) shows more complicated dependence on d. It is not hard to understand why this effect changes non-monotonically with d. We can explain that by analogy with a much simpler case of two uniformly-charged parallel surfaces a distance h apart, with charge densities σ_+ and σ_-, respectively (see Fig. 3.8). The physics of this system has been well studied in the literature [57, 58]. For $|\sigma_+| = |\sigma_-|$, the two surfaces are always attractive (independently of h). There are two driving force for this attraction: (i) Coulomb interactions, (ii) Favorable entropic free energy gain due to release of counterions. Counterintuitively, the latter is dominant [57, 58]. If $|\sigma_+| \neq |\sigma_-|$, however, residual counterions trapped between the plates resist confinement, turning the attraction into a repulsion at short separations, as illustrated in Fig. 3.8 [58] (the residual counterions are to neutralize the excess backbone charges).

Comparison of the peptide-lipid bilayer system with the two plate system is complicated by lipid mixing-demixing. Assuming that a peptide carries a surface charge density of σ_+, the surface charge density of the membrane interacting with this peptide, σ_-, is not a constant, owing to the mobility of anionic lipids. At the expense of their entropy, anionic lipids in the outer layer tend to accumulate around an oppositely charged object (e.g., a cationic AMP), when the peptide carries a higher charge density than the outer layer. This enhances the attraction between the peptide and the lipids. (The opposite would be expected for small peptide charge Q. This means the peptide is repelled eventually; counterions from salts preferentially reside near the outer layer.) How does it explain the d-dependence of the free energy depicted in Fig. 3.5? For large d, a single-peptide picture is expected

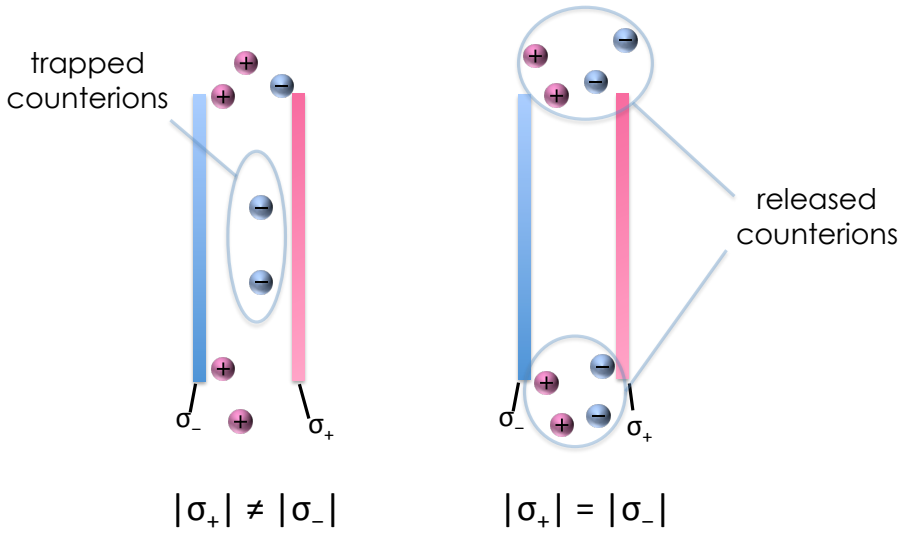

Figure 3.8: Counterions are released when two oppositely charged membrane, $|\sigma_+| = |\sigma_-|$ approach each other. The interaction is always attractive regardless of the distance between membranes. If $|\sigma_+| \neq |\sigma_-|$, however, residual counterions trapped between the membranes will turn attraction into repulsion at short separations.

to work (one peptide interacting with an infinitely large membrane); anionic lipids can adjust such that charges are matched ($|\sigma_+| = |\sigma_-|$) and the total electrostatic free energy varies roughly linearly with the peptide density. As d decreases, however, the number of "available" anionic lipids for subsequent binding also decreases – there is a 'competition' between bound peptides to recruit anionic lipids recalling that the lipid bilayer is not an *un*limited source of anionic lipids (see Ref. [52] for relevant discussion in a somewhat different context). This situation is analogous to the aforementioned repulsive parallel plates ($|\sigma_+| > |\sigma_-|$) at short separations. This also explains how many-body effects arise in this system, which turn the attraction into a repulsion at high densities of bound peptides. Accordingly, the electrostatic free energy changes non-monotonically with d. In the next section, we investigate the effect of peptide charge variation on binding.

3.3.3 Variation of peptide charge

The observed non-monotonicity as a function of d in Fig. 3.6 is a combined effect arising from both electrostatic many-body effects and the balance of two opposing effects in (a) and (b). Fig. 3.7 depicts that the location of the free energy energy minimum changes non-monotonically; it decreases with d for Q up to $\hat{Q} \approx 5$ and increases beyond $\hat{Q}$. At the single-peptide level, the attraction is stronger for large Q; for too large Q, however, the many-body effect diminishes the binding affinity. For a reason evidenced later, $\hat{Q}$ is designated as an "optimal charge." This can be also explained using the analogy we had in the previous subsection. Large Q requires a large number of anionic lipids to ensure the $|\sigma_+| = |\sigma_-|$ condition. While there is a limited number of anionic lipids available on the membrane, for too large Q the density of bound peptides should decrease (d should increase).

A key parameter in our model is σ_I, the surface density on interfacially-inserted peptides. This parameter is determined by d, the peptide-peptide distance, and θ, the fraction of peptides in the membrane-disturbing mode. More insight about the effect of the peptide charge can be gained by considering the free energy as a function of θ [see Fig. 3.6]. The non-monotonic dependence of F on θ can also be understood: binding mode 'S' is favored by the mechanical energy and the electrostatic interactions, while binding mode 'I' is favored by the hydrophobic attraction (insertion reduces the overall backbone charge density and is electrostatically disfavored). When the two sets of competing effects are comparable, one may expect $\theta \approx 1/2$. Obviously, the electrostatic effect is more pronounced for larger Q, thus increasing Q tilts this balance toward smaller θ. Indeed this expectation is consistent with Fig. 3.7, which vividly shows how the equilibrium θ (d) evolves as Q increases; it decreases monotonically from ≈ 1 to ≈ 0, as Q varies from 1 to 10.

A parameter of physical interest is the molar ratio of peptides in binding mode I to lipids, denoted as P_I/L [20, 23, 25] – membrane coverage in the membrane-

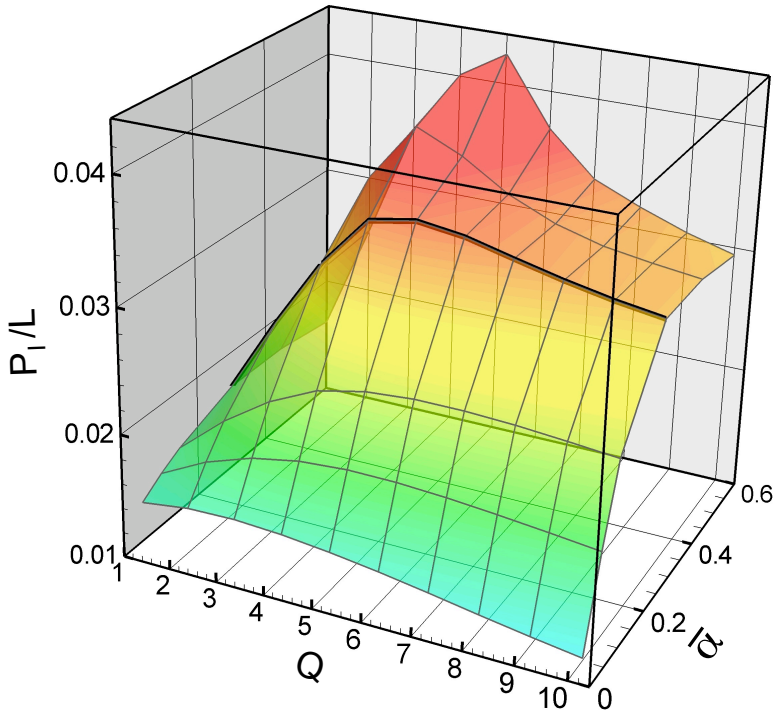

Figure 3.9: Molar ratio of membrane-perturbing peptides to lipids P_I/L, a key parameter that determines the membrane-disrupting activity of peptides, as a function of Q. For $\bar{\alpha} \gtrsim 0.3$, P_I/L has a well-defined peak at a certain value of Q, $\hat{Q} \approx$ 4-5. The existence of an optimal charge $\hat{Q}$ is one of the main attributes of cationic AMPs. (See the text for our choices of parameters not specified in the figures.)

disturbing mode. Fig. 3.9 displays P_I/L, as a function of Q and α. Except for Q and α, we have chosen the same parameters used for Fig. 3.6(a)(b): $\varepsilon_I = -12\, k_B T$, $a_p = 314\,\text{Å}^2$, $c_p = 10\,\mu$M, $\gamma = 0.14\, k_B T/\text{Å}^2$, $\epsilon_w = 80$, $\epsilon_l = 2$, $\epsilon_p = 40$, $\epsilon_H = 4$, $\kappa^{-1} = 10\,\text{Å}$, $T = 300\,\text{K}$, and the peptide-membrane gap chosen to be 3 Å.

As shown in the figure, P_I/L for highly charged surfaces ($\bar{\alpha} \gtrsim 0.2$) changes non-monotonically with increasing Q with its peak at the optimal charge $\hat{Q} \approx 5$ for $\kappa^{-1} = 10\,\text{Å}$. [Recall the parameter R_{WS} can be eliminated in favor of P_I/L.] On the other hand, the curve for the host cells ($\bar{\alpha} \approx 0$) is less sensitive to Q and is almost monotonic. Importantly, P_I/L increases rapidly with $\bar{\alpha}$, especially

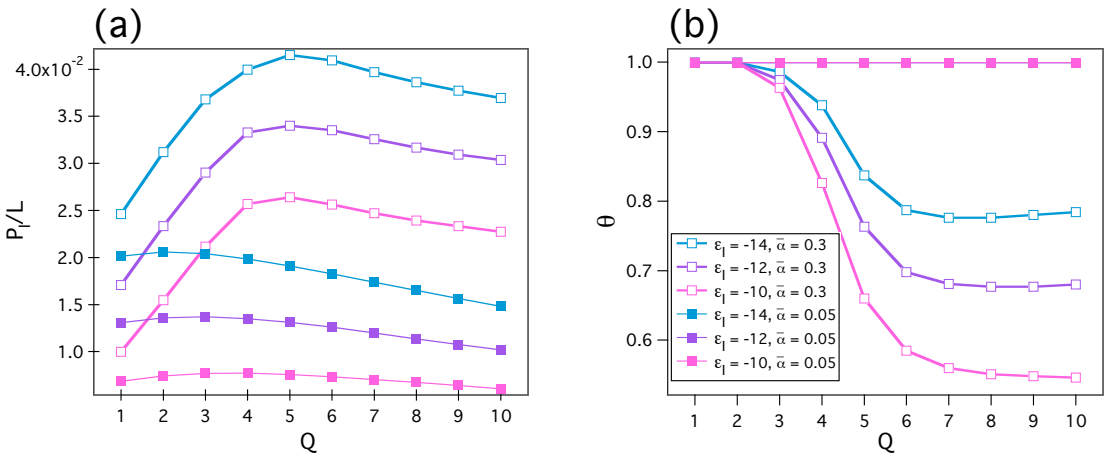

Figure 3.10: (a)P_I/L as a function of peptide charge, Q. Increasing hydrophobicity, $|\varepsilon_I|$, increases P_I/L for both host cells ($\bar{\alpha} = 0.05$, thin lines with filled square) and microbial membranes ($\bar{\alpha} = 0.3$, thick lines with unfilled square). (b) θ as a function of peptide charge, Q. $\theta \approx 1$ for $\bar{\alpha} = 0.05$. Larger $|\varepsilon_I|$ pushes θ to higher values by making insertion mode, I, more energy favorable.

for $Q \approx \hat{Q}$. This is the physical basis of selectivity, as elaborated in the next subsection. It is gratifying to note that the experimentally observed threshold coverage $(P/L)^* \approx 1/30$ for magainin 2 [41] can be reached for microbial membranes if $Q \gtrsim \hat{Q}$, but not for the host cell membrane, as clearly indicated in Fig. 3.6(c).

3.3.4 Effect of peptide hydrophobicity

A main driving force for the insertion of the peptides is hydrophobic energy gain quantified as ε_I in our model. The hydrophobicity of peptides varies depending on the amino acids in their sequence. Unlike electrostatic driven interactions, hydrophobicity has not been proven to discriminate between host cells and bacterial cells. Fig. 3.10(a) depicts P_I/L as a function of Q, for a few different choices of ε_I. Parameters chosen in Fig. 3.10 are similar to those in Fig. 3.5, except for Q, $\bar{\alpha}$, and ε_I, as specified. Not surprisingly, P_I/L increases rather uniformly with increas-

ing $|\varepsilon_I|$. The trend is almost the same for host cell and bacterial cell membranes. This suggest that, despite of the strong antimicrobial activity, peptides with too strong hydrophobicity may not be suitable for therapeutic development due to high hemolytic activity. Fig. 3.10(b) depicts θ, the fraction of inserted peptides (those in state "I"), as a function of Q. For membranes with $\bar{\alpha} = 0.05$, for a wide range of Q and ε_I we can see $\theta \approx 1$, while P_I/L is relatively small. This arises from the fact that binding on weakly charged membranes is solely driven by hydrophobicity of the peptides, and hydrophobically driven binding keeps peptides in state "I". While the surface binding is not favored with $\bar{\alpha} = 0.05$, θ becomes close to 1 regardless of Q and ε_I. For highly charged membranes with $\bar{\alpha} = 0.3$, θ decreases from 1 to smaller values as discussed before. Larger hydrophobicity, $|\varepsilon_I|$ keeps more peptides in the insertion mode, "I" and pushes the curve to the larger values of θ .

3.3.5 Dependence on bulk peptide concentration

Concentration of peptides in the solution, or bulk peptide concentration, affects the density of bound peptides, and thus P_I/L, through the entropic term in Eq. 3.6. Dependence of P_I/L on bulk peptide concentration is of importance in designing peptides for therapeutic purposes. At a given bulk concentration, the viability of host cells has to be conserved while surface coverage on bacterial membranes is disruptive. Fig. 3.11 depicts the P_I/L as a function of bulk peptide concentration, c_p, for a few values of peptide charge, Q, as specified in the legend. Not surprisingly, P_I/L is higher for higher bulk peptide concentration. For large c_p, P_I/L reaches a saturation value. The higher Q, the faster P_I/L gets saturated. Consistent with previous observations, the saturation value of P_I/L becomes smaller beyond peptide charges ~ 5.

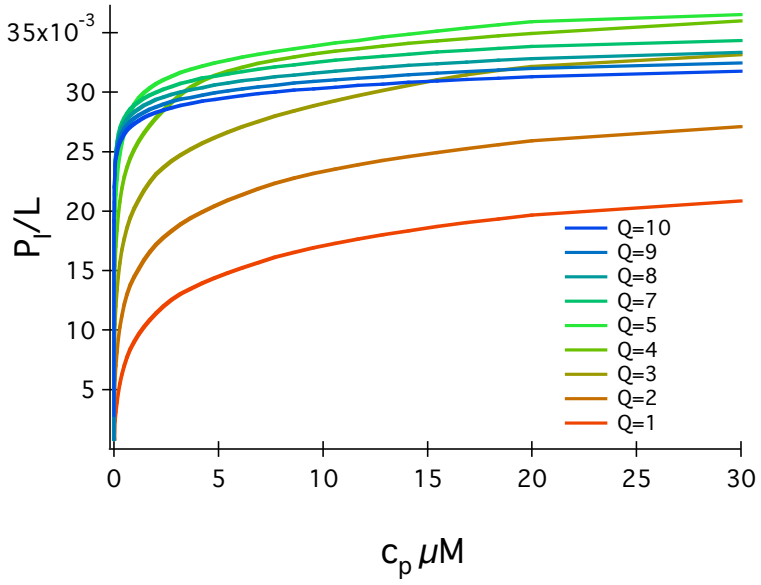

Figure 3.11: P_I/L as a function of bulk peptide concentration, c_p, for different values of peptide charge, Q. P_I/L is saturated for large c_p. The saturation value is lower for peptides with charges beyond $Q \sim 5$.

3.3.6 Membrane disruption

How can peptide binding increase the permeability of a membrane, eventually causing the membrane to rupture via pore formation? To assess quantitatively the fate of such a membrane, we have first calculated the overall fractional area stretch, $\Delta A/A$, induced by peptide binding (see Fig. 3.12); except those described in the legend, the same parameters were used. When the electrostatic compression of lipids is negligible or for small Q (i.e., a_l = constant), there is a simple linear relationship between $\Delta A/A$ and P_I/L (dotted lines), as indicated in Fig. 3.12. For this reason, the optimal charge is the same for P_I/L and $\Delta A/A$. The deviation between the two for large Q ($Q \gtrsim \hat{Q}$) can be attributed to the electrostatic compression of lipids, which is more pronounced for larger Q. As Q increases from 1, $\Delta A/A$ increases rapidly from a small value and reaches its peak at $\hat{Q}$,

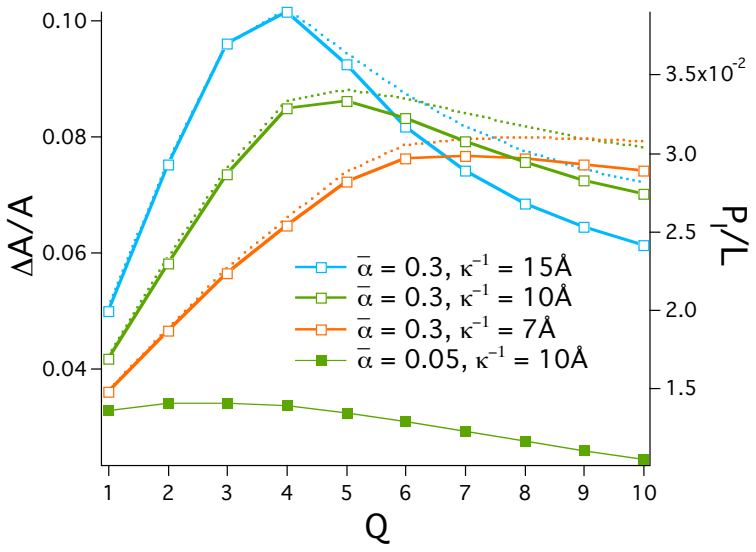

Figure 3.12: Fractional area stretch, $\Delta A/A$, along with P_I/L (dotted lines) as a function of peptide charge Q, for a few choices of κ^{-1}, $\overline{\alpha}$ and γ. See the text for our choices of parameters not specified on the figures. Notice that $\Delta A/A$ changes non-monotonially with Q, which is a direct consequence of the non-monotonicity observed in the P_I/L-Q relationship in Fig. 3.9. As a result, $\Delta A/A$ is maximized at a certain value of Q, i.e., $\hat{Q}$, such that $\hat{Q}$ is larger for a smaller value of κ^{-1}, because of enhanced screening.

in a κ-dependent way. Note this is a crucial attribute of AMPs, which was only crudely captured in Ref. [20], where the overall membrane area was assumed to remain constant upon peptide insertion. This inevitably underestimated the ratio $\left[(P_I/L)_{Q\approx\hat{Q}} - (P_I/L)_{Q\approx 1}\right]/\left(P_I/L\right)_{Q\approx 1}$, which can be viewed as a rough measure of optimal membrane discrimination, resulting in somewhat unrealistic optimal discrimination.

The κ-dependence of $\hat{Q}$ is intriguing: $\hat{Q} \simeq 5$ for $\kappa^{-1} = 10\,\text{Å}$, but $\hat{Q}$ is larger for smaller κ^{-1}. The many-body effect is weaker for smaller κ^{-1}, and thus a "single-peptide picture" (i.e., increasing binding affinity with Q) is expected to work better, resulting in a larger $\hat{Q}$. What are the biological implications of $\hat{Q}$? Interestingly, the majority of AMPs carry a net charge of $Q = 4$-6 [49]. Our results in Fig. 3.12

seem to provide quantitative hints on how AMPs might have evolved to optimize their activity. Diminished membrane perturbation at higher salt concentrations (for $Q \approx$ 4-6) is consistent with known results [4, 40, 50], especially the observation of peptide inactivation in a high-salt environment (e.g., the airway of cystic fibrosis patients), leading to lethal bacterial colonization [50]. Intriguingly, peptide activity in that case can be restored at least partly by increasing the charge. This may offer a strategy for designing a potent peptide antibiotic that remains active in such an unusual environment.

3.3.7 Spontaneous pore formation

Peptide binding will result in membrane disruption likely via pore formation, beyond a certain value of P_I/L, i.e., $(P_I/L)^*$ [18, 22, 23, 25, 41, 47]. In reality, each pore formed this way will be stabilized by a few peptides associated with the pore. This implies that $(P_I/L)^*$ depends on the type of peptide and lipid as well as on lipid arrangements around the pore. The precise mechanism of pore formation will likely be influenced by microscopic details such as chain length and packing shape, which are not taken into account here. Not surprisingly, the available data for $(P_I/L)^*$ have not been fully integrated with binding models [23, 47]. Moreover, pore formation is a kinetic process. Our consideration is limited to transient lipid pores as intermediates, for which molecular details play less significant roles. To utilize this idea, we have mapped peptide binding onto an equivalent external tension τ, i.e., the tension it would take to have the same effect on $\Delta A/A$, following $\tau = K_A \times \Delta A/A$ (see the illustration in Fig. 3.14). A pore can form and grow in a membrane, if stretched. Assuming a circular pore of radius $R_{\rm pore}$, the pore free energy can be expressed as $F_{\rm pore} = 2\pi R_{\rm pore}\lambda - \pi R_{\rm pore}^2\tau$, where λ is the line tension, i.e., the free energy cost for creating a pore per length. Fig. 3.13 depicts the free energy of spontaneous pore as a function of pore radius, $E_{\rm pore}$ for a few different

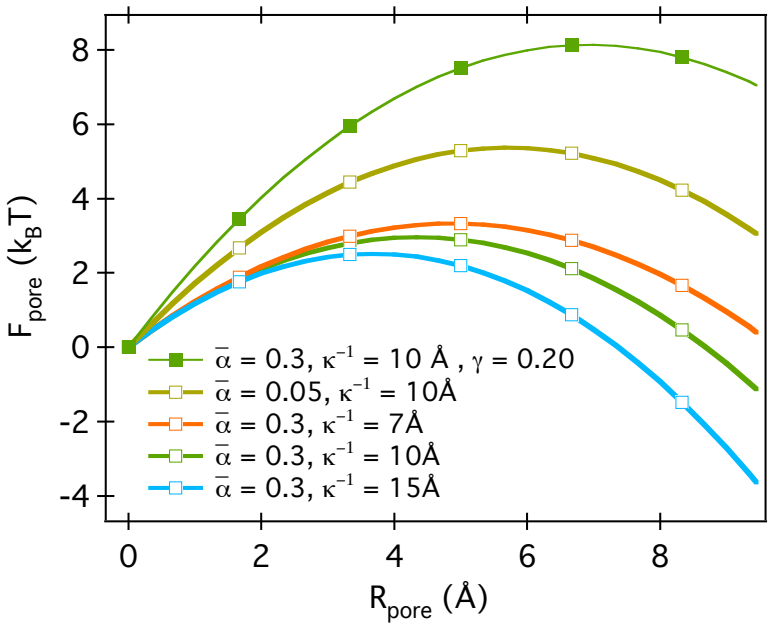

Figure 3.13: Energy of a spontaneous pore as a function of the radius of the pore for different values of $\overline{\alpha}$, κ^{-1}, and γ as specified in the figure.

values of $\bar{\alpha}$, κ, and γ. Parameters in Fig. 3.13 are similar to those in Fig. 3.12 unless otherwise specified. Peptide charge, Q, for each curve is chosen to be the optimal charge. F_{pore} as a function of R_{pore} is an inverted parabola with zero at the origin. It has a maximum at $R_{\rm pore} = R^*$ beyond which $F_{\rm pore}$ drops rapidly – there is a barrier to pore growth. The activation energy or the barrier height is then given by $\Delta F^*_{\rm pore} = \pi\lambda^2/\tau$.

Fig. 3.12 shows our results for $\Delta F^*_{\rm pore}$; we have chosen the same parameters used for Fig. 3.13 as well as $\lambda = 0.22 k_B T/\mathring{A}^2$, a typical value of λ (see ref. [35], for instance), unless otherwise stated in the legend. For $\bar{\alpha} = 0.05$ (host), $\Delta F^*_{\rm pore} \approx 10\, k_B T$, meaning that the "barrier crossing" is improbable. When $\bar{\alpha} = 0.3$ (microbe), the activation energy can be as small as 2-3 $k_B T$ for large Q ($Q \approx \hat{Q}$); for small Q, however, pore growth is kinetically disfavored. The results are informative and consistent with the large-charge requirement for antimicrobial activity/selec-

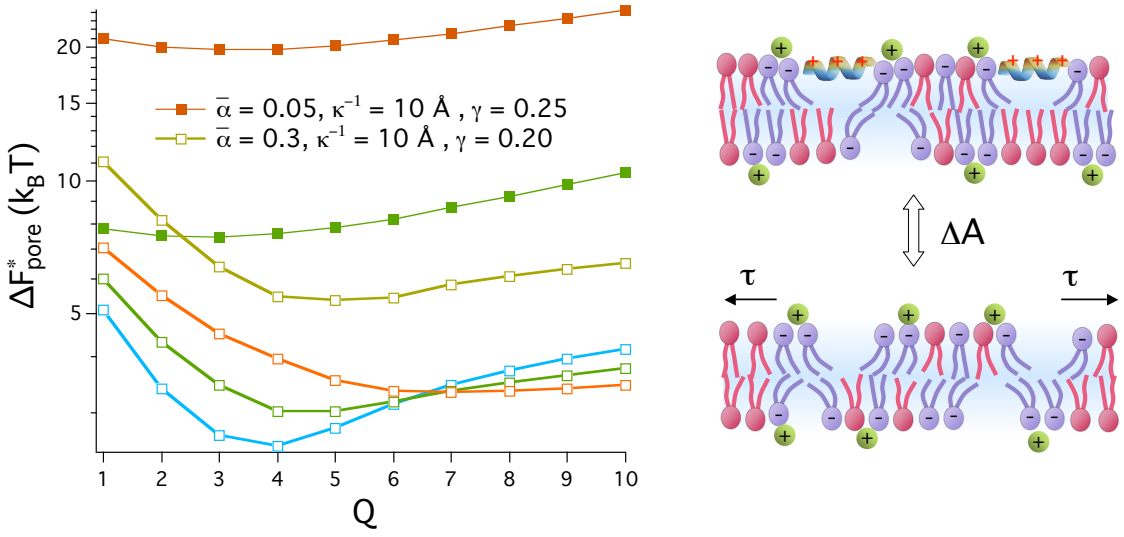

Figure 3.14: The activation free energy for lipid-pore formation, $\Delta F^*_{\rm pore}$, as a function of peptide charge Q, for a few choices of κ^{-1}, $\overline{\alpha}$ and γ. The color scheme is the same as Fig. 3.12 except for the two curves described in the legend. (See the text for our choices of parameters not specified on the figures.) To obtain $\Delta F^*_{\rm pore}$, we have mapped ΔA onto an equivalent tension (τ)-induced stretch (see the inset illustration). For the host cell membrane ($\bar{\alpha} = 0.05$), $\Delta F^*_{\rm pore}$ is too large, but for a microbial membrane ($\bar{\alpha} = 0.3$), $\Delta F^*_{\rm pore}$ is as low as 2-3k_BT for $Q \approx \hat{Q}$.

tivity long observed in experiments [4, 6, 18, 19, 40].

Beside peptide parameters (e.g., Q and ε_I), membrane parameters are also linked to antimicrobial selectivity. For instance, cholesterol found in the host cell membrane is shown to enhance the selectivity by diminishing hemolytic activity [4, 18]. In fact, cholesterol changes K_A (or γ) – K_A increases with increasing content of cholesterol [35, 59]. Fig. 3.12 also shows $F^*_{\rm pore}$ for a different choice of γ: $\gamma = 0.25\, k_BT/\text{Å}$. This roughly corresponds to a lipid bilayer enriched with 40 mol % of cholesterol as in the host cell membrane [35, 59]. In constructing this curve, we have used a linear relationship between γ and λ: $\lambda \sim \gamma$. This is obvious for a hydrophobic pore, since both quantities share the same physical origin, and can be shown to hold for a hydrophilic pore as well [35]. The effect of cholesterol (through

change of γ) is dramatic. The barrier height is doubled, meaning much reduced hemolytic activity and thus much enhanced selectivity. But $\hat{Q}$ remains unchanged, which coincides with the Q value at which $F^*_{\rm pore}$ is minimized. For a similar reason, $\hat{Q}$ will not be influenced by the way peptides are partitioned between the inner and outer layers. We show that $\Delta A/A$ (thus $\hat{Q}$) remains roughly the same for the asymmetric and symmetric cases (data not shown).

What are the implications of our results in Fig. 3.9 and Fig. 3.12 for microbe's strategies to acquire resistance to AMPs, by reducing their surface charge or membrane fluidity (thus redesigning their membrane)? In fact, they illustrate the level of difficulty in doing so. For instance, γ has to increase to $\approx 0.2\, k_BT/\text{Å}^2$ (from $0.14\, k_BT/\text{Å}^2$) to reduce AMP activity against microbes to the level somewhat comparable to that against the host, as indicated in Fig. 3.12 (see the thick curve in light green).

3.4 Conclusions

In conclusion, the theoretical mechanism of electrostatic discrimination and membrane perturbation by cationic AMPs presented here aligns well with the general view of the peptide as an effective and discriminative disrupter of microbial membranes [4, 6, 18, 22, 23, 25, 40]. In this chapter, we have developed a theoretical model that integrates a few distinct and pronounced interactions of AMPs with lipid bilayers. Our results, while reproducing some known and important features of antimicrobial activity, shed light on how peptide parameters can be adjusted (in a membrane and solvent dependent way) to optimize AMP's selective activity.

We have shown how AMPs discriminate microbial membranes from host cell membranes utilizing the structural difference in the composition of anionic and zwitterionic phospholipids on their outer layer. We have shown the optimal charge

$\hat{Q}$ ($\approx$ 5 for $\kappa = 10$ Å) is an overall constraint in optimizing peptide sequences for therapeutic purposes, consistent with and shedding quantitative insights into relevant experiments [19, 49, 60]. Also, our prediction of salt dependence of $\hat{Q}$ suggests how experimental settings may have to be chosen to best mimic the (target-site dependent) physiological condition. An interesting biological implication is that this finding will be especially useful for designing peptide antibiotics, which will remain active in a high-salt environment (e.g., the cystic fibrosis lung) and can thus combat pathogens causing related disease [50]. In this work, we have elaborated on membrane disruption activity of AMPs by linking insertion (P_I/L) to relative area stretch ($\Delta A/A$). Likelihood of formation of spontaneous pores are found by considering the energy barrier for the growth of the pore. The membrane parameters prove to play important role where presence of cholesterol (in host cell) doubles the energy barrier.

Despite this success, other biological details are not to be overlooked. For instance, charge distributions on the polar face of AMPs can influence their activity [60], even though this is less significant than net charge Q, especially for large Q [49]. Also self-association of AMPs in the aqueous phase reduces their surface activity [60], since dimers have less favorable structure for membrane insertion. Lipid packing shapes as well as discrete membrane charges can play some role. Additionally, a more complete picture requires explicit consideration of pore-stabilizing AMPs (see the subsection, Membrane Disruption); our approach can then be extended to the analysis of peptide therapeutic index [60], which in turn may benefit our endeavor in finding better peptide antibiotics. Our coarse-grained approach presented here will be an essential step toward this effort.

3.5 COMSOL scripts

3.5.1 Wigner-seitz cell free energy

The following code calculates a Wigner-Seitz cell free energy with one inserted peptides.

```
flclear 'all'

for epsl = [2]
 for alb = [0.3 ]
  for a2 = [30 40 45 50 52.5 55 57.5 60 62.5 65 67.5 70]
   for Rws = [140 100 80 70 60 55 50 45 40 35 32.5 30 25 27.5 22.5 20 17.5 15]
    for Q=1:10

        %fprintf('\n         Q = %d, Rws = %d \n', Q, IRws);
        %Constants
        smalld = 1;
        Pt = 8;
        Rp = 10;
        Lth = 40;
        kappa = 1/10;
        epsilon = 0.1794422079e-2;
        lB = 1/(80*epsilon);
        coe1 = -2.6; coe2 = -1.0;
        rough_sol = 0; fine_sol = 0;
        a0 = 65;
        clear fem;
        clear fem_f;
        clear fem_c;
        rough_sol = 0; fine_sol = 0;



        % FEM Constants
        fem.const.Q = Q;
        fem.const.Pt = Pt;
        fem.const.alb = alb;
        fem.const.lB = lB;
        fem.const.epsl = epsl;
        fem.const.kappa = kappa;
        fem.const.Rp = Rp;
        fem.const.coe = coe1;
        fem.const.Rws = Rws;
        fem.const.Lth = Lth;
        fem.const.n0 = 'kappa^2/lB/8/pi';
        fem.const.a0 = a0;
        fem.const.a2 = a2;
        fem.const.Nl =  pi*(Rws^2-Rp^2)/a2;

        % Geometry
        g1=rect2(Rws,10/kappa,'base','corner','pos',[0,0]);
        g2=rect2(Rws,Lth,'base','corner','pos',[0,-Lth]);
        g3=rect2(Rws,10/kappa,'base','corner','pos',[0,-Lth-10/kappa]);
        carr = { curve2([0,0],[Pt/2,0],[1,1]), curve2([0,Rp],[0,0],[1,1]), curve2
([Rp, Rp], [0, Pt/2],[1, 1]), curve2([Rp, 0], [Pt/2, Pt/2],[1, 1]) };
        g4=geomcoerce('solid',carr);
        carr = { curve2([0,0],[-Pt/2,0],[1,1]), curve2([0,Rp],[0,0],[1,1]), curve2
([Rp, Rp], [0, -Pt/2],[1, 1]), curve2([Rp, 0], [-Pt/2, -Pt/2],[1, 1]) };
        g5=geomcoerce('solid',carr);

        g1 = g1 - g4;
```

```
        g2 = g2 - g5;

        % Geometry objects
        clear s
        s.objs={g1, g2, g3, g4, g5 };
        s.name={'Water_top', 'Lipids', 'Water_bottom', 'Peptide_top', '
Peptide_bottom'};
        s.tags={'g1', 'g2', 'g3', 'g4', 'g5'};

        fem.draw=struct('s',s);
        fem.geom=geomcsg(fem);

        % (Default values are not included)

        % Application mode 1
        clear appl
        appl.mode.class = 'Electrostatics';
        appl.mode.type = 'axi';
        appl.border = 'on';
        appl.assignsuffix = '_es';
        clear bnd
        bnd.rhos = {0,0,0,'-4*pi*al/a2',0};
        bnd.type = {'V0','cont','ax','r','D'};
        bnd.name = {'Ground','Cont. Bound.','r Axis','Negative Layer','Cell Wall
'};
        bnd.ind = [3,1,3,2,3,2,3,2,3,2,1,2,2,4,5,5,5];
        appl.bnd = bnd;
        clear equ
        equ.epsilonr = {80,epsl,2,40};
        equ.rho = {'-kappa^2/lB*sinh(V)',0,'4*Q/(Rp*Rp*Pt)*0','8*Q/(Rp*Rp*Pt)'};
        equ.name = {'Water','Lipid','Peptide_bottom','Peptide_top'};
        equ.ind = [1,2,3,4,1];
        appl.equ = equ;
        appl.var = {'epsilon0','0.1794422079e-2'};
        fem.appl{1} = appl;
        fem.sdim = {'r','z'};
        fem.frame = {'ref'};
        fem.border = 1;

        % Scalar expressions
        fem.expr.L = 'coe';
        fem.expr.al_CON = '(1-alb)/alb';
        fem.expr.al = 'exp(V-L)/( al_CON+exp(V-L) )';
        fem.expr.np = 'n0*exp(-V)';
        fem.expr.nm = 'n0*exp(V)';
        fem.expr.Ent_V = '(nm - np)*V - np -nm + 2*n0';
        fem.expr.Ent_sur = 'al*log(al/alb) + (1-al)*log( (1-al) / (1-alb) )';

        %Creat rough_mesh and fine_mesh fem structure
        fem_c = fem;
        fem_f = fem;

        % Initialize mesh, Multiphysics, Extend Mesh for rough
        fem_c.mesh=meshinit(fem_c,'hauto',5);
        fem_c=multiphysics(fem_c);
        fem_c.xmesh=meshextend(fem_c);

        % Initialize mesh, Multiphysics, Extend Mesh for rough
        fem_f.mesh=meshinit(fem_f,'hauto',3);
        fem_f=multiphysics(fem_f);
        fem_f.xmesh=meshextend(fem_f);

        % Assign Coe, Solve and find ratios
        fem_c.const.coe = coe1;

        if rough_sol == 0
                        fem_c.sol=femstatic(fem_c,'solcomp',{'V'},'outcomp',{'V
'},'nonlin','on');
                        rough_sol = 1;
```

```
        else
                        fem_c.sol=femstatic(fem_c,'init',fem_c.sol,'solcomp',{'V
'},'outcomp',{'V'},'nonlin','on');
        end
        ratio1 = postint( fem_c, '2*pi*r*(al)/a2', 'unit', '', 'dl', [14], 'edim',
 1) / postint( fem_c, '2*pi*r/a2', 'unit', '', 'dl', [14], 'edim', 1);
        while abs(ratio1 - alb) > 0.00005

        fem_c.const.coe = coe2;
        fem_c.sol=femstatic(fem_c,'init',fem_c.sol,'solcomp',{'V'},'outcomp',{'V
'},'nonlin','on');
        ratio2 = postint( fem_c, '2*pi*r*(al)/a2', 'unit', '', 'dl', [14], 'edim',
 1) / postint( fem_c, '2*pi*r/a2', 'unit', '', 'dl', [14], 'edim', 1);
        coe3 =  ( coe2 - coe1 )/( ratio1 - ratio2 ) * ( ratio1 - alb ) + coe1;

        if abs(ratio1-alb) > abs(ratio2-alb)
                coe1 = coe2; ratio1 = ratio2; coe2 = coe3;
        else
                coe2 = coe3;
        end
                        %fprintf('   coe3 = %g\n', coe3);
        end

        % solve fine mesh wih adaptive solver and coe = coe2;
        fem_f.const.coe = coe2;

        fem_f=adaption(fem_f, 'solcomp',{'V'},'nonlin','on','outcomp',{'V'},'
solver','stationary','l2scale',[1],'l2staborder',[2], ...
                                                        'eigselect',[1],'
maxt',10000000,'ngen',2,'resorder',[0],'rmethod','longest','tppar',1.7, 'geomnum
',1);
        ratio2 = postint( fem_f, '2*pi*r*(al)/a2', 'unit', '', 'dl', [14], 'edim',
 1) / postint( fem_f, '2*pi*r/a2', 'unit', '', 'dl', [14], 'edim', 1);
        fprintf('\nfinal:  coe = %g, ratio   ratio2 = %g, Q=%d, R=%g', coe2,
ratio2, Q, Rws );
        for fine_al_iter=1:15

          II0 = postint( fem_f, '2*pi*r*(alb-al)/a2', 'unit', '', 'dl', [14], '
edim', 1);
          II1 = postint( fem_f, '2*pi*r*(al^2-al)/a2', 'unit', '', 'dl', [14], '
edim', 1);
          fem_f.const.coe = fem_f.const.coe + II0/II1;
          fem_f.sol=femstatic(fem_f,'init',fem_f.sol,'solcomp',{'V'},'outcomp',{'V
'},'nonlin','on');
          ratio2 = postint( fem_f, '2*pi*r*(al)/a2', 'unit', '', 'dl', [14], 'edim
', 1) / postint( fem_f, '2*pi*r/a2', 'unit', '', 'dl', [14], 'edim', 1);
          if abs(II0) < 0.00006 break; end;

        end;

        fprintf('\nrefine coe:  coe = %g, ratio   ratio2 = %g, Q=%d, R=%g', fem_f.
const.coe, ratio2, Q, Rws );
        coe2 = fem_f.const.coe;
        fname = sprintf('../Data_var_a_eps_40_2_kap_10/Ins_Disc_Q=%d_R=%g_a=%
g_alpha=%g_e=%d_Rp=%d.mph', fem_f.const.Q, Rws , a2, alb, epsl, Rp);
        flsave( fname, fem_f );

    end;
   end;
  end;
 end;
end;
```

3.5.2 Minimization of free energy

The following code minimizes the free free energy with respect to d, a_{out}, and θ.

```
flclear 'all'

a0 = 65;

gamma = 0.145;
H = -12;
Rp = 10;
alb_cn_range = 2;
k1 = 10;
peps = 402;
nd = '';
RD = 30;

% for kappa =1/10
if (k1==10)
k_0_09_0_05 = 379.1934; %381.29;
k_0_09_0_10  = 379.3;
k_0_09_0_15 = 371.6254;
k_0_09_0_3  = 368; %352.0135; %397.75;
k_0_09_0_45 = 326.8879;
k_0_09_0_60 = 298.3097;
end

if (k1==7)
% for kappa = 1/7
k_0_09_0_3 = 370.1849;
end

if (k1==15)
% for kappa = 1/15
k_0_09_0_3 = 366;
end

if (k1==5)
% for kappa = 1/5
k_0_09_0_3 = 371;
end

k(2) = a0^2 * ( gamma - 0.09 ) + k_0_09_0_3 ;

if(k1==10)
k(1) = a0^2 * ( gamma - 0.09 ) + k_0_09_0_05 ;
k(3) = a0^2 * ( gamma - 0.09 ) + k_0_09_0_15  ;
k(4) = a0^2 * ( gamma - 0.09 ) + k_0_09_0_45  ;
k(5) = a0^2 * ( gamma - 0.09 ) + k_0_09_0_60  ;
k(6) = a0^2 * ( gamma - 0.09 ) + k_0_09_0_10  ;
end

lambda = 0.217/.145*gamma;

S_M = 1 / ( 2*sqrt(3)*Rp*Rp ) ;
Ap = pi*Rp^2;

c = 10;

f_se = 1;
IRws_exp = [ 11.5 15 17.5 20 22.5 25 27.5 30 32.5 35 40 45 50 55 60 70 80 100 140
150];
IRws = [ 15 17.5 20 22.5 25 27.5 30 32.5 35 40 45 50 55 60 70 80 100 140 ];
IRws_fine = [ 15 15.5 16 16.5 17 17.5 18 18.5 19 19.5 20 20.5 21 21.5 22 22.5 23
23.5 24 24.5 25 26 27.5 30 32.5 35 37.5 40 42.5 45 47.5 50 52.5 55 60 65 70 75 80
90 100 110 120 130 140 ];
```

```
%alb = [ 0.05   0.3  ];
%alb = [ 0.15   0.6  ];
alb  = [ 0.05   0.3   0.15   0.45  0.6  0.1];
epsl = [ 2       80  ];
a2   = [ 30 40 45 50 52.5 55 57.5 60 62.5 65 67.5 70 ];

% Free energy of a Single Peptide  Q= 1..10
%Fsp = [0.5588     2.2199     4.9391     8.6506    13.2810    18.7617    25.0349
  32.0531    39.7782    48.1788];
% Free energy of a Single Peptide  Q= 1..10, Energy and Entropy parts separated
epsilon = 4, 40
%Fsp_ee = [0.479938,   1.87663,   4.0731,   6.92169,   10.2995,   14.1316,
18.3805,   23.0284,   28.0664,   33.4894];
%Fsp_en = [ 0.0696482,   0.3071,   0.787056,   1.59415,   2.78034,   4.35354,
6.29428,   8.57366,   11.1626,   14.0351 ];
% Free energy of a Single Peptide  Q= 1..10, Energy and Entropy parts separated
uniform peptide
%Fsp_ee = [ 0.2785817,  1.103019,  2.440995,  4.244099,   6.45564,  9.019499,
11.88717,  15.02113,  18.39467,  21.98992];
%Fsp_en = [0.05299486, 0.2191902, 0.5188924, 0.9814871,  1.639174,  2.520178,
3.64388,   5.01932,  6.646556,  8.519311];
% Free energy of a Single Peptide  Q= 1..10, Energy and Entropy parts separated
peptide epsilon=20, half charged
%Fsp_ee = [ 0.5041408,  1.990431,  4.386552,  7.595048,  11.52392,  16.10662,
21.30268,  27.08905,  33.45218,  40.38339];
%Fsp_en = [0.06079743, 0.2603243, 0.6447239,  1.271448,  2.185091,  3.404509,
4.926912,  6.738129,   8.82026,  11.15545];
% Free energy of a Single Peptide  Q= 1..10, Energy and Entropy parts separated
peptide epsilon=20, half charged, Rp = 8
%Fsp_ee = [ 0.6739887,  2.652625,  5.815605,  10.00843,   15.1041,  21.02758,
27.74068,    35.223,  43.46205,  52.44924];
%Fsp_en = [0.06926412, 0.3059662, 0.7879786,  1.605302,  2.811753,  4.413747,
6.39131,  8.717142,  11.36464,  14.30982];
% Free energy of a Single Peptide  Q= 1..10, Energy and Entropy parts separated
peptide epsilon=20, half charged, Rp = 12
%Fsp_ee = [ 0.3897864,   1.542888,   3.414185,   5.940783,   9.057732,   12.71085,
   16.86135,   21.48389,   26.56238,   32.08653];
%Fsp_en = [0.05405745,  0.2267005,  0.5462865,   1.049932,   1.771144,   2.730841,
    3.93583,   5.382477,   7.061376,   8.960729];
% Free energy of a Single Peptide  Q= 1..10, Energy and Entropy parts separated
peptide epsilon=20, thin layer charged, Rp = 10
%Fsp_ee = [ 0.4252024,  1.591427,  3.228191,  5.066118,  6.948405,    8.8105,
10.63083,  12.40432,  14.13192,  15.81669];
%Fsp_en = [0.09180918, 0.4401103,  1.213514,  2.544476,  4.457485,  6.909453,
9.839443,  13.18959,  16.91021,  20.95981];
% Free energy of a Single Peptide  Q= 1..10, Energy and Entropy parts separated
peptide infinitely thin layer charged, Rp = 10
%Fsp_ee = [ 0.2760555,  1.060611,  2.239382,  3.671608,  5.236744,  6.854932,
8.481763,  10.09523,  11.68546,  13.24873];
%Fsp_en = [0.07936247, 0.3454726, 0.8687388,  1.726491,  2.968564,  4.607342,
6.628428,  9.004801,  11.70609,  14.70301];
% Free energy of a Single Peptide  Q= 1..10, Energy and Entropy parts separated
peptide, epsilon = 20, half charged, Rp = 10, kappa=1/7
%Fsp_ee = [ 0.4586232,   1.813472,    4.00913,   6.975436,   10.64818,   14.97949,
   19.93745,   25.50136,    31.6574,   38.39585];
%Fsp_en = [ 0.0629702,  0.2649697,  0.6390898,   1.222962,    2.04373,   3.112583,
   4.428017,   5.981465,   7.761509,   9.756171];
% Free energy of a Single Peptide  Q= 1..10, Energy and Entropy parts separated
peptide, epsilon = 20, half charged, Rp = 10, kappa=1/15
%Fsp_ee = [   0.55634,   2.197731,   4.841449,   8.361697,   12.62678,   17.53862,
   23.04196,   29.11054,    35.7323,    42.9011];
%Fsp_en = [ 0.0542825,  0.2360459,  0.6013723,   1.231869,   2.202406,   3.550759,
    5.27651,    7.35836,   9.768944,   12.48177];
```

```
% Free energy of a Single Peptide  Q= 1..10, Energy and Entropy parts separated
peptide, epsilon = 20, half charged, Rp = 10, kappa=1/4
%Fsp_ee = [  0.395923,   1.573177,   3.504404,   6.154839,   9.490942,    13.4848,
   18.11484,   23.36475,   29.22219,   35.67758];
%Fsp_en = [0.05817508,  0.2385531,  0.5555621,   1.025397,   1.660388,    2.46697,
   3.446387,   4.596351,   5.912536,   7.389611];
if (peps==402 & Rp==10 & k1==10)
% Free energy of a Single Peptide  Q= 1..10, Energy and Entropy parts separated
peptide, epsilon = 40,2 , half charged, Rp = 10, kappa=1/10
Fsp_ee = [ 0.4968255,   1.939665,   4.200493,   7.121571,   10.57667,    14.4925,
   18.8338,   23.58438,   28.73619,   34.28452];
Fsp_en = [ 0.0719695,  0.3193627,  0.8236652,   1.673974,   2.920503,   4.566224,
  6.587365,    8.95229,   11.63039,   14.59477];
end

if (peps==402 & Rp==12 & k1==10)
% Free energy of a Single Peptide  Q= 1..10, Energy and Entropy parts separated
peptide, epsilon = 40,2 , half charged, Rp = 12, kappa=1/10
Fsp_ee = [ 0.3952319,   1.548197,   3.371134,   5.752054,   8.591615,   11.82212,
  15.40461,   19.31851,   23.55302,   28.10222];
Fsp_en = [0.06590862,  0.2848969,  0.7119737,   1.410675,   2.424991,    3.76886,
  5.433637,   7.399816,   9.644893,   12.14712];
end

if (peps==402 & Rp==10 & k1==15)
% Free energy of a Single Peptide  Q= 1..10, Energy and Entropy parts separated
peptide, epsilon = 40,2, half charged, Rp = 10, kappa=1/15
Fsp_ee = [ 0.5593109,   2.188664,   4.742958,   8.015042,   11.82164,   16.05853,
  20.68442,   25.68723,    31.0645,   36.81632];
Fsp_en = [0.06182997,  0.2809303,  0.7561793,   1.619032,   2.961028,   4.797693,
  7.095642,   9.807816,   12.88977,   16.30399];
end

if (peps==402 & Rp==10 & k1==7)
% Free energy of a Single Peptide  Q= 1..10, Energy and Entropy parts separated
peptide, epsilon = 40,2, half charged, Rp = 10, kappa=1/7
Fsp_ee = [ 0.4402194,   1.721464,    3.74427,   6.394479,   9.582091,   13.25072,
  17.36845,   21.91712,   26.88564,   32.26656];
Fsp_en = [0.07704489,  0.3328639,  0.8263194,   1.615098,   2.729077,   4.169454,
  5.921112,   7.963215,    10.2746,   12.83579];
end

if (peps==402 & Rp==10 & k1==5)
% Free energy of a Single Peptide  Q= 1..10, Energy and Entropy parts separated
peptide, epsilon = 40,2, half charged, Rp = 10, kappa=1/5
Fsp_ee = [ 0.3896488,   1.530466,   3.353071,   5.778616,   8.742484,   12.20016,
  16.12298,   20.49236,   25.29574,   30.52417];
Fsp_en = [0.07702489,  0.3246309,  0.7808607,   1.481873,   2.447021,   3.678634,
  5.168499,   6.903751,   8.870304,   11.05446];
end

% Free energy of a Single Peptide  Q= 1..10, Energy and Entropy parts separated
peptide, epsilon = 20,2, half charged, Rp = 10, kappa=1/10
%Fsp_ee = [ 0.6884181,    2.69934,   5.891073,    10.1011,   15.21252,   21.16444,
    27.9295,   35.49487,   43.85326,    52.9994];
%Fsp_en = [0.07405076,  0.3320161,  0.8629304,   1.754124,   3.043097,   4.720516,
   6.756627,   9.118737,   11.77758,   14.70852];
% Free energy of a Single Peptide  Q= 1..10, Energy and Entropy parts separated
peptide, epsilon = 20,2, half charged, Rp = 10, kappa=1/7
%Fsp_ee = [ 0.6304307,   2.477393,   5.432982,   9.381678,   14.23995,   19.95914,
   26.51253,   33.88456,   42.06503,   51.04645];
%Fsp_en = [0.07923633,  0.3445008,  0.8583113,   1.675232,    2.81661,   4.276111,
   6.034737,   8.070696,   10.36347,   12.89496];
fprintf('\n loading');

fname_S = sprintf('../Free_Energies/Ads_energies_var_a_eps_40_2_kap_%d_al_%g_Rp=%d
%s', k1, alb(alb_cn_range), Rp, nd );
```

```
fname_I = sprintf('../Free_Energies/Ins_energies_var_a_eps_40_2_kap_%d_al_%g_Rp=%d
%s', k1, alb(alb_cn_range), Rp, nd );
fp_S = fopen( fname_S ,'r');
fp_I = fopen( fname_I ,'r');

temp = fscanf( fp_S, '%s', [1, 16]);
temp = fscanf( fp_I, '%s', [1, 16]);

for a_cn = 1:12
  for alb_cn = alb_cn_range
    for eps_cn=1:1
      for Q=1:10
        for Rcn = 1:(size(IRws))(2)

          temp = fscanf( fp_S, '%g', [1, 16]);
          Elec_S(Rcn, Q, eps_cn, alb_cn, a_cn) = temp(9) + temp(10) + temp(11);
          Ent_salt_S(Rcn, Q, eps_cn, alb_cn, a_cn) = f_se * (temp(12) + temp(13));
          Ent_sur_S(Rcn, Q, eps_cn, alb_cn, a_cn) = temp(14);
          Mech_S(Rcn, Q, eps_cn, alb_cn, a_cn) = 0*temp(15);


          temp = fscanf( fp_I, '%g', [1, 16]);
          %k(alb_cn) = temp(8);
          Elec_I(Rcn, Q, eps_cn, alb_cn, a_cn) = temp(9) + temp(10) + temp(11);
          Ent_salt_I(Rcn, Q, eps_cn, alb_cn, a_cn) = f_se * (temp(12) + temp(13));
          Ent_sur_I(Rcn, Q, eps_cn, alb_cn, a_cn) = temp(14);
          Mech_I(Rcn, Q, eps_cn, alb_cn, a_cn) = 0*temp(15);

        end;
      end;
    end;
  end;
end;


fclose(fp_S);
fclose(fp_I);

fprintf('\n ... calculating ... \n ');

for Rcn = 1:(size(IRws))(2)
  fprintf('Rcn = %g\n', Rcn);
  for Q = 1:10
    for alb_cn = alb_cn_range
      for eps_cn = 1:1
        for f_cn = 1:20
          for a_cn = 1:12

          f = (f_cn-0.001)/20;

          F_I = H + Elec_I(Rcn, Q, eps_cn, alb_cn, a_cn) + Ent_sur_I(Rcn, Q,
eps_cn, alb_cn, a_cn) + Ent_salt_I(Rcn, Q, eps_cn, alb_cn, a_cn) - Fsp_ee(Q) -
Fsp_en(Q) + 0;
          F_S =     Elec_S(Rcn, Q, eps_cn, alb_cn, a_cn) + Ent_sur_S(Rcn, Q,
eps_cn, alb_cn, a_cn) + Ent_salt_S(Rcn, Q, eps_cn, alb_cn, a_cn) - Fsp_ee(Q) -
Fsp_en(Q) + 0;
          F_I_check(Rcn,Q) = Elec_I(Rcn, Q, 1, alb_cn, 10) + Ent_sur_I(Rcn, Q,
eps_cn, alb_cn, 10) + Ent_salt_I(Rcn, Q, eps_cn, alb_cn, 10) - Fsp_ee(Q) - Fsp_en(
Q);
          F_S_check(Rcn,Q) = Elec_S(Rcn, Q, 1, alb_cn, 10) + Ent_sur_S(Rcn, Q,
eps_cn, alb_cn, 10) + Ent_salt_S(Rcn, Q, eps_cn, alb_cn, 10) - Fsp_ee(Q) - Fsp_en(
Q);
          %F_I_fake =  H -Fsp_ee(Q) - Fsp_en(Q);
          %F_S_fake =  -Fsp_ee(Q) - Fsp_en(Q);

          %N_I = ( 2 * sqrt(3) * IRws(Rcn)^2 - Ap ) / a2(a_cn);
          %N_S = ( 2 * sqrt(3) * IRws(Rcn)^2 ) / a2(a_cn);
          N_I = ( pi * IRws(Rcn)^2 - Ap ) / a2(a_cn) ;
```

```
          N_S = ( pi * IRws(Rcn)^2 ) / a2(a_cn) ;

          F_I_plot(Rcn, Q, eps_cn, alb_cn, a_cn) = ( F_I - H ) / N_I;
          F_S_plot(Rcn, Q, eps_cn, alb_cn, a_cn) = F_S / N_S;

          S_I =    f  /  ( 2 * sqrt(3) * IRws(Rcn)^2 );
          S_S = (1-f) / ( 2 * sqrt(3) * IRws(Rcn)^2 );

          CV = ( c * (1e-6*6.02e23/1e27*Ap*8) );

          Del_Ent = (S_S) * ( log(S_S/S_M) ) + (S_I) * ( log(S_I/S_M) ) + (S_M -
S_I - S_S)*( log( (S_M - S_I - S_S)/(S_M) ) ) - (S_S + S_I) * log(CV) + ((S_S +
S_I));
          temp1 = ( f * N_I + (1-f) * N_S + (2*sqrt(3) - pi) * IRws(Rcn)^2/a0 ) ;

          a_in = a2(a_cn) + f * Ap / (temp1);

           a_out = a2(a_cn) ;


          %F_mech_in  = gamma * 65  + k(alb_cn) / 65 ;
          F_mech_in  = gamma * a_in  + k(alb_cn) / a_in ;
          %F_mech_out = gamma * 65  + k(alb_cn) / 65 ;
          F_mech_out = gamma * a_out + k(alb_cn) / a_out ;

          Del_Ent_per_lipid(Rcn, Q, eps_cn, alb_cn, f_cn, a_cn ) = Del_Ent * a_in
;
          Ftotal(a_cn) =  f * F_I / temp1 + (1-f) * F_S / temp1 + F_mech_in +
F_mech_out + Del_Ent_per_lipid(Rcn, Q, eps_cn, alb_cn, f_cn, a_cn );
          Ftotal_no_ent(a_cn) =  f * (F_I-H) / temp1 + (1-f) * F_S / temp1 +
F_mech_in + F_mech_out + 0*Del_Ent_per_lipid(Rcn, Q, eps_cn, alb_cn, f_cn, a_cn );
          %Ftotal_fake(a_cn) =  0*f * F_I_fake / temp1 + 0*(1-f) * F_S_fake /
temp1 + F_mech_in + F_mech_out + 0*Del_Ent_per_lipid(Rcn, Q, eps_cn, alb_cn, f_cn,
 a_cn );
          if(a_cn == 10)
              F_salt_ent_65(Rcn, Q, eps_cn, alb_cn, f_cn) = f * Ent_salt_I(Rcn, Q,
 eps_cn, alb_cn, a_cn) + (1-f) * Ent_salt_S(Rcn, Q, eps_cn, alb_cn, a_cn) - Fsp_en
(Q) ;
              F_salt_ent_65(Rcn, Q, eps_cn, alb_cn, f_cn) = F_salt_ent_65(Rcn, Q,
eps_cn, alb_cn, f_cn) / temp1;
              F_elec_65(Rcn, Q, eps_cn, alb_cn, f_cn)     = f * Elec_I(Rcn, Q,
eps_cn, alb_cn, a_cn) + (1-f) * Elec_S(Rcn, Q, eps_cn, alb_cn, a_cn) - Fsp_ee(Q) ;
              F_elec_65(Rcn, Q, eps_cn, alb_cn, f_cn)     = F_elec_65(Rcn, Q,
eps_cn, alb_cn, f_cn) / temp1;
              PiL_65(Rcn, f_cn) =  f/2/sqrt(3)/IRws(Rcn)^2  * a_in ;
              PsL_65(Rcn, f_cn) =  (1-f)/2/sqrt(3)/IRws(Rcn)^2  * a_in ;
          end;

          end;

          %[temp, i] = min( Ftotal_fake );
          [temp, i] = min( Ftotal_no_ent );
          %[temp, i] = min( Ftotal );

          if(i==12)  i=11;   end;
          if(i==1) i=2; end;

          a2_fine = a2(i-1):0.01:a2(i+1);

          %Ft_fine = spline( a2, Ftotal_fake, a2_fine);
          Ft_fine = spline( a2, Ftotal_no_ent, a2_fine);
          %Ft_fine = spline( a2, Ftotal, a2_fine);
          [temp, i] = min( Ft_fine );

          a_min(Rcn, Q, eps_cn, alb_cn, f_cn) = a2_fine(i);
          %a_min_in(Rcn, Q, eps_cn, alb_cn, f_cn) = a_min(Rcn, Q, eps_cn, alb_cn,
f_cn) + f*Ap / temp1;
```

```
          %TEMP1(Rcn, f_cn) = temp1;

          N_I_a_min(Rcn) = ( pi * IRws(Rcn)^2 - Ap ) / a_min(Rcn, Q, eps_cn,
alb_cn, f_cn);
          N_S_a_min(Rcn) = ( pi * IRws(Rcn)^2 ) / a_min(Rcn, Q, eps_cn, alb_cn,
f_cn);
          temp_N(Rcn, f_cn) = (  f * N_I_a_min(Rcn)  +  (1-f) * N_S_a_min(Rcn)  +
(2*sqrt(3) - pi) * IRws(Rcn)^2/a0 ) ;

          temp_N_a_min(Rcn, f_cn) = temp_N(Rcn, f_cn); %spline(a2, temp_N(Rcn,
f_cn, :), a_min(Rcn, Q, eps_cn, alb_cn, f_cn) );

          Elec_I_min(Rcn, Q, eps_cn, alb_cn, f_cn) = spline(a2, Elec_I(Rcn, Q,
eps_cn, alb_cn, : ), a_min(Rcn, Q, eps_cn, alb_cn, f_cn) );
          Ent_sur_I_min(Rcn, Q, eps_cn, alb_cn, f_cn) = spline(a2, Ent_sur_I(Rcn,
Q, eps_cn, alb_cn, : ), a_min(Rcn, Q, eps_cn, alb_cn, f_cn) );
          Ent_salt_I_min(Rcn, Q, eps_cn, alb_cn, f_cn) = spline(a2, Ent_salt_I(Rcn
, Q, eps_cn, alb_cn, : ), a_min(Rcn, Q, eps_cn, alb_cn, f_cn) );
          Mech_I_min(Rcn, Q, eps_cn, alb_cn, f_cn) = spline(a2, Mech_I(Rcn, Q,
eps_cn, alb_cn, : ), a_min(Rcn, Q, eps_cn, alb_cn, f_cn) );

          Elec_S_min(Rcn, Q, eps_cn, alb_cn, f_cn) = spline(a2, Elec_S(Rcn, Q,
eps_cn, alb_cn, : ), a_min(Rcn, Q, eps_cn, alb_cn, f_cn) );
          Ent_sur_S_min(Rcn, Q, eps_cn, alb_cn, f_cn) = spline(a2, Ent_sur_S(Rcn,
Q, eps_cn, alb_cn, : ), a_min(Rcn, Q, eps_cn, alb_cn, f_cn) );
          Ent_salt_S_min(Rcn, Q, eps_cn, alb_cn, f_cn) = spline(a2, Ent_salt_S(Rcn
, Q, eps_cn, alb_cn, : ), a_min(Rcn, Q, eps_cn, alb_cn, f_cn) );
          Mech_S_min(Rcn, Q, eps_cn, alb_cn, f_cn) = spline(a2, Mech_S(Rcn, Q,
eps_cn, alb_cn, : ), a_min(Rcn, Q, eps_cn, alb_cn, f_cn) );

          Del_Ent_per_lipid(Rcn, Q, eps_cn, alb_cn, f_cn) = spline(a2,
Del_Ent_per_lipid(Rcn, Q, eps_cn, alb_cn, f_cn, : ), a_min(Rcn, Q, eps_cn, alb_cn,
 f_cn) );

          Ftotal_a_min(Q, eps_cn, alb_cn, Rcn, f_cn)  = spline(a2, Ftotal(:),
a_min(Rcn, Q, eps_cn, alb_cn, f_cn) );

          %Ftotal(a_cn) =  f * F_I / temp1 + (1-f) * F_S / temp1 + F_mech_in +
F_mech_out + Del_Ent_per_lipid(Rcn, Q, eps_cn, alb_cn, f_cn, a_cn );

          a_in_a_min(Q, eps_cn, alb_cn, Rcn, f_cn) = a_min(Rcn, Q, eps_cn, alb_cn,
 f_cn) + f * Ap / ( temp_N_a_min(Rcn, f_cn) );
          a_out_a_min(Q, eps_cn, alb_cn, Rcn, f_cn) = a_min(Rcn, Q, eps_cn, alb_cn
, f_cn);

          Felec_a_min(Q, eps_cn, alb_cn, Rcn, f_cn) = f*Elec_I_min(Rcn, Q, eps_cn,
 alb_cn, f_cn) + (1-f)*Elec_S_min(Rcn, Q, eps_cn, alb_cn, f_cn) - Fsp_ee(Q) ;
          Felec_a_min(Q, eps_cn, alb_cn, Rcn, f_cn) = Felec_a_min(Q, eps_cn,
alb_cn, Rcn, f_cn)/temp_N_a_min(Rcn, f_cn);
          Fent_sal_a_min(Q, eps_cn, alb_cn, Rcn, f_cn)  = f*Ent_salt_I_min(Rcn, Q,
 eps_cn, alb_cn, f_cn) + (1-f)*Ent_salt_S_min(Rcn, Q, eps_cn, alb_cn, f_cn) -
Fsp_en(Q) ;
          Fent_sal_a_min(Q, eps_cn, alb_cn, Rcn, f_cn)  = Fent_sal_a_min(Q, eps_cn
, alb_cn, Rcn, f_cn)/temp_N_a_min(Rcn, f_cn);
          Fent_sur_a_min(Q, eps_cn, alb_cn, Rcn, f_cn)  = f*Ent_sur_I_min(Rcn, Q,
eps_cn, alb_cn, f_cn) + (1-f)*Ent_sur_S_min(Rcn, Q, eps_cn, alb_cn, f_cn);
          Fent_sur_a_min(Q, eps_cn, alb_cn, Rcn, f_cn)  = Fent_sur_a_min(Q, eps_cn
, alb_cn, Rcn, f_cn)/temp_N_a_min(Rcn, f_cn);
          Fmech_a_min(Q, eps_cn, alb_cn, Rcn, f_cn)  =  gamma * a_in_a_min(Q,
eps_cn, alb_cn, Rcn, f_cn) + k(alb_cn) / a_in_a_min(Q, eps_cn, alb_cn, Rcn, f_cn)
+ gamma * a_min(Rcn, Q, eps_cn, alb_cn, f_cn) + k(alb_cn) / a_min(Rcn, Q, eps_cn,
alb_cn, f_cn);
        end;
      end;
    end;
  end;
end;

fprintf('\n ... saving ... \n');


f= 1:20;
```

```
f = f - 0.001;
f = f/20;

[RR, ff] = meshgrid(f, IRws);

%-------------------------------------------------------------------------------%


for eps_cn = 1:1
  for alb_cn = alb_cn_range
    for Q = 1:10

      FF2(:,:) = Ftotal_a_min(Q, eps_cn, alb_cn, :, :); % (R,f)
      AA_in2(:,:) = a_in_a_min(Q, eps_cn, alb_cn, :, :); % (R,f)
      AA_out2(:,:) = a_min(: , Q, eps_cn, alb_cn, : ); % (R,f)

      FF(:,:) = transpose( spline(IRws, transpose( FF2(:,:) ), IRws_exp) );
      AA_in(:,:) = transpose( spline(IRws, transpose( AA_in2(:,:) ), IRws_exp) );
      AA_out(:,:) = transpose( spline(IRws, transpose( AA_out2(:,:) ), IRws_exp) )
;
      [ FFf, iif ] = min(FF);
      [ FFfR, iifR ] = min(FFf);   %var f

      Rcn_min = iif(iifR); %var f
      fcn_min = iifR;      %var f

      %Rcn_min = iif(20);  %fixed f
      %fcn_min = 20;       %fixed f

      Rcn_min_start = Rcn_min - 1;
      Rcn_min_end = Rcn_min + 1;

      fcn_min_start = fcn_min - 1;
      fcn_min_end = fcn_min + 1;

      if(Rcn_min_start < 1) Rcn_min_start = 1; end;
      if(Rcn_min_end > (size(IRws_exp))(2) ) Rcn_min_end = (size(IRws_exp))(2);
end;
      if(fcn_min_start <= 0) fcn_min_start = .0000001; end;
      if(fcn_min_end > 20 ) fcn_min_end = 19.9999999; end;

      f_fine = ( (fcn_min_start-0.001) / 20 ):0.001:( (fcn_min_end-0.001) / 20 );
      R_fine = IRws_exp(Rcn_min_start):0.005:IRws_exp(Rcn_min_end);

      clear FF_fine1
      clear FF_fine2
      clear FF_fine3

      clear AA_in_fine1
      clear AA_in_fine2
      clear AA_in_fine3

      clear AA_out_fine1
      clear AA_out_fine2
      clear AA_out_fine3

      FF_fine1(:,:) = spline( f , FF(:,:), f_fine );
      FF_fine2(:,:) = spline( IRws_exp , transpose(FF_fine1(:,:)), R_fine );
      FF_fine3(:,:) = transpose( FF_fine2(:,:) );

      AA_in_fine1(:,:) = spline( f , AA_in(:,:), f_fine );
      AA_in_fine2(:,:) = spline( IRws_exp , transpose(AA_in_fine1(:,:)), R_fine );
      AA_in_fine3(:,:) = transpose( AA_in_fine2(:,:) );

      AA_out_fine1(:,:) = spline( f , AA_out(:,:), f_fine );
      AA_out_fine2(:,:) = spline( IRws_exp , transpose(AA_out_fine1(:,:)), R_fine
);
      AA_out_fine3(:,:) = transpose( AA_out_fine2(:,:) );
```

```
      [ FFf_fine, iif_fine ] = min(FF_fine3);
      [ FFfR_fine, iifR_fine ] = min(FFf_fine);  %var f

      Req_cn = iif_fine(iifR_fine); %var f
      feq_cn = (iifR_fine);   %var f

      %Req_cn = iif_fine( (size(f_fine))(2) ); %fix f
      %feq_cn = (size(f_fine))(2);   %fix f

      Req(Q, -H, eps_cn, alb_cn) = R_fine(Req_cn);
      feq(Q, -H, eps_cn, alb_cn) = f_fine(feq_cn);
      a_in(Q, -H, eps_cn, alb_cn) = AA_in_fine3( Req_cn , feq_cn);
      a_out(Q, -H, eps_cn, alb_cn) = AA_out_fine3( Req_cn , feq_cn);
      PL(Q, -H, eps_cn, alb_cn) = ( f_fine(feq_cn)/2/sqrt(3)/(R_fine(Req_cn))^2 )
* AA_in_fine3( Req_cn , feq_cn) ;
      %PL(Q, -H, eps_cn, alb_cn) = ( f_fine(feq_cn)/pi/(R_fine(Req_cn))^2 ) *
AA_in_fine3( Req_cn , feq_cn) ;
    end;
  end;
end;

%-------------------------------------------------------------------------------------------------%

for eps_cn = 1:1
  for alb_cn = alb_cn_range

   fname = sprintf('../PL_C/XX_v_Q_H=%d_al=%g_epsl=%d_d=3_gam=%g_f_se=%
g_eps_40_2_kap_%d_Rp=%d%s_no_mech2', H, alb(alb_cn), epsl(eps_cn), gamma, f_se, k1
, Rp, nd);
  fp = fopen(fname, 'wt' );
  fprintf(fp,'Q                Del_A                  PIL                  a_in
              a_out                DA/A                  Req
feq                Sig                  PiR\n');
  for Q = 1:10
    fprintf(fp,'%2g%20.10g   %20.10g   %20.10g  %20.10g  %20.10g  %20.10g  %20.10g
  %20.10g  %20.10g\n', Q, ...
    ( a_in(Q, -H, eps_cn, alb_cn) - a_out(Q, -H, eps_cn, alb_cn) ), ...
    PL(Q, -H, eps_cn, alb_cn), ...
    a_in(Q, -H, eps_cn, alb_cn), ...
    a_out(Q, -H, eps_cn, alb_cn), ...
    (a_in(Q, -H, eps_cn, alb_cn)-65)/65, ...
    Req(Q, -H, eps_cn, alb_cn), ...
    feq(Q, -H, eps_cn, alb_cn), ...
    Q*PL(Q, -H, eps_cn, alb_cn)/a_in(Q, -H, eps_cn, alb_cn)/feq(Q, -H, eps_cn,
alb_cn) - alb(alb_cn)/a_in(Q, -H, eps_cn, alb_cn), ...
    pi * lambda^2/ ( 4*gamma*( a_in(Q, -H, eps_cn, alb_cn)/65 - 1) )     );

    end;
  end;
end;

fclose(fp);
```

Chapter 4

Spontaneous Bending of Lipid Bilayers: How are Lipid and Electrostatic Properties Interrelated?

4.1 Introduction

A lipid bilayer membrane is a self-assembled structure studded with membrane proteins [15, 35, 61, 62]. Its ability to deform its shape and topology complements its integrity as a "self-sealing" object. This is correctly a particular realization of lipid aggregates. The rich phase behavior of lipid aggregates is not only a direct manifestation of single-lipid properties, i.e., lipid packing, but also a result of external parameters such as salts and temperatures [61–63]. Along this line, the electrostatic bending of a possibly asymmetrically-charged lipid membrane has been considered for some time [64–66]. It not only complements protein-induced bending [67] but also has relevance in a variety of different contexts: cell shape transformation [61, 68], vesicle budding, and lipid tubulation [64–66], as well as Ca^{2+}-induced membrane fusion [69–71]. An intimately-related point is that lipid charges can alter lipid packing stress, which in turn influences membrane functions by modifying the "working" condition for membrane-protein activity (Ref. [72]

and references therein). For instance, the gating (open vs. closed) properties of 'mechanosensitive' (MS) channels (as in *E. coli*) are sensitive to lipid packing or membrane curvature [73]. The opening or closure of such channels can be controlled by counterion valence and membrane charges [74]. It is worth noting that the electrostatic mechanisms of spontaneous membrane curvature and lipid packing stress share the same physical origin in common, i.e., electrostatic modification of lipid headgroups. Indeed, headgroup properties are shown to play a fundamental role in self-assembly of lipid aggregates [75].

On the other hand, what remains unclear is the relative roles of electrostatic [64–66] and protein-based [67, 73] mechanisms in "shaping" lipid membranes. In the case of MS channels, for instance, channel shapes are also implicated in their gating properties. Also, cells use a variety of proteins specialized in membrane bending as for membrane vesicle formation [76]. Nevertheless, a better understanding of electrostatic bending will be useful for identifying relevant parameters for determining lipid packing and membrane curvature. In fact, the lipid contribution to membrane curvature is influenced by lipid charges, whether proteins are involved or not (see for instance Ref. [75]), and is shown to have nontrivial impact on MS channels [74].

Despite much effort, however, the electrostatic bending of a lipid membrane has not been well understood theoretically, owing to the presence of large degrees of freedom such a system presents (e.g., lipid flexibility and the "ionic cloud" forming near a charged surface [57]). Accordingly, spontaneous membrane curvature has been considered under a few assumptions about how bending modifies lipid arrangements and surface charges [64–66]. In this sense, lipid and electrostatic properties are not fully integrated. In fact, the electrostatic interaction between constituent lipids can modify lipid parameters, while the latter can influence the way charged lipids interact with each other. As evidenced later, this interdependence, which has been under-appreciated in the past, is a key feature of lipid assemblies. Furthermore, it has been shown that charge discreteness can play an important role,

especially when counterions are multivalent [77, 78]. Owing to all these complexities, it still remains challenging to describe the electrostatic bending of a lipid membrane consistently, without suppressing its important degrees of freedom.

This work is aimed at presenting a unified theoretical approach to the spontaneous bending of lipid membranes (or lipid aggregates) consisting of neutral and anionic lipids immersed in a salty solution, possibly containing multivalent counterions. Our approach is distinct from previous attempts [64–66] in several respects. First, in our approach, the elastic and charge properties of lipids are integrated at the single-lipid level. Accordingly, bending, stretching, and surface charges are taken into account simultaneously and coherently. To this end, we allow lipid parameters to relax at their equilibrium values, which turn out to depend on external parameters within our model – without invoking any further simplification. While our electrostatic analysis is based on the nonlinear Poisson-Boltzmann (PB) equation, it is implemented by incorporation of charge discreteness (thus nonuniform charge distributions), so as to capture 'lateral' and 'transverse' charge correlations [77,78]. This is particularly important when the solution contains multivalent counterions, which give rise to non-uniform charge distributions on the membrane surface. In fact, it has been shown that Ca^{2+} can trigger lipid-tail ordering [70], primarily by shrinking lipid headgroups [79]. This illustrates limitations of any approach that leaves out charge discreteness or heterogeneity in surface charge distributions. Furthermore, charge discreteness has nontrivial impact on how charged (anionic) lipids interact with their counterions, as is particularly the case for multivalent counterions. It tends to enhance lipid-counterion association. Better understanding of the spontaneous bending of a lipid membrane would necessitate a more consistent treatment of the various effects described above.

Our results show how the spontaneous curvature of a membrane, denoted as C_0, can be controlled by the elastic and charge properties of lipids and counterion valence [80]. While the general picture for C_0 emerged from our study in the

absence of multivalent counterions is similar to those presented earlier [64–66], it also points to the significance of treating the elastic and charge properties of lipids consistently. Interestingly, its sign can be inverted by the presence of a small concentration of divalent salts. As a result, the membrane tends to bend toward a more highly charged layer, in contrast to what one may expect from meanfield-type approaches [64–66]. This finding is paralleled by the earlier observation that divalent counterions can induce lipid tail ordering [70] or a negative lateral pressure on the charged layer [71, 79]. Also, this is closely related to and thus may offer a quantitative basis for the observed sensitivity of MS channels to counterion valence [74]. This electrostatic modulation of membrane curvature can be considered as a particular realization of preferred structures (amphiphilic) lipids form in aqueous solution [62], thus offering a molecular basis for the aforementioned various membrane phenomena, which implicate spontaneous membrane curvature or more generally lipid packing properties. Our results show that electrostatic modification of headgroups is a key determinant of the preferred structure (and phase) of lipid aggregates: inverted micelles vs. bilayers (reverse hexagonal vs. lamellar phases).

4.2 Model

In this section, we present our molecular model. After introducing a free-energy description of individual lipids forming a monolayer or a bilayer, we develop our electrostatic model for lipid-counterion interactions: their association and its impact on lipid parameters and membrane bending.

4.2.1 Single-lipid free energy

The free energy of a lipid aggregate (e.g., a monolayer or bilayer) can be expressed in terms of single lipid parameters. Each lipid (ı.e., its packing shape) is fully characterized by its geometrical parameters: the headgroup area (a_h), the area

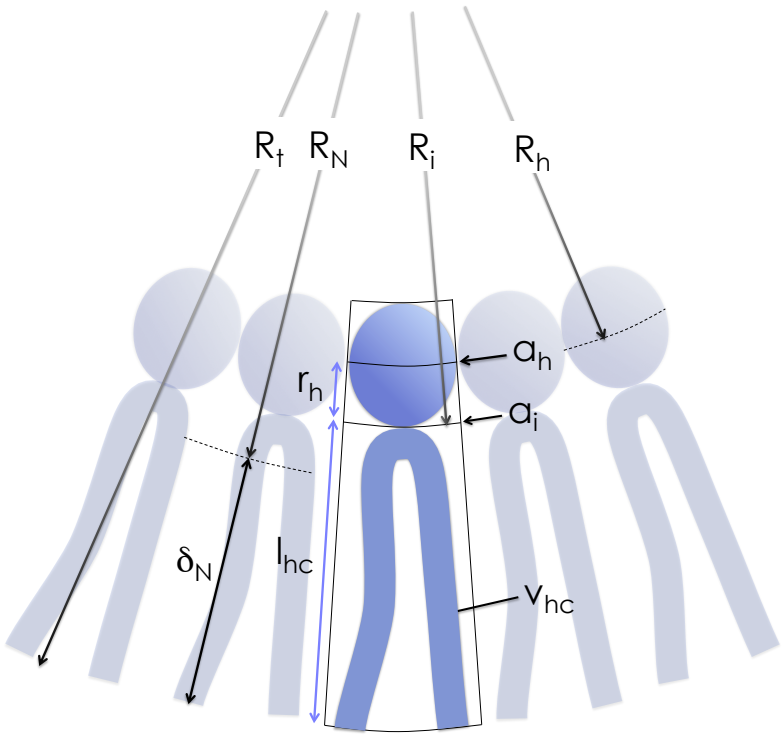

Figure 4.1: The packing shape of a lipid in a lipid membrane is characterized by a few geometrical parameters such as a_h (the headgroup area), a_i (the lipid interfacial area), l_{hc} (the hydrocarbon-chain length), and v_{hc} (the hydrocarbon-chain volume assumed to be constant). There is a simple geometrical relationship between different radii of curvature (see Eq. 4.8).

per each lipid at the headgroup-tail interface (a_i), and the length of its tail or hydrocarbon chain (l_{hc}), as illustrated in Fig. 4.1. The parameter conjugate to a_i is the interfacial tension, γ, arising from the hydrophobicity of hydrocarbon chains, i.e., their tendency to avoid contact with water. The resulting free energy per lipid is γa_i. Similarly, the free energy cost for overlapping two headgroups is described as K/a_h, where K is a constant characterizing the strength of their repulsion. On the other hand, the free energy of a lipid tail assumes the Hookean form of τl_{hc}^2, where τ measures the energy cost for deforming l_{hc}. The total free energy per lipid

in an aggregate can be written as [81]

$$f = K/a_h + \gamma a_i + \tau l_{hc}^2. \tag{4.1}$$

While the first and last term tend to swell the area per lipid, the second term opposes this. Note that different models have been used [82–84] (see Ref. [84] for comparative studies on a few models).

These phenomenological energy terms deserve some discussion. First, the parameters K, γ, and τ reflect the elastic nature of individual lipid molecules, which behave as "molecular springs." On the other hand, the shape parameters, a_h, a_i, and l_{hc} are interrelated, since their changes are subject to the constraint that the volume of each tail, v_{hc}, remains invariant [81,82], which is a reasonable assumption for the lipids in the fluid phase, as is the case for a biologically active membrane.

4.2.2 Electrostatic free energy of a lipid membrane

In addition to the free energy in Eq. 4.1, one has to include the electrostatic contribution. The lipid membrane we consider here consists of zwitterionic (neutral polar) and anionic lipids such as phosphatidylserine (PS) or phosphatidylglycerol (PG). The charged lipids interact not only with each other but also with surrounding counterions, especially multivalent counterions. The crudest simplification may amount to smearing out the lipid charges, but this meanfield-type approximation underestimates their attraction with counterions. While their mutual repulsion tends to keep them equidistant from each other, their association with multivalent counterions can modulate their spatial distribution – one counterion may neutralize more than one lipid charge. In general, lipid demixing can alter how the membrane interacts with opposite charges, especially for multivalent cases. Here we restrict ourselves to the case of monovalent or divalent counterions. In this case, lipid demixing is not expected to be pronounced, since the resulting entropic loss can easily counterbalance the energy gain.

In our approach, anionic lipids are considered as forming a hexagonal lattice as depicted in Fig. 4.2. The solution of the PB equation with this arrangement can be used to calculate the electrostatic free energy without suppressing lipid-charge discreteness. Electrostatic effects on lipid parameters can be analyzed by allowing them to relax at new preferred values – by free-energy minimization. For simplicity, we assume that the geometrical parameters (a_h, a_i, and l_{hc}) take on the same value for both neutral and anionic lipids in the same layer. The regularity in the hexagonal geometry allows us to construct and focus on a unit cell, often referred to as a Wigner-Seitz (WS) cell. Below we present our strategy for constructing the WS cell and calculating the electrostatic free energy.

The monovalent case

In the absence of divalent counterions, each anionic lipid on a hexagonal lattice naturally defines its WS cell; it is placed at the center of the cell (see Fig. 4.3(a)). Depending on the curvature of the membrane, the WS cell resembles a cylinder, a cone, or an inverted cone [62]. The boundary of each WS cell can be approximated as circular one – on average, each anionic lipid will experience radially symmetrical interactions [52]. The average electrostatic energy per charged lipid can be obtained by solving the Poisson-Boltzman (PB) equation in the aqueous phase within a WS cell. The PB equation in the presence of a $(1:1)$ salt can be written as [66]

$$\nabla^2\Psi = \kappa^2 \sinh(\Psi), \tag{4.2}$$

where $\Psi = e\Phi/k_BT$ is the *reduced* electrostatic potential with e the electronic charge, Φ the electrostatic potential, k_B the Boltzmann constant, and T the temperature. The Debye screening length, κ^{-1}, is given by the relation, $\kappa^2 = 8\pi n_0 \epsilon_0 \epsilon_w / k_B T$, where ϵ_0 is the permittivity of free space and ϵ_w is the dielectric constant of water. The PB equation has to be solved with the following appropriate boundary conditions.

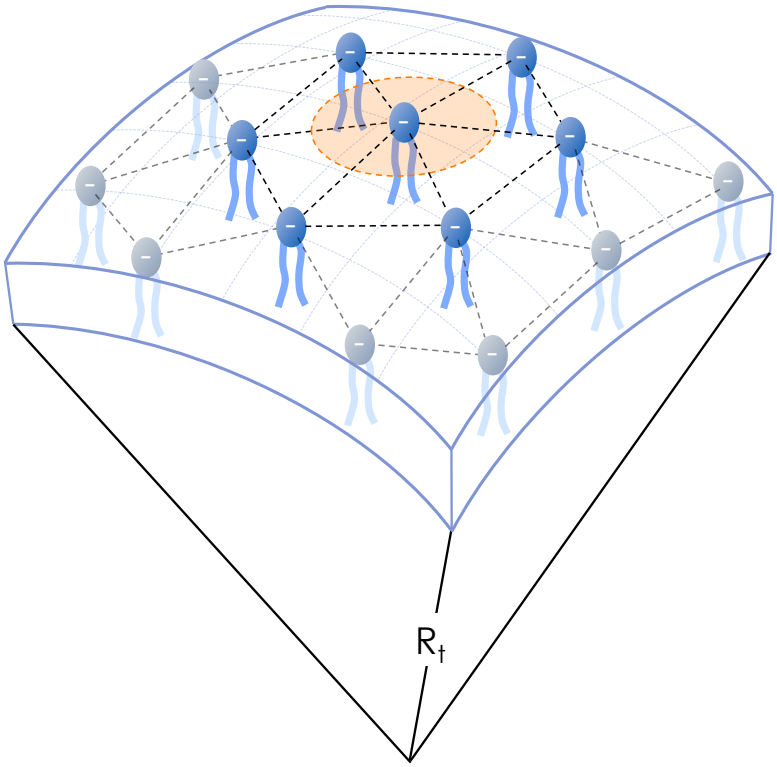

Figure 4.2: Charge discreteness and the spatial distribution of anionic lipids on a spherically curved membrane; for simplicity, neutral lipids are not shown. A hexagonal lipid arrangement as well as a Wigner-Seitz cell (the dashed circle) are highlighted. The central lipid, i.e., the one at the center of the dashed circle, experiences radially symmetrical interactions on average. It thus suffices to consider the central one explicitly and absorb others into a boundary condition (cf. Eq. 4.3).

- The vanishing normal component of electrostatic fields on the cell boundary to reflect the symmetry of WS cells:

$$\mathbf{n} \cdot \nabla \Phi(\mathbf{r})|_{r=R_{\mathrm{WS}}} = 0, \tag{4.3}$$

  with $\mathbf{n}$ the unit vector normal to the WS cell boundary.

- The vanishing electric potential at infinity:

$$\lim_{\mathbf{r}\to\infty} \Phi(\mathbf{r}) = 0. \tag{4.4}$$

- Discontinuity of the electric field across a charged surface with a planar charge density, σ:

$$\epsilon_w \epsilon_0 \frac{\partial \Phi(\mathbf{r})}{\partial r}\bigg|_{\text{above}} - \epsilon_l \epsilon_0 \frac{\partial \Phi(\mathbf{r})}{\partial r}\bigg|_{\text{below}} = \sigma(\mathbf{r}). \tag{4.5}$$

  where ϵ_l is the dielectric constant of lipids and $\sigma_S(\mathbf{r})$ the surface charge density at $\mathbf{r}$.

The electrostatic free energy of a WS cell can be written as [52]

$$\mathcal{F}_{elec} = \frac{\epsilon_0}{2} \int \epsilon_r(\mathbf{r}) \left[\nabla \Phi(\mathbf{r})\right]^2 d\mathbf{r} + k_B T \int \left[n_+ \ln \frac{n_+}{n_1} + n_- \ln \frac{n_-}{n_1} - (n_+ + n_- - 2n_1) \right] d\mathbf{r} \tag{4.6}$$

The first term accounts for the electrostatic energy of the cell, where the integral runs over the entire volume of the WS cell; $\epsilon_r(\mathbf{r})$ is the dielectric constant at $\mathbf{r}$ (e.g., $\epsilon_r = \epsilon_l$ in the lipid phase). The second term describes the entropic penalty for redistributing monovalent salt ions, where $n_+ = n_+(\mathbf{r})$ ($n_- = n_-(\mathbf{r})$) is the concentration of positive (negative) salt ions at the position $\mathbf{r}$ and n_1 is the concentration at infinity. The second integral is over the aqueous phase of the WS cell.

The divalent case

The previous WS approach suppresses finite ionic sizes of counterions. It is thus expected to work well for the monovalent case. Monovalent counterions can only form a *loose* diffusive layer near a charged surface, and their size is not a crucial parameter. However, multivalent counterions interact more strongly with anionic charges [62, 77], and thus charge discreteness plays a more significant role [77]. Accordingly, we implement our WS approach by incorporation of finite ionic sizes of bound divalent counterions. An important consequence is that the counterion charge overcompensates that of an anionic lipid, thus producing nonuniform charge distributions on the membrane surface. To capture this, we treat bound divalent counterion as charged spheres of some diameter D ($D = 3\,\text{Å}$). On the other hand,

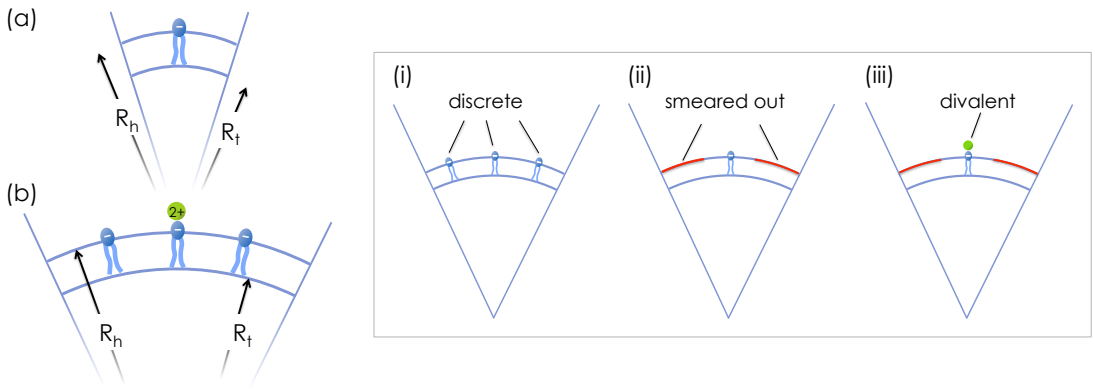

Figure 4.3: Side view of a Wigner-Seitz cell for the monovalent (a) and divalent case (b). For simplicity, neutral lipids are not shown. The radius of curvature R_t (R_h) is measured with reference to the surface of tail ends (headgroups). For the monovalent case (on the left), one anionic lipid defines one WS cell. In the divalent case, however, each WS cell is constructed so as to contain one divalent counterion. Finite ionic sizes of both the lipid and counterion charges are thus taken into account. Our electrostatic analysis in this case consists of three steps (see the box on the right). (i) First, we consider a membrane with discrete backbone charges in a (1:1) salt. The electrostatic free energy of this setting is $\mathcal{F}_1^{\rm WS}$. (ii) Compared to (ii), the membrane charges are smeared out except the central one. The corresponding electrostatic free energy is $\mathcal{F}_2^{\rm WS}$. (iii) Finally, we introduce a divalent counterion in (b). The electrostatic free energy of this distribution is denoted as $\mathcal{F}_3^{\rm WS}$.

monovalent ions will remain as featureless particles as often assumed in the PB approach. Eq. 4.6 can still be used to calculate the electrostatic free energy. The difference is that the WS cell now contains a divalent counterion at its center. This can be implemented through the electrostatic boundary conditions as discussed earlier (see Eq. 4.3).

To further proceed with the free energy calculation in the presence of divalent counterions, we "reconstruct" our WS cells so that each cell now contains one divalent counterion paired with a central anionic charge right below, as illustrated in Fig. 4.3(c). While the central lipid is treated as discrete as before, other lipid charges are assumed to be smeared out on the surface of the membrane. The motivation is that the ion (counterion-central lipid) pair as a whole will not interact

strongly with other lipids, since the pair is monovalent and distant from other backbone charges. As a result of this simplification, the WS cell restores cylindrical symmetry, which significantly reduces the computational load. There is, however, *energy shift* because of this alternation of the backbone charges, which is equivalent to shifting the energy reference and has to be corrected.

To compensate for the energy shift, compare the two different backbone charge distribution within each WS cell: (a) a discrete lipid charge distribution (Fig. 4.3a) and (b) a discrete central lipid charge in the uniform background of other lipid charges (Fig. 4.3a). The free energy difference between the two is the free energy change caused by the reference shift. In the former case, the free energy of each lipid is calculated based on the approach presented in the previous subsection (the monovalent case), where a WS cell was defined by one charged phospholipid. The electrostatic free energy of the WS cell defined here is the single-lipid WS free energy times the number of anionic lipids in the WS cell, and can thus be obtained.

In summary, our free energy calculation consists of three intermediate steps, as depicted in Fig. 4.3. First, the free energy, $\mathcal{F}_1^{\mathrm{WS}}$, is calculated for the WS cell in the absence of any bound divalent counterion (Fig. 4.3a). Second, the free energy of the WS cell in (b), $\mathcal{F}_2^{\mathrm{WS}}$, is the same as in (a) except for the backbone charge distribution. The correction term to compensate for the energy shift would be $\Delta\mathcal{F}^{\mathrm{WS}} = \mathcal{F}_2^{\mathrm{WS}} - \mathcal{F}_1^{\mathrm{WS}}$. Third, the free energy, $\mathcal{F}_3^{\mathrm{WS}}$, is calculated for the WS cell with a bound counterion on the top of the central lipid charge and all other lipid charges smeared (Fig. 4.3c). The correct free energy of the WS cell with a bound divalent counterion is, thus, $\mathcal{F}_{\mathrm{WS}} = \mathcal{F}_3^{\mathrm{WS}} - \Delta\mathcal{F}^{\mathrm{WS}} = \mathcal{F}_3^{\mathrm{WS}} - \mathcal{F}_2^{\mathrm{WS}} + \mathcal{F}_1^{\mathrm{WS}}$.

4.3 Membrane Free Energy

4.3.1 Monolayers

In this section, we construct the total free energy of a lipid bilayer membrane (per lipid), as a function of a few independent parameters. Our preferred membrane parameters are the membrane curvature (C) and the headgroup area (a_h), from which other parameters are derivable. In the divalent case, an important electrostatic parameter is the planar density of divalent counterions, which sets the area of each WS cell, $A_{\rm WS}$. Notice that C_0 is specified only with respect to a reference surface. A convenient choice is the so called 'neutral surface,' where bending and stretching are decoupled [81, 83, 84]. For a monolayer, the location of the neutral surface can vary appreciably as the elastic properties of constituent lipids are altered, as evidenced later (see Fig. 4.5).

The monolayer free energy (in the presence of divalent counterions) can be written as

$$F(C, a_h, A_{\rm WS}) = \frac{K}{a_h} + \gamma a_i + \tau l_{hc}^2 + \mathcal{F}_{\rm WS}\frac{a_h}{A_{\rm WS}} + \frac{1}{A_{\rm WS}} \ln\left(\frac{a_{\rm ion}}{n_2 A_{\rm WS} v_{\rm ion}}\right), \qquad (4.7)$$

where $a_{\rm ion}$ and $v_{\rm ion}$ are the cross sectional area and volume of divalent ions, respectively, and n_2 the bulk density of divalent ions. (Recall a_i is the average area per lipid water interface, l_{hc} is the hydrocarbon length; K, γ, and τ are corresponding conjugate parameters characterizing the elastic properties of phospholipid molecules.) The second last term accounts for the electrostatic free energy per lipid molecule. The last term in Eq. 4.7 represents the entropic penalty for confining divalent ions to the membrane surface. For $n_2 = 0$, the last term should be dropped; also the meaning of $A_{\rm WS}$ is different, as discussed earlier.

Other parameters such as a_i and l_{hc} are not independently changeable but are derivable from C, a_h, and v_{hc}, the volume of each lipid tail (assumed to be a constant). To see this, note that a_h and a_i subtend the same solid angle with

respect to the common origin but represent different radii of curvature (they are 'parallel surfaces' of each other [82,84]), i.e., $R_{\rm h} = 1/C + l_{hc} + r_h$ and $R_{\rm i} = 1/C + l_{hc}$, respectively. With the convention that the curvature C of the monolayer in Fig. 4.1 is negative, the area a_i can be written as

$$a_i = a_h \left(\frac{1/C + l_{hc}}{1/C + l_{hc} + r_h} \right)^2 . \tag{4.8}$$

To relate l_{hc} to other geometrical parameters, consider the volume of a spherical shell specified by its outer and inner radii, $R_{\rm h}$ and $R_{\rm i}$, respectively. The volume v_h is then the shell volume divided by $4\pi R_{\rm h}/a_h$. This consideration leads to

$$v_{hc} = \frac{a_i}{3\left(\frac{1}{C} + l_{hc}\right)^2} \left[\left(\frac{1}{C} + l_{hc} \right)^3 - \left(\frac{1}{C} \right)^3 \right] . \tag{4.9}$$

This equation can be solved for l_{hc} in terms of v_{hc}, C, and a_h. The relations in Eqs. 4.8 and 4.9 enable us to express the free energy of a lipid monolayer in terms of C, a_h, and $A_{\rm WS}$, as assumed in Eq. 4.7.

4.3.2 Bilayers

In principle, our free energy analysis can be extended to the case of a bilayer membrane. Imagine coupling two monolayers into a bilayer and bending it. Some subtlety arises from the fact that the bilayer coupling represents a *global* constraint. How this constraint is felt by individual lipids is model dependent [35,66,84,85]. A few molecular models for lipid arrangements in a bilayer have been known. Good examples are 'connected' and 'unconnected' bilayers [84]. The connected bilayer model assumes that the two layers are not allowed to slide against each other; they are "glued" together. In the unconnected bilayer model, each layer is permitted to slide past the other. Not surprisingly, there is no unique way of analyzing lipid arrangements caused by bending, and thus the computation of bending moduli replies on a specific model [35, 84]. On the other hand, the (local) spontaneous

curvature of a lipid bilayer membrane reflects any asymmetry in molecular "shapes" of lipids between the two layers and is considered as a *local* quantity (unless the two layers are physically coupled by any mechanism) [67]. It suffices to use the unconnected model in the computation of C_0 [80].

In contrast to the case of monolayers, the neutral surface of a symmetric bilayer membrane always coincides with its midplane. A charge imbalance between the two layers, for instance, can alter this picture. Nevertheless, one can argue that this effect is minor: The electrostatic effect can be considered as renormalizing γ, which has a minor effect on the neutral surface, as evidenced later (see Fig. 4.5). With this simplification, we measure C of a bilayer membrane with respect to the midplane, whether the membrane is symmetrically charged or not, while we explicitly construct the neutral surface of each layer.

In our approach, the radius of curvature is always measured from the end of the hydrocarbon tails of lipid molecules (See Fig. 4.1). For a monolayer, a more convenient choice is its neutral surface, which is significantly different from the surface formed by the tail ends. However, our monolayer analysis is only an intermediate step in our approach. For a bilayer, however, it proves useful to use the tail-end surface as a reference, which approximately represents the neutral surface as discussed earlier. (Note that since the thickness is not necessarily the same for the two layers if bent, the interface between the layers is not always identical to the midplane) Even in the unconnected case, the two layers should remain attached to each other, and their curvatures with reference to their interface are the same in magnitude but are opposite in sign. This is the only constraint imposed on each layer. This implies that the total free energy of the bilayer per lipid can be written as

$$F_{\rm bl} = F^{out}(C, a_h^{out}, A_{\rm WS}^{out}) + F^{in}(-C, a_h^{in}, A_{\rm WS}^{in}), \tag{4.10}$$

where the superscripts 'out' and 'in' refer to the inner and outer layer, respectively.

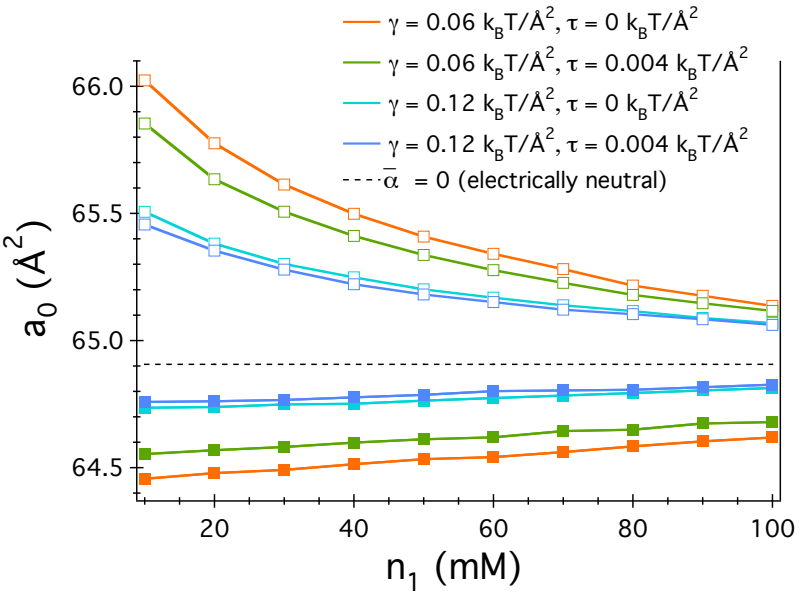

Figure 4.4: Relaxed headgroup area lipids in a monolayer as a function of monovalent salt concentration, n_1, in presence (filled squares) or absence (unfilled squares) of divalent counterions. Here $\overline{\alpha} = 0.3$, lipid parameters γ and τ are adjusted together with K such that $a_0 = 64.9\,\text{Å}$ for $\overline{\alpha} = 0$ (uncharged case). In the presence of 5 mM divalent counterions, the headgroup area shrinks compared to the corresponding uncharged case.

This free energy is to be minimized with respect to five parameters: C, a_h^{in}, a_h^{out}, A_{WS}^{in}, and A_{WS}^{out}, as detailed in the next section.

4.4 Results

4.4.1 Monolayers

Optimal headgroup area

We have first calculated the equilibrium or optimal headgroup area a_0 of a monolayer by free energy minimization for a planar surface ($a_0 = a_h = a_i$), in the presence or absence of divalent counterions, and plotted our results in Fig. 4.4. This effort illustrates how lipid and electrostatic parameters influence each other. We have

chosen $\overline{\alpha} = 0.3$ and used various choices of lipid parameters as depicted in different colors (see the legend). In all cases, we have chosen K such that $a_0 = 64.9\,\text{Å}^2$ for the corresponding electrically neutral surface ($\bar{\alpha} = 0$, not to be confused with the 'neutral surface'), as marked by the dotted line. This explains why a_0 values tend to the dotted line as n_1 increases, i.e., as the electrostatic interaction becomes more screened. In the absence of divalent counterions (the top four curves with unfilled symbols), lipid charges enlarge the headgroup more effectively at lower salt concentrations, as expected.

In the presence of as small a concentration as 5 mM of divalent counterions (the bottom four curves with filled symbols), however, the headgroup shrinks compared to the corresponding uncharged case (the dotted line). Intriguingly, the general trend observed for the monovalent case is reversed. This is not unexpected, since in this case nonuniform charge distributions on the membrane surface can induce a negative lateral pressure, which tends to shrink the area occupied by each lipid. An important consequence of this is that the presence of a small concentration of multivalent counterions can reverse the sign of C_0 of a lipid membrane, as evidenced later. Importantly, the headgroup shrinkage in this case is well correlated with the observed MS channel closing induced by trivalent counterions (Gd^{3+}) [74] – the main difference is that Gd^{3+} is expected to shrink lipid headgroups more effectively than Mg^{2+} or Ca^{2+}.

In both cases (filled and unfilled symbols), the electrostatic effect is less significant if γ is larger (thus the monolayer is stiffer). This is already hinted in our finding that the tail elasticity is less important for larger γ. Our results in Fig. 4.4 illustrate how the elastic and charge properties of lipids are interrelated.

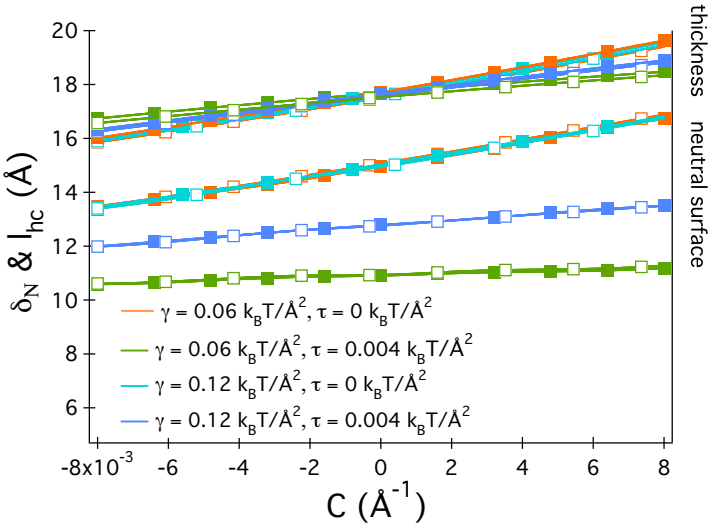

Figure 4.5: Location of neutral surface, δ_N, and thickness, l_{hc}, of a lipid monolayer, as a function of the curvature C. We have chosen $n_1 = 50\,\text{mM}$ and $\overline{\alpha} = 0.3$. Our results here show how δ_N implicates lipid elastic parameters γ and τ. Intriguingly, δ_N is almost independent of salt ions. Despite the *seeming* gradual change in δ_N with C, the location of the neutral surface remains invariant if "corrected" for thickness change (see l_{hc} curves).

Neutral surface

Our analysis in this section so far is limited to a flat surface. The free energy of a monolayer (or a bilayer), if bent, is most conveniently expressed with respect to its neutral surface, which will not suffer from stretching upon bending. Imagine bending a uniform elastic sheet, which has constant material properties and thickness. By symmetry, the geometric midplane coincides with its neutral surface. However, this picture does not necessarily apply to a lipid aggregate, except when it is a symmetrical bilayer.

In our approach, it is straightforward to find the neutral surface. For a flat layer, $a_h = a_i = a_0$. Upon bending, a_h will no longer remain the same as a_0 but its equilibrium value can be obtained by free energy minimization; similarly, the equilibrium l_{hc} can be estimated. For spherical bending we consider here, the

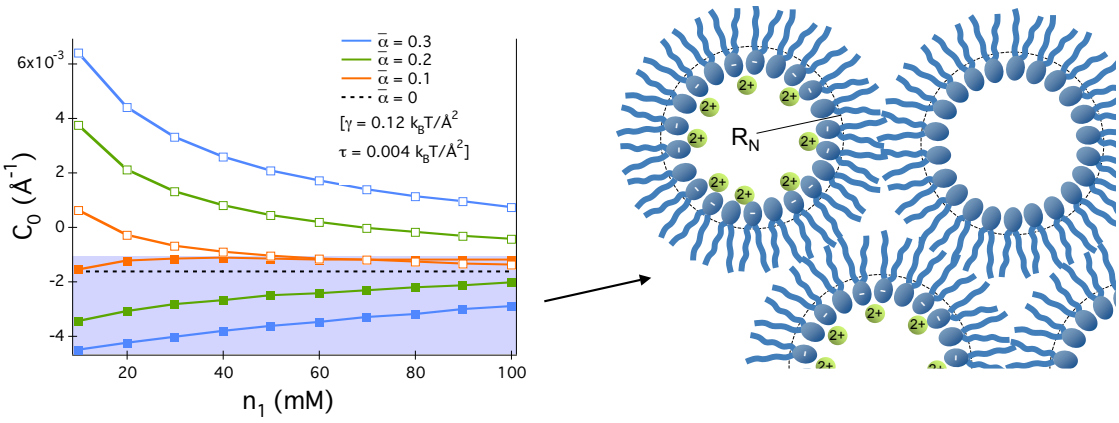

Figure 4.6: Spontaneous curvature of a charged lipid monolayer as a function of monovalent salt concentration n_1 for a few choices of $\bar{\alpha}$: $\overline{\alpha} = 0, 0.1, 0.3$. The lipid parameters have been chosen to mimic PS (phosphatidylserine): $\gamma = 0.12\, k_BT/\text{Å}^2$ and $\tau = 0.004\, k_BT/\text{Å}^2$. When the charge on the lipid is turned off by lowering pH, the spontaneous curvature C_0 is negative. When the fraction of charged lipids increases, the sign of C_0 can be inverted, as is particularly the case for $\bar{\alpha} > 0.2$. In the presence of 5 mM divalent counterions in solution, however, $C_0 < 0$ for the entire range of n_1. Divalent counterions invert the sign of C_0 more effectively for larger $\bar{\alpha}$.

neutral surface can be located from a purely geometrical consideration: Imagine translating the equilibrium headgroup area a_h in the normal direction – the neutral surface is where the cross-sectional area of lipid is the same as a_0.

Let δ_N be the location of the neutral surface for a monolayer, defined as the distance from the end of lipid tails (see Fig. 4.1). To examine the dependence of δ_N on the elastic and charge properties of lipids, we have plotted δ_N (as well as l_{hc}) in Fig. 4.5, in the presence or absence of divalent counterions. We have chosen a few combinations of γ and τ (see the legend). Let's compare the two cases: $\gamma = 0.06\, k_BT/\text{Å}^2$ and $\gamma = 0.12\, k_BT/\text{Å}^2$ (with the same $\tau = 0.004\, k_BT/\text{Å}^2$). The neutral surface for the "stiffer" case (larger γ) is closer to the headgroup-tail interface, as expected from the following picture; as $\gamma \to \infty$, the neutral surface is expected to coincide with the interface at which the interfacial tension operates. As $\tau \to 0$, the neutral surfaces for the stiffer and softer cases tend to collapse onto

each other. This is not surprising, since the location of the neutral surface is solely determined by the competition between the headgroup repulsion and the surface tension; for our particular choice of the monolayer free energy in Eq. 4.7, one can show that for $\tau = 0$ the neutral surface coincides with the headgroup region [84], independently of γ, as also shown in our results for $\tau = 0$. The gradual change of δ_N is to reflect the thickness change. If the hydrocarbon chain deforms uniformly, the "relative" position (or the position along the contour of the chain) of the neutral surface is invariant.

Importantly, the position of the neutral surface is almost insensitive to salts. This implies that it is mainly determined by non-electrostatic contributions. In light of our results in Fig. 4.4, this finding is puzzling but can be understood as follows. The electrostatic contribution to the free energy in Eq. 4.7 can be considered as renormalizing γ. As indicated above, for $\tau = 0$, δ_N is independent of γ [84] (electrostatic effects as well), in good agreement with our results in Fig. 4.5. For $\tau > 0$, δ_N changes as γ changes, but the change is only moderate ($\approx 10\,\%$), even when γ doubles. We expect the change to be more pronounced for larger τ. It is also conceivable that the dependence of δ_N on electrostatic effects may be model dependent. (Another commonly used model is the "harmonic-spring" model for a lipid aggregate [83, 84].) We believe that experimentally more accessible quantities such as C_0 are not quite model dependent, as is particularly the case for a bilayer, where the non-electrostatic contributions to C_0 of the two layers balance out. This together with our results in Fig. 4.5 allow us to choose the midplane of a bilayer as its neutral surface, even if the bilayer is asymmetrically charged, as long as the non-electrostatic properties of the two layers are the same. This does not mean that the C_0 of a bilayer is not sensitive to charge asymmetry as shown below.

Spontaneous curvature of a monolayer and the formation of H_{II} phases

The preferred structure of lipid membranes is controlled by packing shapes of the constituent lipids [62] and thus by the ionization status of headgroups [75]. Indeed, a recent experiment on PS-containing membranes shows that at low pH ($\bar{\alpha} \simeq 0$) the membrane prefers to form reverse hexagonal (H_{II}) phases (thus $C_0 < 0$), while the sign of C_0 is inverted at neutral or high pH. Recall that we only consider spherical bending so as to utilize the symmetry assumed in Fig. 4.2. However, this will not limit the applicability of our results. What our approach predicts is the preferred structure or morphology of lipid aggregates, which will eventually dictate phases they form. The only structural requirement for the formation of H_{II} phases is the inverted cone shape [63], which translates into $C_0 < 0$. To offer a theoretical basis of the observation with PS-containing membranes, we have calculated the spontaneous curvature of a monolayer for a few choices of $\bar{\alpha}$ and plotted our results in Fig. 4.6, as a function of n_1. The lipid parameters have been chosen so as to mimic PS – negative C_0 when $\bar{\alpha} = 0$: $\gamma = 0.12\, k_B T/\text{Å}^2$ and $\tau = 0.004\, k_B T/\text{Å}^2$. Our results (open symbols) are illuminating, since they imply that at low pH ($\bar{\alpha} \simeq 0$) PS-containing membranes tend to form H_{II} phases (see the illustration), while at higher pH lamellar phases (or positively-curved structure) are stabilized by headgroup repulsions. Our results also offer an alternative mechanism of H_{II}-phase formation at neutral pH, i.e., H_{II} phases stabilized by charge correlations due to divalent counterions. Charge correlations reduce the optimal area of charged headgroups, as already hinted in Fig. 4.4. This theoretical prediction is paralleled with the longstanding observation that divalent counterions induce H_{II} phases of lipids, which would otherwise form lamellar phases [63].

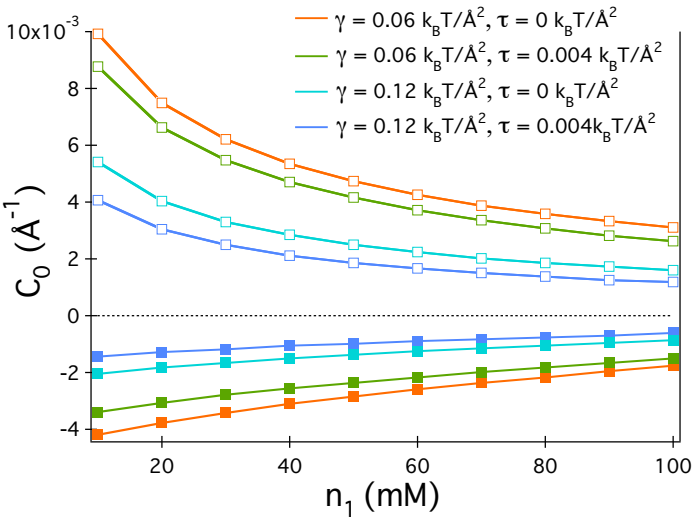

Figure 4.7: Spontaneous curvature of an asymmetrically charged lipid bilayer ($\overline{\alpha} = 0$ for the inner layer, and, $\overline{\alpha} = 0.3$ for the outer layer) as a function of monovalent salt concentration n_1. The presence of 5 mM divalent counterions in solution inverts the sign of C_0. In other words, the bilayer tends to bend toward the charged layer.

4.4.2 Bilayers: spontaneous curvature of asymmetrically charged bilayers

In contrast to the case of a lipid monolayer, the preferred curvature of a lipid bilayer, i.e., the value of C at which the membrane free energy is minimized, is determined by *asymmetries* between the two layers. As a result, a perfectly symmetrical bilayer has a vanishing preferred curvature. There are two kinds of asymmetry (see Refs. [67, 68, 85] and references therein). First, any asymmetry in packing shapes between the constituent layers results in a nonzero spontaneous curvature. This reflects local properties of the bilayer. Second, any mismatch in relaxed areas of the two layers can induce membrane bending. Here the relaxed areas refer to the neutral surfaces, and are invariant upon bending if the two layers are 'unconnected' [86]. The resulting preferred curvature has a global or non-local character. For a bilayer we consider here (one consisting of two identical layers

except for charge properties), the non-local preferred curvature can be expressed as $C_0^{nl} = (a_0^{out} - a_0^{in}) / [(a_0^{out} + a_0^{in})\,\delta_N]$ [67]. Note here that δ_N is the location of the neutral surface of each layer for $C = 0$ and is essentially the same for both layers. In our approach, we mainly focus on the computation of C_0, the (local) spontaneous curvature; C_0^{nl} can be readily read off from our results in Fig. 4.4. Furthermore, in a more general case, C_0^{nl} is also influenced by the number of lipids in each layer [67,68,85]. In this sense, C_0^{nl} is a less intrinsic quantity than C_0. Also, as it turns out, the interrelationship between lipid properties and bending is much less obvious for C_0 (cf. Fig. 4.8), and we focus on calculating C_0.

The simultaneous presence of both local and global effects makes it challenging to determine C_0 and C_0^{nl} separately. To focus on C_0, we allow the bilayer to relax at its preferred area difference per lipid, i.e., $\Delta a_0 = a_0^{out} - a_0^{in}$. This is equivalent to minimizing the free energy of each layer independently of the other layer with respect to the curvature of the bilayer. To be specific, we have considered a bilayer, in which the inner layer is neutral, while the outer layer contains 30% ($\overline{\alpha} = 0.3$) charged lipids. Our results can then be extended to the case in which the inner layer is charged – simply by changing the sign of C_0. Except for the charge properties, the two layers are assumed to be identical. Fig. 4.7 displays C_0 as a function of monovalent salt concentration, n_1, in the presence or absence of divalent counterions. In the absence of divalent counterions (unfilled symbols), the electrostatic repulsion between charged lipids induces a positive curvature. In other words, the membrane tends to bend toward the electrically-neural, inner layer. This is paralleled by our finding that the repulsion enlarges the headgroup area (see Fig. 4.4). However, it is worth noting that our C_0 results reflect both in-plane and out-of plane deformations of the membrane, while only in-plane deformations are taken into account in our a_0 calculations. Curvature can be induced not only through in-plane lipid deformations (i.e., a_0 changes in the outer layer) but also through the modification of the ionic cloud of the outer layer. Upon bending toward the inner

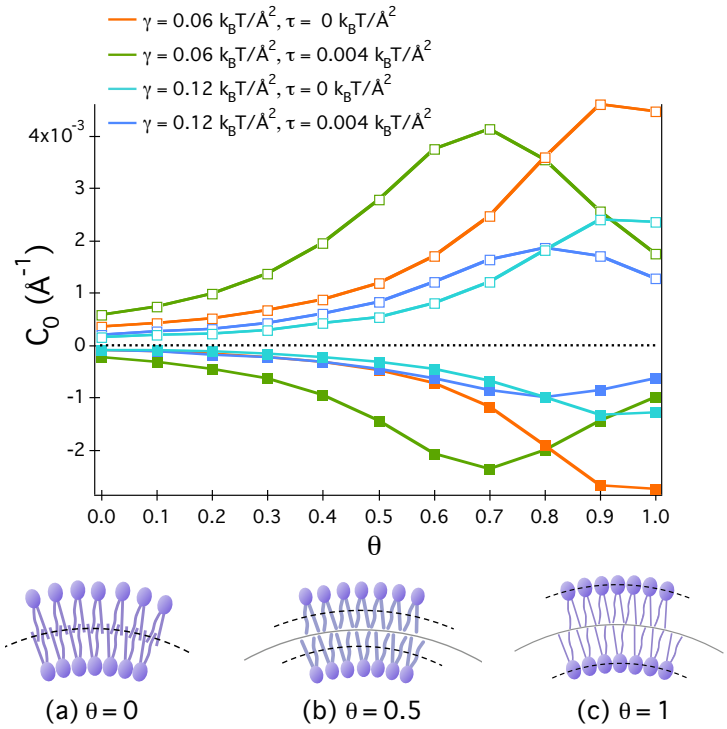

Figure 4.8: Spontaneous curvature of an asymmetrically charged lipid bilayer ($\overline{\alpha} = 0$ for the inner layer and $\overline{\alpha} = 0.3$ for the outer layer) as a function of θ, the relative position of the neutral surface pre-chosen for each monolayer. These results show that C_0 is sensitive to θ, demonstrating the significance of determining the location of the neutral surface consistently – by free energy minimization. (a)-(c). Illustrations of a few hypothetical models of bilayer bending, corresponding to a few choices of θ. While (a) represents the connected model, (c) can be realized if tails are flexible (or headgroups are "bulky"); these two limiting features are combined in (b).

layer, the ionic cloud expands [66]. It is this entropic gain that induces a positive C_0.

On the other hand, the presence of 5 mM of divalent ions inverts the sign of spontaneous curvature for the entire range of n_1 shown in the figure, as already hinted in Fig. 4.4: the non-uniform charge distribution on the outer layer in this case means that the layer can lower the electrostatic free energy by curving inward (via both in-plane and out-of plane deformations), inducing a negative spontaneous

curvature. As n_1 increases, however, the electrostatic effect diminishes as indicated in the figure.

In both monovalent and divalent cases, the electrostatic effect is more pronounced for smaller γ or τ, since the membrane is more easily deformable in that case; it is worth noting that τ is also implicated in C_0.

So far we have determined C_0 and δ_N simultaneously and systematically without using any ad hoc assumption about surface charges, which may obscure the physical picture of electrostatic bending. Our approach has enabled us to determine such parameters as δ_N and a_0 consistently with electrostatic interactions. In the past, however, simplification has often been invoked, which amounts to using pre-chosen δ_N for a membrane without the benefit of derivation [66]. To test this, we have used pre-chosen values of the position of the neutral surface and plotted the resulting C_0 in Fig. 4.8. Here θ describes the relative position of the neutral surface, For instance, $\theta = 1$ means that the neutral surface coincides with the headgroup region, while $\theta = 0$ corresponds to the connected case; for $\theta = 0.5$, the neutral surface lies halfway between the head-tail interface and the midplane of the bilayer. As θ changes between 0 and 1, C_0 changes appreciably and nontrivially. (In our calculations, $\theta \approx 0.7$-0.8 for $\tau = 0.004\, k_B T/\text{Å}^2$ and $\theta \approx 0.8$-0.9 for $\tau = 0$.) Our results in Fig. 4.8 clearly suggest that θ has to be determined according to the energetics of each layer. Interestingly, the peak of C_0 appears to occur around our estimated θ value. This is not unexpected, since each layer tends to bend with respect to its neutral surface.

4.5 Conclusions

In conclusion, we have presented a unified approach to the electrostatic modification of lipid headgroups and its impact on the spontaneous curvature of a lipid

membrane, interacting with monovalent or divalent salt ions. Our effort is distinct from the existing approaches in two major respects. First, in our approach, the elastic and charge parameters are combined in a more coherent manner. This is accomplished by free-energy minimization with respect to lipid parameters for given C (in a salt-dependent manner). Accordingly, the lipid parameters are allowed to relax at their equilibrium values for given C. Our approach thus does not rely on any assumption about how bending influences surface charges. Second, our approach captures lateral and transverse charge correlations; to this end, we have implemented the Poisson-Boltzmann approach by incorporation of finite ionic sizes, especially for describing the association of a divalent counterion with an anionic lipid.

A general picture that has emerged from our approach is paralleled by the experimental observation that the electrostatic modification of lipid headgroups is one of the key determinants of lipid packing, which in turn influences membrane functions [74] or the structure and phase of lipid aggregates [75]. On the other hand, the relative role of electrostatic [64–66] and protein-based bending [67] is unclear. Nevertheless, our results reported here can offer a quantitative basis for various experiments with pure lipid membranes (e.g., Ca^{2+}-induced membrane fusion [69–71]) or those with biological membranes where ion valence is a key parameter (e.g., Ref. [74]).

In principle, our approach can be extended to the analysis of other membrane parameters such as (both mean and Gaussian) bending moduli as well as to the study of Ca^{2+}-induced lipid ordering and lipid phase transitions. A related (but more involved) problem is membrane perturbations by cationic antimicrobial peptides (CAPs) [4,6,20,87]. CAPs are known to selectively disrupt bacterial (cytoplasmic) membranes – initially by asymmetrical incorporation into the outer layer, carrying a large fraction of anionic lipids (PG). Interestingly, they can significantly soften their binding membranes [88], likely through the combined effects: membrane thin-

ning and charge-correlations. Both effects can soften the membrane. We leave this membrane-softening mechanism for future consideration.

Chapter 5

Conclusions and Proposal for Future Considerations

5.1 Conclusions

In this thesis, we have developed coarse-grained models to account for the interactions of charged lipid membranes with antimicrobial peptides (AMPs) and surrounding salt ions. Our approach integrates the electric and elastic properties of lipids and AMPs in an unified manner as they are intrinsically interrelated. The charge properties of a lipid membrane is determined by the collective organization of constituent lipids which is itself adjusted by electrostatic interactions. Lipid membranes can undergo conformational changes in response to external perturbations. Cationic AMPs utilize the difference in the composition of anionic and zwitterionic phospholipids to discriminate and attack their target cells from a crowd of host cells. Salt ions can induce spontaneous curvature or modify the bending rigidity of a lipid bilayer through electrostatic interactions.

Our model for the membrane-disrupting activity of AMPs integrates a few distinct and pronounced interactions of AMPs with lipid bilayers. Poisson-Boltzmann approach has been implemented for description of electrostatic interactions while hydrophobic energy has been added to account the amphipathicity of AMPs. We

have calculated the surface coverage of AMPs embedded in the lipid headgroup-tail interface and resulting fractional area change, $\Delta A/A$, for a wide range of peptide parameters. Our results, while reproducing some known and important features of antimicrobial activity, shed light on how peptide parameters can be adjusted (in a membrane and solvent dependent way) to optimize AMPs selective activity. We have shown that antimicrobial activity of AMPs, can be optimized at peptide charge $Q \gtrsim 4$. The optimal charge is larger for larger salt concentration. The underlying physics of this phenomenon has been traced back to the interplay between electrostatic energy and entropic penalty of the redistribution of salt ions (around AMPs and membrane) in minimizing the free energy of the system. We have also studied the formation of spontaneous AMP-induced pores on a lipid bilayer, considering the growth of a pore as a barrier crossing process. Our results show that, for host cells, a large energy barrier makes the growth of a spontaneous pore improbable while this barrier is significantly smaller for microbial membranes.

In this thesis, we have also presented an approach to the electrostatic modification of lipid headgroups and its impact on the spontaneous curvature of a lipid membrane. We have combined the elastic and electrostatic properties in a coherent manner by minimizing the free energy over a wide range of parameter space. Lateral and transverse charge correlations are incorporated by considering the finite size and discrete distribution of ions. Our results can offer a quantitative basis for various experiments with pure lipid membranes.spontaneous bending of an asymmetrically charged lipid membrane. We have shown the significant effect of salt ions on the spontaneous curvature, C_0, of a lipid membrane. Presence of a small concentration (5 mM) of divalent ions in solution inverts the sign of C_0, compelling the membrane to bend toward the charged surface, thus stabilizing reverse hexagonal (H_{II}) phases. .

5.2 Proposals for Future Works

5.2.1 An analytical approach for peptide-lipid bilayer binding

In chapter three of this thesis, we presented a detailed computational approach to calculate the energetics of peptide binding. The calculation scheme was based on solving the nonlinear Poisson-Boltzmann (PB) equation. The results of PB equation were utilized in a statistical physics formalism to compute the free energy of membrane-peptide-solution system. The equilibrium state of the system was found by minimization of the free energy. Regarding the computing time, solving the nonlinear PB equation was the major part of the calculations. Nevertheless, the PB equation was not a dominant part of the computational flowchart of the whole project. In this section, we propose an approach to lower the computational load of PB equation. In systems with low charge densities, the PB equation can be replaced by its linear version, the Debye-Hückel (DH) equation. However, for the peptide-lipid bilayers system, the DH equation cannot be applied due to the high electric charge of the peptides.

In this section, we develop a coarse-grained semi-analytical approach to calculate the binding energy of a thin peptide on a lipid membrane. More specifically, we find an analytical approach to compute the free energy of a Wigner-Seitz (WS) cell as a function of its radius R_{WS} and peptide-membrane parameters. As introduced in chapter 3 of this thesis, a WS cell defines the area per each bound peptide. The method we present in this section applies to peptides that are adsorbed on the membrane- water interface and are not inserted among headgroup area of the lipids.

A peptide is modeled as a thin disk with area a_p and electric charge of Q. However, the following approach can be extended to account for other geometries with the thickness suppressed. The membrane is a thin layer, assumed to be made of

neutral and charged lipids with $\overline{\alpha}$ the average fraction of charged lipids and a_0 the average headgroup area of the lipid molecules. Also, the membrane is immersed in a (1:1) salt solution with the Bjerrum length, ℓ_B , and inverse Debye length, κ , defined by $\kappa^2 = 8\pi n_0 e^2/\epsilon_w \epsilon_0 k_B T$ where n_0 is the salt concentration, $-e$ the electronic charge, ϵ_w and ϵ_0 the dielectric permittivity of water and vacuum, and $k_B T$ is the thermal energy. The geometrical consideration for peptide and membrane in this section is similar to that in Reference [20]. Suppressing the thickness of membrane is justified by the low dielectric constant of lipids ($\epsilon_l = 2$) and the typical thickness of lipid bilayers $\sim 40\,\text{Å}$. Low dielectric constant and large thickness prevents the electric field to penetrate to the other side of the membrane. Thus, the membrane acts like a semi-infinite plate or, alternatively, a thin layer through which the electric field cannot cross.

The approach we propose here is based on the solution of the one-dimensional Poisson-Boltzmann equation. The electrostatic energy and the free energy of a charged surface immersed in an (1:1) salt can be derived analytically following reference [89]. A mean-field approach to calculate the free energy of a peptide bound to the membrane is to consider the average charge density: all peptide charges are smeared out on the surface. The net charge density reads $\sigma_{net} = -e\overline{\alpha}/a_0 + Q\sigma_S$ where σ_S is the surface density of bound peptides. One can use σ_{net} to calculate the free energy of binding. However, the main drawback is that this approach underestimates the effect of the charge correlations which is mainly through the demixing of charged lipids. Charge correlations increase the binding energy and trigger more peptide binding.

Here, we suggest a method to take into account the demixing of lipids in a non-trivial way and calculate the free energy of a WS cell. That is, the membrane is divided into two main zones: (*i*) the zone that includes a peptide and membrane within a specified area from the peptide, A_S, surrounded by solvent; (*ii*) bare membrane in solvent. Zones 1 and 2 are illustrated in Fig. 5.1. In this approach,

phospholipid molecules are able to relocate between zones 1 and 2. Intuitively, the fraction of charged lipids should depend on the distance to bound peptide due to electrostatic interaction. On average, zone 1 should be more populated with anionic lipids than zone 2. For simplicity, we assume the fraction of charged lipids is uniform in each zone and is denoted by α_1 and α_2 in zones 1 and 2, respectively. α_1 and α_2 are to be determined by minimization of the free energy subject to the constraint that the total number of lipids is conserved over the WS cell area. To find the free energy of the WS cell, zones 1 and 2 are treated separately, each zone is considered as a charged layer in an electrolyte. This is a nontrivial approximation, its accuracy can be, however, checked *a posteriori*. The average surface charge density in each zone is $\sigma_1 = Q/A_S - e\alpha_1/a_0$ and $\sigma_2 = -e\alpha_2/a_0$. Following reference [89] the free energy per unit area for each zone is written as

$$\mathcal{F}_{el}(\sigma_i, \kappa, \ell_B) = \sigma_i \Psi_i^0 - \frac{\kappa}{\pi \ell_B} \left[\cosh\left(\frac{\Psi_i^0}{2} \right) \right] \tag{5.1}$$

with Ψ_i^0 the electrostatic potential on the surface of charge density σ_i given by

$$\Psi_i^0 = 2 \sinh^{-1}(2\pi \sigma_i \ell_B / \kappa). \tag{5.2}$$

The WS free energy is approximately given as

$$F_{\mathrm{WS}} = A_S \mathcal{F}_{el}(\sigma_1, \kappa, \ell_B) + (A_{\mathrm{WS}} - A_S) \mathcal{F}_{el}(\sigma_2, \kappa, \ell_B) \tag{5.3}$$

There is ambiguity in choosing the area of the zone 1, A_S. In principle, A_S includes the peptide area as well as the surrounding in which lipids effectively interact with the peptide. What is the area of surrounding membrane? To answer this question, one can use the *two-dimensional* Debye screening length, κ_2^{-1}, introduced by E. S. Velazquez and L. Blum in reference [90], assuming the lipids within this screening length interact with the peptide and are in zone one. For instance, in

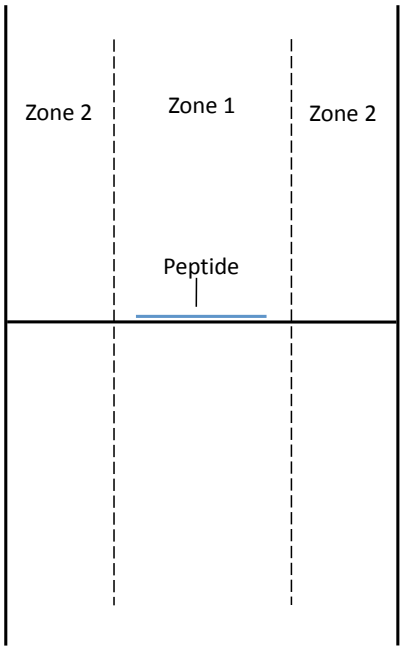

Figure 5.1: A side view of a cylindrical Wigner-Seitz cell with a peptide adsorbed on the surface of a thin membrane. Zone 1 is a cylinder and zone 2 is a cylindrical shell around zone 1. In the approximation scheme developed in this section, the membrane in each zone is assumed to have a uniform surface charge density.

case of a disk peptide with area $a_p = \pi R_P^2$ adsorbed on the membrane, we can define the interaction zone area by $A_S = \pi(R_P + \kappa_2^{-1})^2$, where $\kappa_2 = 2\pi e^2 \overline{\alpha}/a_0 \epsilon_w \epsilon_0 k_B T$ for a membrane with $\overline{\alpha}$ the average fraction of charged lipids and a_0 the headgroup area of lipid molecules.

The approximation scheme introduced here is rather non-trivial in the sense that the electrostatic potential is not fully and consistently solved for the solvent. A valid concern one can raise is the discontinuity of the electric potential on the boundary between zone 1 and zone 2. Since we treated the two zones separately, there was no mechanism to match the potentials at this boundary. One explanation is that, if the electrostatic free energy is overestimated in one zone due to the mismatch

of electric potential, it is, on the other hand, underestimated in the other zone. Thus, the uncertainty of the free energy in each zone tends to counterbalance that of the other zone. To further discuss the accuracy of the approach presented here, we show some results compared with the results of the exact PB solution.

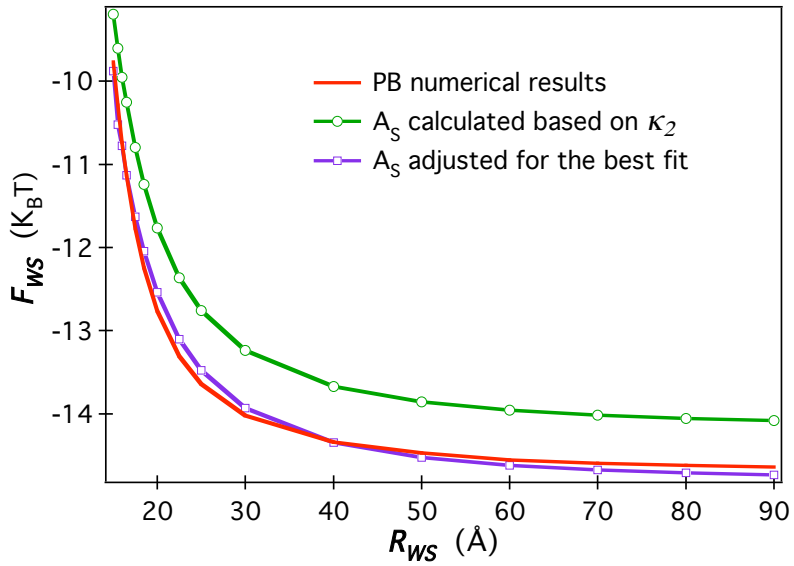

Figure 5.2: Free energy of a cylindrical Wigner-Seitz cell as a function of the radius of the cell. The red line shows the result of numerical Poisson-Boltzmann solution. The results from the approximation scheme developed in this section is shown using $A_S = \pi(R_P + \kappa_2^{-1})^2$ (green line) and A_S manually adjusted to get the best fit with the PB result (blue line). We have used $\overline{\alpha} = 0.3$, $Q = 4$, $a_p = 314$, $a_0 = 65\,\text{Å}^2$, $\kappa = 0.1\,\text{Å}^{-1}$, $\ell_B = 6.9\,\text{Å}$, $T = 300\,\text{K}$.

The results in Fig. 5.2 depict the WS cell free energy, F_{WS}, as a function of the WS cell radius, R_{WS}. Parameters are chosen as follows: $\overline{\alpha} = 0.3$, $Q = 4$, $a_p = 314$, $a_0 = 65\,\text{Å}^2$, $\kappa = 0.1\,\text{Å}^{-1}$, $\ell_B = 6.9\,\text{Å}$, $T = 300\,\text{K}$. The solid red line in Fig. 5.2 show the result obtained by numerical solution of PB equation for a WS cell subject to boundary conditions. The green line shows the result obtained by the semi-analytical approach proposed here, where A_S is calculated using the two-dimentional Debye screening length, κ_2, as explained above. For the blue line,

the same semi-analytical approach is used, however, A_S is manually adjusted to get the best fit. The accuracy of the approach is impressive – it's within 5% of the numerical result.

A future direction along this line is designing a similar method to calculate energetics of surface-inserted peptides (See Chapter 3 for details about surface-inserted mode). In this case, the results reported in chapter 3 can be reproduced with a fast-paced approach that enables us to research and discover other possibly important parameters and degrees of freedom. This has been cumbersome due to the slow and time consuming nature of solving the nonlinear PB equation. With this alternative approach one can explore to a larger range of values for parameters such as fraction of charged lipids, $\overline{\alpha}$, Debye length, κ, and peptide area, a_p, which can provides us with a more comprehensive picture of the antimicrobial peptide and membrane interactions.

5.2.2 Threshold of pore formation by antimicrobial peptides

In this thesis, we presented a theoretical model to capture the essence of the interaction of antimicrobial peptides with lipids bilayers. We studied the binding of peptides onto lipid bilayers as influenced by a variety of parameters. We elaborated on the modes of peptide binding, i.e., surface-adsorption and surface-insertion, and discovered how insertion of peptides disrupts the bilayer structure through stretching the overall area that can lead to formation of transient pores. Our analysis of pore formation, however, has been limited to spontaneous pores. While this provides us with the valuable information on the likelihood of formation and expansion of a transient pore, a comprehensive understanding of peptide induced pores may require a detailed modeling of pores stabilized by peptides (See Chapter 1 for a review on the process of pore formation). One important aspect is the threshold of pore formation. If the molar ratio of bound peptides to lipids, P/L, exceeds a

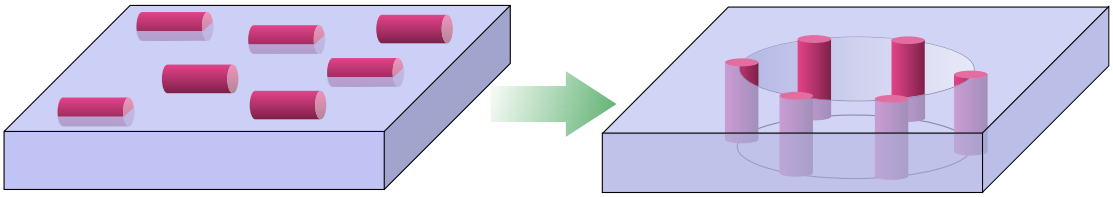

Figure 5.3: As the density of bound peptides reaches a threshold value, $(P/L)^*$, the stress on the bilayer becomes great such that peptides can self-assemble into a pore to relief the stress.

threshold value, $(P/L)^*$, pores start to form on the surface (Fig. 5.3). This threshold is not a universal value and is dependent on the characteristics of peptides and lipid membrane. There has been experimental observation of $(P/L)^*$ for a few different choices of peptides and lipid bilayers [23,24]. On the theoretical side, however, there has not been a concrete model to provide predictions of $(P/L)^*$ based on the peptide and lipid bilayers parameters.

In this section, we propose a theoretical modeling scheme to calculate the energetics of peptide-stabilized pores. Comparison of the energies of peptides participating in pore formation with those bound on the surface of the lipid bilayer determines if the formation of the pore is favorable (Fig. 5.4). In chapter 3 of this thesis, we have calculated energy of bound peptides where we used a disk model for the peptides. To compare the energy of bound peptides with those in pore, one should, however, change the geometry of the model peptide to cylinder, the most simple geometry for alpha-helical peptides forming a pore. Since the comparison between the energies leads to determining the threshold (P/L) for pore formation and since the energy is influenced by geometry, for those peptides bound on the surface, we should also use the cylindrical model.

The Wigner-Seitz cell (WSC) approximation is applicable as long as we have cylindrical symmetry. In chapter 3, it was due to the disk model for peptide which was surrounded by the symmetrical radial distribution of other bound peptides.

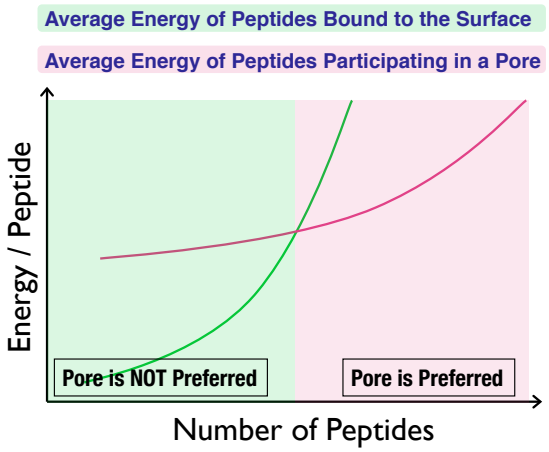

Figure 5.4: Schematic representation of the comparison between the free energy per peptide in a pore and bound on the surface can determine if the formation of a pore on the lipid bilayer is favorable.

For cylindrical peptides bound parallel to the membrane, we have to use different methods, as there is no cylindrical symmetry for unit cells on the surface.

An approximation method one can invoke to calculate the energetics of cylindrical peptide bound to the surface of the lipid membrane is to ignore the direct interaction between the bound peptides. While it may sound naïve at first glance, this approximation can be justified considering that the direct distance between bound peptides is $\sim 20\,\text{Å}$, almost two times longer than the Debye screening length. The direct interaction between peptides is screened by salt ions to a large extent. Can we assume there is absolutely no interaction between peptide? Can we write the electrostatic energy of peptide-membrane as $N_P \times F_{single}$, where N_P is the number of peptides bound to the surface and F_{single} is the energy one single peptide bound to the surface? (By single peptide, we indicate the energy of only one peptide bound to an infinitely large membrane).

Our observations in chapter 3 shows that energy of WSCs strongly depends on the radius of the WSC (Fig. 5.5). This implies that the electrostatic free energy

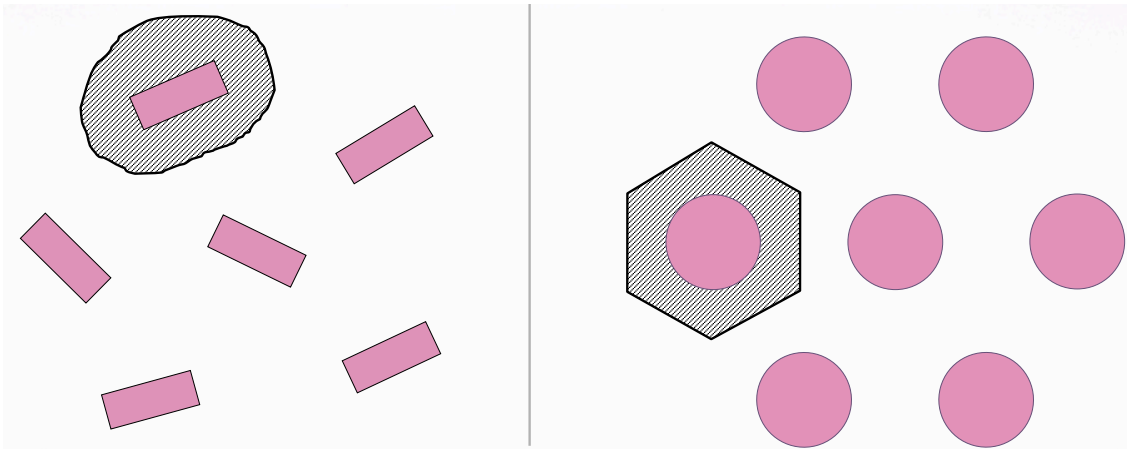

Figure 5.5: Typically, the planar density of peptides is such that there is no direct electrostatic interaction between peptides. Yet the electrostatic free energy per peptide is a function of the distance between peptides. This dependence is through the number of anionic lipids that each peptide can potentially attract to increase its binding affinity. This observation from the disk peptides (right figure) lead us to define unit cells of constant area with variable number of anionic lipids. This can be applied to cylindrical peptides bound parallel to the surface of the membrane.

of peptide-membrane system is not linearly proportional to the number of bound peptides. Our results indicate that, while peptide-peptide distance is larger than the Debye length, the interactions between peptides is rather through anionic lipids that tend to accumulate around bound peptides. To understand this, imagine there is one single peptide bound to the surface, anionic lipids migrate to the vicinity of the peptide to neutralize peptide charge. If the density of peptides bound to surface is large, anionic lipids are shared by all peptides. Thus, there is a smaller number of anionic lipids accumulated around each peptide. As a result, the binding energy of peptides is dependent on the number of available anionic lipids for each peptide which is proportional to the membrane area per bound peptide. This observation, suggests that we can use a modified the WS cell approach for cylindrical peptides bound to the surface. That is, each WS cell includes one cylindrical bound peptide and membrane within the Debye length from the peptide. Assuming the number

of the number of anionic lipids is variable, we can calculate the WSC free energy as a function of the number of anionic lipids present in the WSC. Using this free energy, we can construct the free energy of the membrane as a function of the planar density of bound peptides which is inversely proportional to number of available anionic lipids per peptide.

As for peptides participating in pore formation, one can solve the Poisson-Boltzmann equation subject to boundary conditions to find the electrostatic free energy of a pore. Since peptides are symmetrically distributed around each pore, one can divide a pore to $2 \times N_{peptide}$ slices, where $N_{peptide}$ is the number of peptides in a pore. Energy of a pore can be calculated as a function of $N_{peptide}$ and radius of the pore, R_{pore}. Minimization of free energy with respect to these quantities gives us the preferred state of the pore. Comparison of the free energy per peptide in the pore with the free energy of peptides bound to the surface demonstrates if the formation of peptides-stabled pore is favored.

Besides the electrostatic energy, the elastic energy of phospholipid molecules plays an important role. Their effect can be included by integrating their energetics, similar to our approach in chapter 4 of this thesis. Due to the time consuming nature of the calculations of this project and technical difficulties in computation of pore energy (e.g., arising from the narrow edges of the slices of a pore) we have not been able to include it in this thesis. However, the framework we proposed in this section can open a route for the better understanding of AMP interactions with cell membranes.

Bibliography

[1] Laxminarayan, R., A. Malani, D. Howard and D. Smith. 2007. *Extending The Cure: Policy Resposes to the Growing Threat of Antibiotic Resistance*, Resources for the Future, Washington.

[2] *Nobel Lectures, Physiology or Medicine 1942-1962*, 1964. Elsevier Publishing Company, Amsterdam.

[3] Gordon, Y. J., and E. G. Romanowski. 2005. A Review of Antimicrobial Peptides and Their Therapeutic Potential as Anti-Infective Drugs. Curr. Eye Res. 30: 505-515.

[4] Zasloff, M. 2002. Antimicrobial peptides of multicellular organisms. Nature. 415: 389-395.

[5] Giuliani, A., G. Pirri and S. F. Nicoletto. 2007. Antimicrobial Peptides: an Overview of a Promising Class of Therapeutics. Cent. Eur. J. of Biol. 2: 1-33.

[6] Brogden, K. A. 2005. Antimicrobial peptides: pore formers or metabolic inhibitors in bacteria? Nature Reviews Microbiology. 3: 238-250.

[7] Skarnes, R. C., and D. W. Watson. 1957. Antimicrobial Factors of Normal Tissues and Fluids. Bacteriol. Rev. 4: 273-294.

[8] Zasloff, M. 1987. A class of antimicrobial peptides from *Xenopus* skin: isolation, characterization of two active forms, and partial cDNA sequence of a precursor. Proc. Natl. Acad. Sci. USA. 84: 5449-5453.

[9] Steiner, H., D. Hultmark, A. Engstrom, H. Bennich and H. D. Boman. 1981. Sequence and specificity of two antibacterial proteins involved in insect immunity. Nature. 292: 246-248.

[10] Ganz, T., M. E. Selsted and R. I. Lehrer. 1990. Defensins. Eur. J. Haematol. 44: 1-8.

[11] Zaasloff, M. 2002. Antimicrobial Peptides in Health and Disease. N. Engl. J. Med. 347: 1199.

[12] Ganz, T., J. A. Metcalf, J. I. Gallin, L. A. Boxer and R. I. Lehrer. Microbicidal/cytotoxic proteins of neutrophils are deficient in two disorders: Chediak-Higashi syndrome and "specific" granule deficiency. J. Clin. Invest. 82(2): 552-556.

[13] Harder, J. and J.-M. Schröder. 2005. Psoriatic scales: a promising source for the isolation of human skin-derived antimicrobial proteins. J. Leukoc. Biol. 77: 476-486.

[14] Ganz, T. and R. I. Lehrer. 1997. Antimicrobial peptides of leukocytes. Curr. Opin. Hematol. 4: 53-58.

[15] Alberts, B., A. Johnson, J. Lewis, M. Raff, K. Roberts, and P. Walter. 2002 *Molecular Biology of the Cell*. Garland Science.

[16] Cooper, G. M. and R. E. Hausman. 2004. "The cell: a molecular approach". (3rd ed.). Sinauer.

[17] Matsuzaki, K., O. Murase, N. Fujii, and K. Miyajima. 1995. Translocation of a Channel-Forming Antimicrobial Peptide, Magainin 2, across Lipid Bilayers by Forming a Pore. Biochemistry. 34: 6521-6526.

[18] Matsuzaki, K. 1999. Why and how are peptide-lipid interactions utilized for self-defense? Magainins and tachyplesins as archetypes. Biochim. et Biophys. Acta. 1462: 1-10.

[19] Dathe, M., H. Nikolenko, J. Meyer, M. Beyermann, and M. Bienert. 2001. Optimization of the antimicrobial activity of magainin peptides by modification of charge. FEBS Letters. 501: 146-150; also see a commentary by M. Kardar at http: //www.condmatjournalclub.org/?p=557.

[20] Taheri-Araghi, S. and B.-Y. Ha. 2007. Physical Basis for Membrane-Charge Selectivity of Cationic Antimicrobial Peptides. Phys. Rev. Lett. 98: 168101.

[21] Chan, B.-P., K.-S. Yi, K. Matsuzaki, M.-S. Kim and S.-C. Kim. 2000. Structure-activity analysis of buforin II, a histone H_2A-derived antimicrobial peptide: The proline hinge is responsible for the cell-penetrating ability of buforin II. Proc. Natl. Acad. Sci. USA. 97: 8245-8250.

[22] Shai, Y. 1999. Mechanism of the binding, insertion and destabilization of phospholipid bilayer membranes by α-helical antimicrobial and cell non-selective membrane-lytic peptides. Biochim. et Biophys. Acta. 1462: 55-70.

[23] Lee, M.-T., F.-Y. Chen, and H. W. Huang. 2004. Energetics of Pore Formation Induced by Membrane Active Peptides. Biochemistry. 43: 3590-3599.

[24] Wu, Y., H. W. Huang, and G. A. Olah. 1990. Method of Oriented Circular Dichroism. Biophys. J. 57: 797-806.

[25] Huang, H. W., F.-Y Chen, and M.-T. Lee. 2004. Molecular Mechanism of Peptide-Induced Pores in Membranes. Phys. Rev. Lett. 92: 198304-1–198304-4.

[26] Yang, L., T. A. Harroun, T. M. Weiss, L. Ding and H. W. Huang. 2001. Barrel-stave model or toroidal model? A case study on melittin pores. Biophys. J. 81: 1475-1485.

[27] Matsuzaki, K., O. Murase, N. Fujii and K. Miyajima. 1996. An antimicrobial peptide, magainin 2, induced rapid flip-flop of phospholipids coupled with pore formation and peptide translocation. Biochemistry. 35: 11361-11368.

[28] Christensen, B., J. Fink, R. B. Merrifield and D. Mauzerall. 1988 Channel-forming properties of cecropins and related model compounds incorporated into planar lipid membranes. Proc. Natl. Acad. Sci. USA. 85: 5072-5076

[29] Spaar, A., C. Munster and T. Salditt. 2004. Conformation of peptides in lipid membranes studied by X-ray grazing incidence scattering. Biophys. J. 87: 396-407.

[30] He, K., S. J. Ludtke, H. W. Huang and D. L. Worcester. 1995. Antimicrobial peptide pores in membranes detected by neutron in-plane scattering. Biochemistry. 34: 15614-15618.

[31] Yamaguchi, S., T. Hong, A. Waring, R. I. Lehrer and M. Hong. 2002. Solid-state NMR investigations of peptide-lipid interaction and orientation of β-sheet antimicrobial peptide, protegrin. Biochemistry. 41: 9852-9862.

[32] Pouny, Y., D. Rapaport, A. Mor, P. Nicolas and Y. Shai. 1992. Interaction of antimicrobial dermaseptin and its fluorescently labeled analogues with phospholipid membranes. Biochemistry. 31: 12416-12423.

[33] Deryagin, B. V. and Y. V. Gutop. 1962. Theory of the breakdown (rupture) of free films. Kolloidnyi Zh. 24: 431-437.

[34] Lister, J. D. 1975. Stability of lipid bilayers and red blood cell membranes. Phys. Lett. 53A: 193-194.

[35] Boal, D. 2002. *Mechanics of the Cell*, Cambridge University Press.

[36] Playfair, J., and G. Bancroft. 1994. *Infection and Immunity*, Oxford University Press.

[37] Singleton, P. 1997. *Bacteria in Biology, Biotechnology and Medicine*. 4th edition, John Wiley and Sons.

[38] Ha, B.-Y., and A. J. Liu. 1997. Counterion-mediated attraction between two like-charged rods. Phys. Rev. Lett. 79: 1289-1292.

[39] Li, Y., and B.-Y. Ha. 2005. Molecular theory of asymmetrically charged bilayers: Preferred curvatures. Europhys. Lett. 70: 411-417.

[40] Ganz, T. 2003. Defensins: antimicrobial peptides of innate immunity. Nature Reviews Immunol. 3: 710-720.

[41] Ludtke, S. J., K. He, Y. Wu, and H. W. Huang. 1994. Cooperative membrane insertion of magainin correlated with its cytolytic activity. Biochim. et Biophys. Acta. 1190: 181-184.

[42] Lee, M.-T., W.-C. Hung, F.-Y. Chen, and H. W. Huang. 2008. Mechanism and kinetics of pore formation in membranes by water-soluble amphipathic peptides. Proc. Nat. Acad. Sci. 105: 5087-5092.

[43] Jelokhani-Niaraki, M., R. S. Hodges, J. E. Meissner, U. E. Hassenstein, and L. Wheaton. 2008. Interaction of gramicidin S and its aromatic amino-acid analog with phospholipid membranes. Biophys. J. 95: 3306-3321.

[44] Hancock, R. E. W. and H.-G. Sahl. 2006. Antimicrobial and host-defense peptides as new anti-infective therapeutic strategies. Nature Biotechnology. 24: 1551-1557.

[45] Hancock, R. E. W. 2001. Cationic peptides: effectors in innate immunity and novel antimicrobials. Infectious Diseases. 1: 156-164.

[46] The main targets of some peptides are internal components, leading to intracellular killing [6, 44]. Interestingly, membrane-active AMPs can catalyze the entry of these cell-penetrating peptides into the cytoplasm. See, for instance, G. Kragol et al. 2001. The Antibacterial Peptide Pyrrhocoricin Inhibits the ATPase Actions of DnaK and Prevents Chaperone-Assisted Protein Folding. Biochemistry. 40: 3016-3026.

[47] Melo, M. N., R. Ferre and M. A. R. B. Castanho. 2009. Antimicrobial peptides-linking partition, activity and high membrane-bound concentrations. Nature Reviews Microbiology. 7: 245-250.

[48] See Refs. [4, 44] for the interaction of AMPs and the outer membrane of gram negative bacteria.

[49] Zelezetsky, I. and A. Tossi. 2006. Alpha-helical antimicrobial peptides – Using a sequence template to guide structureactivity relationship studies. Biochim. et Biophys. Acta. 1758: 1436-1449.

[50] Goldman, M. J., G. M. Anderson, E. D. Stolzenberg, U. P. Kari, M. Zasloff, and J. M. Wilson. 1997. Human β-defensin-1 is a salt-sensitive antibiotic in lung that is inactivated in cystic fibrosis. Cell. 88: 553-560.

[51] "Good" AMPs are those that are coil-like in bulk but undergo compaction on a membrane [18,60]. The particular one in Fig. 3.1 assumes α-helical structure; see Refs. [4, 6, 40] for other structures.

[52] May, S., D. Harries, and A. Ben-Shaul. 2000. Lipid demixing and protein-protein interactions in the adsorption of charged proteins on mixed membranes. Biophys. J. 79: 1747-1760.

[53] Brent, R.P. 1973. "Algorithms for minimization without derivatives" Prentice-Hall.

[54] Because of its thickness ($\approx 40\,\text{Å}$) and low dielectric constant of the membrane ($\epsilon_l = 2$), the composition of the inner layer is much less crucial, especially in the presence of salts. For simplicity, we will treat the inner layer, "dressed" with its own counterions, as overall neutral.

[55] Wieprecht, T., M. Beyermann, and J. Seelig. 1999. Binding of antibacterial magainin peptides to electrically neutral membranes: Thermodynamics and structure. Biochemistry. 38: 10377-10387.

[56] Rawicz, W., K. C. Olbrich, T. McIntosh, D. Needham, and E. Evans. 2000. Effect of chain length and unsaturation on elasticity of lipid bilayers. Biophys. J. 79: 328-339.

[57] Gelbart, W. M., R. Bruinsma, P. A. Pincus, and V. A. Parsegian. 2000. DNA-inspired electrostatics. Physics Today. 53: 38-44.

[58] Parsegian, V. A. and D. Gingell. 1972. On the electrostatic interaction across a salt solution between two bodies bearing unequal charges. Biophys. J. 12: 1192-1204.

[59] Needham, D. and R. S. Nunn. 1990. Elastic deformation and failure of lipid bilayer membrane containing cholesterol. Biophys. J. 58: 997-1007.

[60] Jiang, Z., A. I. Vasil, J. D. Hale, R. E. W. Hancock, M. L. Vasil, and R. S. Hodges. 2007. Effects of net charge and the number of positively charged

residues on the biological activity of amphipathic α-helical cationic antimicrobial peptides. Biopolymers. 90: 369-383.

[61] For a pedagogical introduction to lipid membranes and vesicle shapes, see Wortis, M. and E. Evans, Physics in Canada, Sep./Oct. 281-288 (1997).

[62] Israelachvili, J. N., *Intermolecular and Surface Forces*, 2nd Edt. (Academic Press, 1992).

[63] Gruner, S. M., P. R. Cullis, M. J. Hope, and C. P. S. Tilcock. 1985. Lipid polymorphism: the molecular basis of non-bilayer phases. Ann. Rev. Biophys. Biophys. Chem. 14: 211-238.

[64] Winterhalter, M., and W. Helfrich. 1992. Bending elasticity of electrically charged bilayers: coupled monolayers, neutral surfaces, and balancing stresses J. Phys. Chem. 96: 321-330.

[65] Mitchell, D. J., and B. W. Ninham. 1989. Curvature elasticity of cLargedmembranes. Langmuir 5: 1121-1123.

[66] Chou, T., M. V. Jari, and E. D. Siggia. 1997. Electrostatics of lipid bilayer bending. Biophys. J. 72: 2042-2055.

[67] Zimmerberg, J., and M. M. Kozlov, 2006. How Proteins Produce Cellular Membrane Curvature. Nature Rev. Mol. Cell Biol. 7: 9-19. Also see the supplementary information.

[68] Lim, G., H. W., M. Wortis, and R. Mukhopadhyay. 2002. Stomatocyte-discocyte-echinocyte sequence of the Human red blood cell: Evidence for the bilayer- couple hypothesis from membrane mechanics. Proc. Nat. Acad. Sci. 99: 16766-16769.

[69] Papahadjopoulos, D. 1969. Stability of asymmetric phospholipid membranes. Science. 30: 1075-1077.

[70] Papahadjopoulos, D.. and A. Portis.1978. Calcium-induced lipid phase transitions and membrane fusion. Ann. of N.Y. Acad. of Sci. 308: 50-66.

[71] Chanturiya, A., P. Scaria and M. C. Woodle, J. 2000. The role of membrane lateral tension in calcium-induced membrane fusion. J. Membr. Biol. 176: 67-75.

[72] Bezrukov, S. M., R. P. Rand, I. Vodyanoy, and V. A. Parsegian. 1998. Lipid packing stress and polypeptide aggregation: alamethicin channel probed by proton titration of lipid charge. Faraday Discuss. 111: 173-183.

[73] Perozo, E., A. Kloda, D. M. Cortes, and B. Martinac. 2002. Physical principles underlying the transduction of bilayer deformation forces during mechanosensitive channel gating. Nature Struct. Biol. 9: 696-703.

[74] Ermakov, Y. A., K. Kamaraju, K. Sengupta, and S. Sukharev. 2010. Gadolinium ions block mechanosensitive channels by altering the packing and lateral pressure of anionic lipids. Biophys. J. 98: 1018-1027.

[75] Fuller, N., C. R. Benatti, and R. P. Rand. 2003. Curvature and bending constants for phosphatidylserine-containing membranes. Biophys. J. 85: 1667-1674.

[76] Kirchhausen, T. 2000. Three ways to make a vesicle. Nature Rev. Mol. Cell Biol. 1 : 187.

[77] Travesset, A., and D. Vaknin. 2006. Bjerrum pairing correlations at charged interfaces. Europhys. Lett. 74: 181-187.

[78] Henle, M. L. , C. D. Santangelo, D. M. Patel, and P. A. Pincus. 2004. Distribution of counterions near discretely charged planes and rods. Europhys. Lett. 66: 284-290.

[79] Li, Y.,and B.-Y. Ha. 2005. Molecular theory of asymmetrically charged bilayers: Preferred curvatures. Europhys. Lett. 70: 411-417.

[80] One of the main differences between monolayers and bilayers in the context of bending is that any mismatch in the areas of outer and inner layers in the latter can induce spontaneous bending. This effect can cooperate with or compete against the spontaneous curvature arising from local properties of lipids such as lipid packing as detailed later (see subsection 4.4.2). However our description in this section is common for both cases.

[81] May, S., and A. Ben-Shaul. 1999. Molecular Theory of Lipid-Protein Interaction and the L_α-H_{II} Transition Biophys. J. 76: 751-767.

[82] S. Safran, *Statistical Thermodynamics of Surfaces, Interfaces, and Membranes* (Westview Press, 2003).

[83] See S. Leibler in *Statistical Mechanics of Membranes and Surfaces* (World Scientific, 2004), 2nd Edt., edited by D. Nelson, T. Piran, and S. Weinberg.

[84] Petrov, A. G., and I. Bivas. 1984. Elastic and flexoelectic aspects of out-of-plane fluctuations in biological and model membranes. Prog. in Surf. Sci. 16: 369-512.

[85] Miao, L., U. Seifert, M. Wortis, and H.-G. Döbereiner. 1994. Budding transitions of fluid-bilayer vesicles: The effect of area-difference elasticity. Phys. Rev. E. 49: 5389-5407.

[86] This does not mean that two neutral surfaces are needed for describing bilayer bending. A common neutral surface can be constructed as discussed here and

in Ref. [85]. In our case, however, the midplane essentially coincides with the bilayer neutral surface, as discussed in subsection 4.4.1.

[87] Taheri-Araghi, S. and B.-Y. Ha. 2010. Cationic antimicrobial peptides: a physical basis for their selective membrane-disrupting activity. Soft Matter 6: 1933-1940.

[88] Bouvrais, H., P. Mèlèrd, T. Pott, K. J. Jensen, J. Brask and J. H. Ipsen. 2008. Softening of POPC membranes by magainin. Biophys. Chem. 137: 7-12.

[89] Jähnig, F. Electrostatic Free Energy and Shift of the Phase Transition for Charged Lipid Membranes. 1976. Biophys. Chem. 4: 309-318

[90] Velàsquez, E. S., L. Blum. 1997. Electrolytes confined to a plane in the Debye-Huckel theory. Physica A, 244: 453-460.